UNIVERSITÀ DEGLI STUDI DI TRENTO
FACOLTÀ DI SCIENZE MATEMATICHE FISICHE E NATURALI
DIPARTIMENTO DI FISICA

Two-fluid Hydrodynamics of a quasi-1D unitary Fermi gas

Thesis submitted for the degree of
Doctor Philosophiae

CANDIDATE:
Yan-Hua Hou

SUPERVISORS:
Prof. Sandro Stringari
Prof. Lev P. Pitaevskii

December 6 2013

for my husband, Wenjun Hu

Abstract

This thesis is devoted to the study of the hydrodynamic behavior of the unitary Fermi gas trapped by a highly elongated harmonic potential. Propagation of sound is one of the most exciting features exhibited by interacting many-body systems. It provides crucial information on the dynamic behavior of the system as well as on key thermodynamic quantities. The propagation of sound is particularly interesting in superfluids where two-fluid hydrodynamic theory predicts the occurrence of two different sounds: first sound, where the normal and superfluid component oscillate in phase, and second sound, where the two components oscillate with opposite phase.

In the thesis, we investigate the propagation of sound waves of the unitary Fermi gas in a cylindrical geometry by solving the equations of two-fluid hydrodynamics in the '1D' scenario at finite temperature. The relevant thermodynamic functions entering the hydrodynamic equations are discussed in the superfluid and normal regimes in terms of universal scaling functions. Both the first sound and second sound solutions are calculated as a function of temperature and the role of the superfluid density is explicitly pointed out. The density fluctuations in the second sound wave are found to be large enough to be measured as a consequence of the finite thermal expansion coefficient of the gas, which is the strategy used in a recent experiment carried out at Innsbruck where second sound was detected in the unitary Fermi gas.

We also provide an investigation of the temperature dependence of the collective oscillations of first sound nature exhibited by a highly elongated harmonically trapped Fermi gas at unitarity, including the region below the critical temperature for superfluidity. Differently from the lowest axial breathing mode, the hydrodynamic frequencies of the higher-nodal excitations show a temperature dependence,

which is calculated starting from Landau two-fluid theory and using the available experimental knowledge of the equation of state.

Acknowledgement

First I would like to thank my supervisors Prof. Lev Pitaevskii and Prof. Sandro Stringari for their great scientific supports, invaluable guidance and continuous encouragement. I appreciate the insightful scientific atmosphere they have created in the seminars, in the office-discussions, during the car-trip to Innsbruck... I am deeply impressed by their enthusiasm, attitude and knowledge in physics. Sandro and Lev showed me how to work with great patience. Although I am a slow walker and very often I walked badly, they gave me encouragement and guidance step by step. The three years' study with them will be a great treasure in my academic life.

The BEC group is like a big family and, from big festivals to small parties, picnics, excursions,..., we are sharing every piece of joys together. Every memory is beautiful, happy and sweet. I do cherish this family and I want to express my deep gratitude to all the members that I met in the group. In particular, I am indebted to Alessio Recati for providing me the first two months' visit to the group before I was enrolled as a PhD student and for his helpful discussions and suggestions and Stefano Giorgini for his patience and help in solving my puzzles. I want to thank all the members for discussing with me during my first visit and in the past three years, among them are Franco Dalfavo, Iacopo Carusotto, Chiara Menotti, Gabriele Ferrari, Giacomo Lamporesi, Philipp Hyllus, Robin Scott, Gianluca Bertaina, Francesco Piazza, Rifat Onur Umucalhar, Stefano Finazzi, Yun Li, David Papoular, Riccardo Rota, Marta Abad Garcia, Tomoki Ozawa, Zeng-Qiang Yu, Natalia Matveeva, Marco Larcher, Nicola Bartolo, Giovanni Martone, Luis Aldemar Pena Ardila, Alberto Sartori, Simone Donadello, Grazia Salerno. I want to thank Peng Zou especially for his friendship and numerous helps in my life and study. I also want to thank Zhen-Yi Cai for sharing his latex template for the

thesis, especially his effort in maintaining the bibliography working well, Zeng-Qiang for helpful discussions during writing the thesis and Natalia and Luis for valuable discussions in many respects. Especially I appreciate the suggestions from Marta, Tomoki, Peng, and Zeng-Qiang on the presentation.

I have been very fortunate to have the chance to collaborate with some of the best experimentalists in the world in ultracold atom physics. I would like to acknowledge systematic discussions and fruitful collaborations with Prof. Rudolf Grimm, Meng Khoon Tey, Leonid A. Sidorenkov, Edmundo R. Sánchez Guajardo and Prof. Martin. W. Zwierlein and Mark J. H. Ku. Especially I am grateful to Meng Khoon for his answering my naive questions on experiments and many valuable advices not only in physics but also in attitudes towards science and life. The helpful discussions with Mark are also greatly appreciated, in his providing the relevant experimental data used in the thesis and on his interpretations and suggestions to manipulate those data.

Thanks also go to the secretaries, Beatrice Ricci, Flavia Zanon, Micaela Paoli and the technician Giuseppe Fronter for all the help they have provided over the years. Especially, I want to thank Beatrice for helping me twice to get a room (which is quite a challenging task) from Opera Universitaria di Trento for the last three months and to have a quiet place to continue the thesis. I also acknowledge the librarians for always managing to find materials that I need.

I dedicate my deepest love and appreciation to my husband Wen-Jun Hu for his loves, listening to my complaints, encouraging me to continue. Without Wen-Jun, I wouldn't have been able to face all the difficulties that I met in life and studies. Finally, I want to thank my family for their unconditional love and support.

Contents

List of Figures

Chapter 1

Introduction

1.1 Historical overview

With the discovery of superfluid helium, the study of strongly interacting systems entered a new era. Following the discovery that liquid ^{4}He exhibits a superfluid phase when cooled below the λ-point [1, 2], L. Tisza suggested the existence of two types of sound-like oscillations in the superfluid phase [3, 4]. Landau [5] developed a successful quantitative two-fluid model (comprising a normal component, which behaves like an ordinary fluid, and a superfluid component with zero viscosity and zero entropy), that could account for many of the properties of superfluid ^{4}He. The two-component nature in the superfluid phase is manifested in the occurrence of 'second sound', an entropy wave in which the superfluid and the non-superfluid components oscillate with opposite phases, as opposed to ordinary 'first sound', where they oscillate in phase. Second sound has attracted much attention in the literature mainly because the velocity of this peculiar sound is determined by the superfluid density. Actually in liquid ^{4}He the most accurate determination of the temperature dependence of the superfluid density is obtained through the measurement of the second sound velocity [6, 7]. These data allowed Landau to establish the correct form of the spectrum of the elementary excitations of ^{4}He, including the roton minimum [8].

The search for other systems possessing similar properties has been carried out extensively and successful achievements have been made in ultracold atomic gases. In 1995, the first BEC in a dilute atomic gas was realized in the laboratory on vapors

of rubidium [9], and very quickly in the same year on sodium and lithium [10, 11]. The degenerate Fermi gas was obtained a few years later in several laboratories [12, 13, 14, 15, 16]. In contrast to bosons (particles with integer spins) which can form a condensate at sufficient low temperatures, fermions (particles with half-integer spin) avoid to occupy the same single particle state because of the Pauli principle. However, also the Fermi gas exhibits a transition to the superfluid phase due to the presence of the atom-atom interactions. The exclusion principle actually poses a challenge (in cooling) and at the same time, yields a unique opportunity (in view of the suppression of the three-body recombination rate) to achieve a stable strongly interacting degenerate Fermi gas, contrary to a strongly interacting Bose gas, which is unstable due to three-body collisions. In 2002, a strongly interacting Fermi gas was first achieved by the Duke group [17], where fermionic atoms are cooled down to quantum degeneracy and the atomic interactions are dramatically enhanced through a Feshbach resonance [18].

In the case of ultracold dilute gases, only s-wave scatterings are important and interactions are well characterized by a single parameter, i.e., the so-called s-wave scattering length 'a'. In this approximation, only fermions in different hyperfine states interact due to the Pauli principle, therefore two different internal states are considered instead in this case, and the system is often called a two-component Fermi gas. By tuning an external magnetic field across a Feshbach resonance [18], the interatomic interactions in a two-component Fermi gas can be changed precisely from weak to infinitely strong, leading to the observation of crossover from a BEC-type system (for positive scattering length) to a fermionic superfluid with Bardeen-Cooper-Schrieffer (BCS) type pairing (for negative scattering length). At resonance, the s-wave scattering length a is infinite and the effective range of interaction is negligible, leading to a strongly interacting system with universal behavior [19]. Under this circumstance, the s-wave cross section reaches its largest possible value (unitary limit). This regime is called unitarity and the strongly interacting degenerate Fermi gas is also referred to as the unitary Fermi gas. Due to the precise control of geometry, purity and interactions in these systems, they have become ideal laboratories to explore important quantum phenomena and provided a fruitful playground to test many-body theories of quantum systems (see [20, 21, 22] and [23, 24, 25] for reviews).

A peculiar feature of ultracold gases is that they are confined, the confinement being often of harmonic shape. In the case of highly elongated configurations, it is possible to investigate directly the propagation of sound waves, by generating a perturbation in the center of the trap and subsequently investigating the time and space propagation of the resulting signal along the long axis [26, 27, 28]. Propagation of sound provides crucial information on the dynamic behavior of the system as well as on key thermodynamic quantities. Most of theoretical investigations in trapped atomic gases have been so far carried out at zero temperature, where only the first sound oscillations exist, both in the Bose-Einstein condensed gas and in the interacting Fermi gas. The propagation of sound near zero temperature, and in particular the value of the sound velocity, have been the object of systematic studies, and the general agreement between theory [29, 30] and experiments [26, 27] is satisfying, both for Bose and Fermi superfluids (for a review see, for example, [20] and [24]).

Much less is known about the behavior of sound at finite temperature. This is due to various reasons. On one hand the realization of the collisional regime in the thermal component of a Bose gas, needed to apply the equations of hydrodynamics, is not obvious due to the very dilute and weakly interacting nature of the system. On the other hand the accurate control of temperature requires sophisticated experimental techniques. From the theoretical point of view the implementation of dynamic theories at finite temperature is much more difficult than at zero temperature [31], especially in the realistic case of trapped configurations. The situation becomes particularly challenging in the study of second sound, due to the intrinsic difficulties in generating and monitoring temperature waves and in providing accurate theoretical predictions for their behavior. The first attempt to investigate the relative motion of the condensate and the thermal component was carried out [32] after the creation of the Bose-Einstein condensate by the MIT group and followed almost 10 years later by R. Meppelink et al in Ref. [33] where the use of denser samples permitted one to explore collisional damping effects. The corresponding temperature dependence of the speed of sound has been measured in Ref. [34], stimulating a recent theoretical interpretation in Ref. [35]. However, in weakly interacting Bose-Einstein condensed gases, second sound behaves quite differently from the case of liquid helium II. In such systems, over the experimentally relevant

temperature range, second sound reduces to an oscillation of the condensate, the thermal component remaining practically at rest. In contrast to dilute Bose gases, the unitary Fermi gas characterized by strong interactions is more similar to liquid helium II as revealed in a recent experimental observation of the propagation of sounds in Ref. [36]. We will investigate the sound propagations in the unitary Fermi gas in highly elongated harmonic traps, where the Landau two-fluid description of finite temperature collisional dynamics is expected to be valid, through the formulation of the so-called one-dimensional (1D) hydrodynamic approach [37].

When the wavelength is comparable with the size of the sample, the confinement causes the discretization of sound waves in the form of collective oscillations. Collective oscillations provide powerful tools to understand the physical behavior of quantum many-body systems from different points of view and to test fundamental theories. On one hand, collective modes can be used to explore different dynamical regimes of the system, such as superfluid, collisional, or collisionless regimes, for both Bose and Fermi statistics [20, 21, 22, 23, 24, 25]. On the other hand, the mode frequencies allow to probe and test the equation of state (EOS) of the system, including its temperature dependence. Collective modes have been studied very early in BEC gases, both experimentally [38, 39] and theoretically [40]. Collective modes in strongly interacting Fermi gases attracted immediate attention [41, 42, 43] as soon as these systems became experimentally available. In the case of BEC gases these studies have permitted to check the validity of superfluid hydrodynamic theory at zero temperature [40] and investigate new interesting phenomena [44, 32, 45, 46, 47]. In the case of interacting Fermi gases, along the BEC-BCS crossover, they have permitted to investigate fine details caused by the interactions and quantum statistical effects in the excitation spectrum of the discretized oscillations [41, 48], including the beyond mean field Lee-Huang-Yang effect [49]. The temperature dependence has been studied experimentally in Refs. [50, 51, 52]. Remarkably, at unitarity all these modes turned out to be insensitive to the superfluid v.s. non-superfluid nature of the gas, with their frequencies remaining independent of temperature throughout the hydrodynamic regime. Recently, a joint theoretical and experimental investigation of the temperature dependence of the higher-nodal collective modes in a highly elongated harmonically trapped unitary Fermi gas have been provided [53, 54]. The frequency of these modes exhibits a useful temperature dependence. We will discuss

this behavior explicitly in chapter 5.

1.2 Thesis outline

We give here a brief outline of the chapters of the thesis. In this chapter, we have begun with reviewing the background and developments in the physics of ultracold atomic gases, pointing out the new opportunities provided by the availability of the Feshbach resonances, allowing for the tuning of the value of the scattering length through the modulation of an external magnetic field. In the case of Fermi gases the availability of Feshbach resonances allows for the BEC-BCS crossover, including the strong-interaction region close to unitarity. The specific system we concentrate on in this thesis is the two-component Fermi gas at unitarity.

One of the peculiarities concerning the unitary Fermi gas is that its thermodynamic functions exhibit a universal behavior due to the absence of any length scale apart from the mean interparticle spacing and thermal wavelength at finite temperatures [19]. In **chapter** 2, we discuss the universal thermodynamic behavior of the unitary Fermi gas in both the uniform (Secs. 2.1–2.4), and trapped geometry (Sec. 2.5) assuming that the local density approximation (LDA) holds in the presence of a smooth harmonic trap. As we will show later, all the thermodynamic quantities can be expressed in terms of universal functions of density or pressure. Since the microscopic calculations of the thermodynamic functions are available only in limited regions of temperature, we choose the strategy of using the data directly derivable from the recent experimental analysis of the MIT team at unitarity [55], implemented and completed at high temperature by the virial expansion ([56, 57] with references therein) and, at very low temperature, by calculating explicitly the phonon contribution which is known to give the leading exact behavior in superfluids as $T \to 0$ [21]. The matching turns out to be rather satisfying (see Figs. 2.1 and 2.2). Therefore, for the goals of the dissertation, the equation of state of the unitary Fermi gas can be considered known with reasonably good accuracy at all temperatures. The superfluid density is another independent and fundamental quantity. However, its present theoretical knowledge, as a function of temperature, is rather poor and we will make use of simple phenomenological ad-hoc expressions

in order to provide explicit predictions. We will discuss the superfluid density in further detail after discussing its first recent experimental detection [36].

By virtue of the strong interactions between the atomic fermions in different hyperfine states, unitary two-component Fermi gases can be used to probe the collisional hydrodynamic regime at finite temperatures. The dynamic behavior of such gases are described by Landau's two-fluid hydrodynamics. This is the basis of the thesis. In **chapter** 3, we review Landau's theory of two-fluid hydrodynamics (Sec. 3.1), as originally developed for ^{4}He (Sec. 3.2), and discuss its application to the weakly interacting Bose gas (Sec. 3.3) and the unitary Fermi gas (Sec. 3.4), both in the homogeneous and in the harmonically trapped case.

In **chapter** 4, we discuss sound propagations of the unitary Fermi gas in the cylindrical geometry. In Sec. 4.1, we develop a theoretical frame for the so-called quasi-1D geometry, which can be experimentally realized in highly elongated traps. We use the notation 'quasi-1D' to indicate configurations which are still Thomas-Fermi in the radial direction (and hence they are actually 3D configurations), but at the same time exhibit peculiar 1D features in the sense that the relevant dynamic behaviour can be described in terms of 1D variables, like for the 1D density, corresponding to the radially integrated 3D density. From the theoretical side the use of highly elongated configurations allows for an important simplification of the formalism, through the formulation of the so-called 1D hydrodynamic approach [37] whose derivation and implementation are discussed in detail. In Sec. 4.2, we implement the reduced 1D two-fluid hydrodynamic equations to get solutions, in the case of cylindrical harmonic traps, for the propagation of first sound (the in-phase motion of the two fluids) and present also the results for second sound (an out-of-phase oscillation of the normal and superfluid components), the most spectacular prediction of Landau two-fluid hydrodynamic equations. We show that the second sound can be detected experimentally due to the finite value of the thermal expansion. In Sec. 4.3, we discuss the experimental excitation and observations of the two sound modes in the cylindrical geometry. Since second sound is particularly sensitive to the behavior of the superfluid density, the recent experimental investigation of second sound [36] has provided the first access to this quantity of fundamental interest, as discussed in Sec. 4.4.

In **chapter** 5, we focus on the discretized axial modes and study its temperature

dependence across the superfluid phase transition within our 1D two-fluid hydrodynamic formalisms. We start in Sec. 5.1, by considering the zero temperature hydrodynamic behavior of the unitary Fermi gas. In Sec. 5.2, we discuss the universal behavior exhibited by the scaling modes, showing that there exist exact solutions for those modes characterized by a linear spatial dependence of the velocity field. The frequencies of these modes turn out to be temperature independent. For the more interesting temperature-dependent higher-nodal modes involving nonlinear dependence in the velocity field, we apply the variational formalism, first developed by Taylor et al [58, 59, 60], to the case of highly elongated traps. In Sec. 5.3, we show that one can solve the classical collisional hydrodynamics in the high temperature limit, as a complement to the limiting case $T = 0$ (as discussed in Sec. 5.1); then we introduce the variational scheme and extend it to our 1D configurations. In Sec. 5.4, we use the variational approach to provide our main results for the discretized collective modes of first sound nature. In Sec. 5.5, we discuss the experimental excitation and observation of higher-order modes of first sound nature. The comparison between the theoretical prediction and the experimental measurement shows excellent agreement and thus represents a sensitive test for the validity of the theoretical approach and of the equation of state. In Sec. 5.6, we investigate the simplest discretized collective modes of second sound nature using the second sound ansatz, namely, assuming there is no net current. We also estimate the coupling between the unperturbed second sound and the lowest coupled first sound mode with the same parity symmetry.

In **chapter** 6, we provide an explicit discussion of the applicability of the 1D approximation implemented in the thesis.

Finally, in **chapter** 7, we draw the conclusions and discuss the perspectives.

Chapter 2

Universal thermodynamics of the unitary Fermi gas

The unitary Fermi gas plays a fundamental role in broad areas of physics, like in condensed matter physics (e.g. high temperature superconductors) and in astrophysics (neutron stars). It is, however, a difficult system to describe microscopically because of the absence of a small interaction parameter. There are numerous efforts to develop strong coupling many-body theories for such a system (see [24] and [57] with references therein and [61, 62, 63, 64, 65, 66, 67, 68]). The use of standard strong-coupling theories [69, 70] requires infinite order expansions and the truncation to a particular order cannot be fully justified a priori. For instance, the Nozières and Schmitt-Rink treatment of fluctuations [71] agrees reasonably well with the experimental data at unitarity at all temperatures except in regions close to the superfluid transition temperature [70]. At present, numerical QMC simulations [72, 73, 61] suffer from either the notorious sign problem for fermions [72] or, in the case of lattice calculations, the need for extrapolation to the zero filling factor limit [73, 61]. Recently, a new Monte Carlo technique (BDMC) [74] has made a breakthrough in calculating the equation of state, showing an excellent agreement with the precise experiment carried out by the MIT group at unitarity [55] in the normal state. However, successful calculations below the superfluid transition are still missing.

On the other hand, due to infinitely large scattering length and zero effective range of interaction, the absence of a characteristic length scale in unitary Fermi gases implies that the type and details of the interaction are not important. A universal thermodynamic behavior, identical for all systems belonging to such a class of systems is expected [19]. Such "universality" can lead to simplifications. Since the seminal work of T.-L. Ho [19], there is an explosive research on the universality of the unitary Fermi gas. Systematic experimental [75, 76, 28, 55] and theoretical (see for example [24, 25] and refs therein) efforts have been made to explore this universal thermodynamic behavior in the superfluid as well as in the normal phase. A breakthrough was achieved by the MIT group [55] in 2012. They measured with high accuracy the critical temperature ($T_c/T_F = 0.167(13)$, see Eq. (2.2) for the definition of T_F) and the so-called Bertsch parameter $\xi = 0.376(4)$ accounting for the interaction effects of the unitary Fermi gas (see Secs. 2.2 and 2.4), providing a benchmark for many-body theories of strongly interacting fermions.

In our work, due to the uncertainties of the theoretical calculations in the relevant temperature range below T_c, we will choose the strategy of using, for the equation of state, the data available from the experimental analysis of the MIT team at unitarity [55]. Universality can then be used to build the thermodynamic functions for all values of T and the particle density n (see Sec. 2.1). Actually the experimental MIT data do not cover the whole range of temperatures and the information on the equation of state can be implemented and completed at high temperature by making use of the virial expansion (Sec. 2.3) and, at very low temperature, by calculating explicitly the phonon contribution (Sec. 2.2) which is known to give, in superfluids, the exact behavior as $T \to 0$ [21]. As far as the superfluid density is concerned, its present theoretical knowledge is rather poor and we will introduce simple ad-hoc parameterizations (see chapter 4). In addition to thermodynamic behavior in the uniform geometry (Sec. 2.1), we also present its nontrivial corresponding counterparts in highly elongated harmonic trap, a geometry favored by experiments in the investigation of hydrodynamic collective modes and sound waves [27, 36, 53, 54].

2.1 3D thermodynamic functions

At unitarity the s-wave scattering length diverges and, in uniform matter, the remaining length scales are the thermal wavelength

$$\lambda_T = \sqrt{2\pi\hbar^2/mk_BT}, \tag{2.1}$$

and the inter-particle distance $n^{-1/3}$, where $\hbar$ is the Planck constant divided by 2π, k_B is the Boltzmann constant, m is the atomic mass, and n is the number density. For the same reason the remaining energy scales are fixed by the temperature T and by the Fermi temperature

$$T_F = \frac{1}{k_B}\frac{\hbar^2}{2m}(3\pi^2 n)^{2/3}, \tag{2.2}$$

or, alternatively, by the chemical potential μ. It follows that at unitarity all the thermodynamic functions can be expressed [19] in terms of a universal function $f_p(x)$ depending on a dimensionless parameter $x \equiv \mu/k_BT$. This function can be defined in terms of the pressure of the gas as

$$\frac{P}{k_BT}\lambda_T^3 \equiv f_p(x)\ . \tag{2.3}$$

Using the thermodynamic relation $n = (\partial P/\partial\mu)_T$, which follows from the Gibbs-Duhem identity: $dP = sdT + nd\mu$, the density of the gas can then be written as

$$n\lambda_T^3 = f_p'(x) \equiv f_n(x)\ . \tag{2.4}$$

From Eq. (2.4) one derives the useful expression

$$\frac{T}{T_F} = \frac{4\pi}{[3\pi^2 f_n(x)]^{2/3}}, \tag{2.5}$$

for the ratio between the temperature and the Fermi temperature (2.2).

In addition to the functions $f_p(x)$ and $f_n(x)$ it is also useful to define the function

$$f_q(x) = \int_{-\infty}^{x} dx' f_p(x'), \tag{2.6}$$

which, as we will show soon, enters in some relevant 1D thermodynamic quantities.

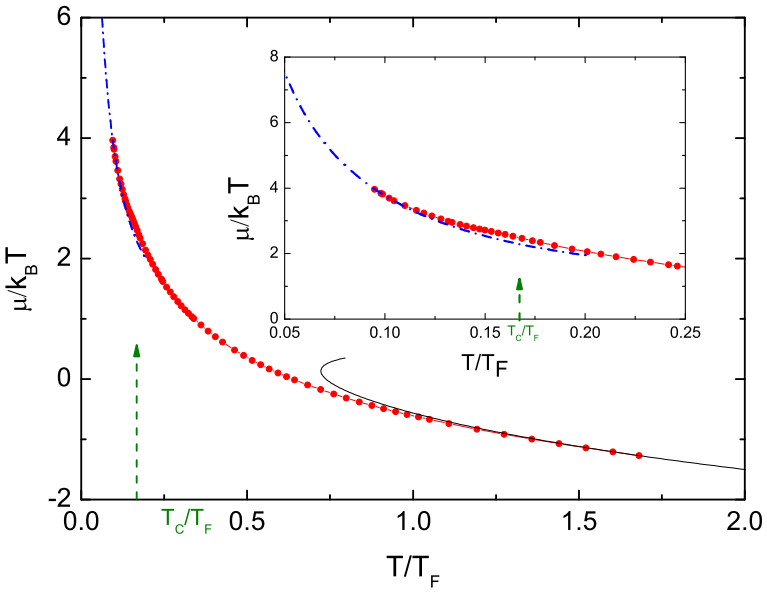

Figure 2.1: Equation of state μ/k_BT versus T/T_F. The blue dash-dotted line corresponds to the phonon contribution to thermodynamics. The red filled circles correspond to the experiment data in the intermediate T regime, while the black solid line to the virial expansion in classical limit. The green arrow indicates the critical point $T_c/T_F = 0.167(13)$. The inset on the upper right corner is an amplification in the lower T regime.

In terms of f_n and f_p we can calculate directly the thermodynamic functions of the uniform Fermi gas at unitarity. For example, using the relation $s = (\partial P/\partial T)_\mu$, we find

$$\frac{S}{Nk_B} = \frac{s}{nk_B} = \frac{1}{nk_B}(\frac{\partial P}{\partial T})_\mu = \frac{5}{2}\frac{P}{nk_BT} + \frac{T}{n\lambda_T^3}f_n(\frac{\partial x}{\partial T})_\mu = \frac{5}{2}\frac{f_p}{f_n} - x, \tag{2.7}$$

while the specific heat at constant volume (hence constant density, and T_F) becomes

$$\frac{C_V}{Nk_B} = \frac{c_v}{nk_B} = T(\frac{\partial S/Nk_B}{\partial T})_{V,N} = \frac{T}{T_F}(\frac{\partial S/Nk_B}{\partial T/T_F})_{V,N} = \frac{15}{4}\frac{f_p}{f_n} - \frac{9}{4}\frac{f_n}{f_n'}, \tag{2.8}$$

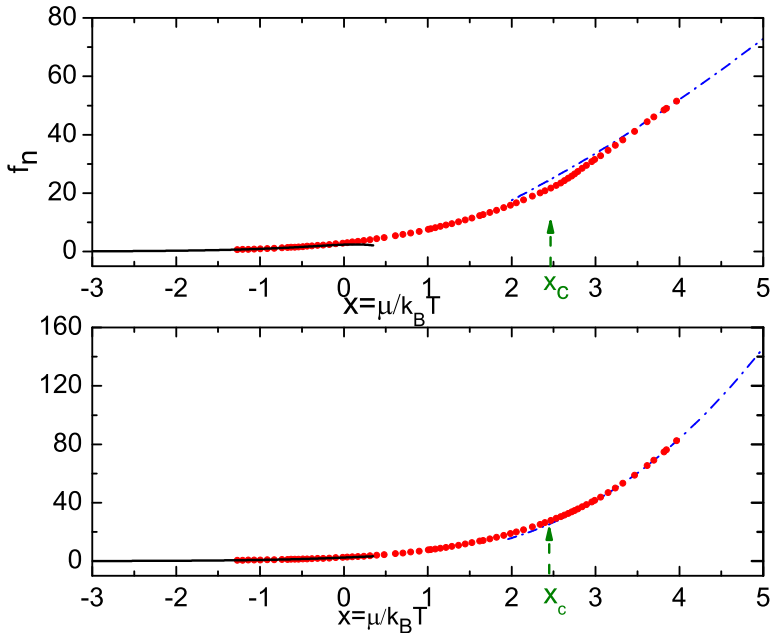

Figure 2.2: Universal scaling functions f_n and f_p as a function of the dimensionless variable μ/k_BT. See Fig. 2.1 for the notation.

and the specific heat at constant pressure becomes

$$\begin{aligned}\frac{C_P}{Nk_B} &= \frac{c_p}{nk_B} = T(\frac{\partial S/Nk_B}{\partial T})_{P,N} \\ &= T\frac{d\beta\lambda_T^3}{dT}P(\frac{\partial S/Nk_B}{\partial \beta\lambda_T^3 P})_{P,N} = \left(\frac{15}{4}\frac{f_p}{f_n} - \frac{9}{4}\frac{f_n}{f_n'}\right)\frac{5}{3}\frac{f_n' f_p}{f_n^2}\,,\end{aligned} \tag{2.9}$$

where $\beta = 1/k_BT$. According to thermodynamics the ratio between isobaric heat capacity C_P and isochoric heat capacity C_V coincides with the ratio between the isothermal (κ_T) and the adiabatic (κ_s) compressibility

$$\frac{C_P}{C_V} = \frac{\kappa_T}{\kappa_s} = \frac{5}{3}\frac{f_n' f_p}{f_n^2}, \tag{2.10}$$

with κ_T and κ_s given, respectively, by:

$$\kappa_T = \frac{1}{n}\left(\frac{\partial n}{\partial P}\right)_{T,N} = \frac{\lambda_T^3 f_n'}{k_B T f_n^2}, \tag{2.11}$$

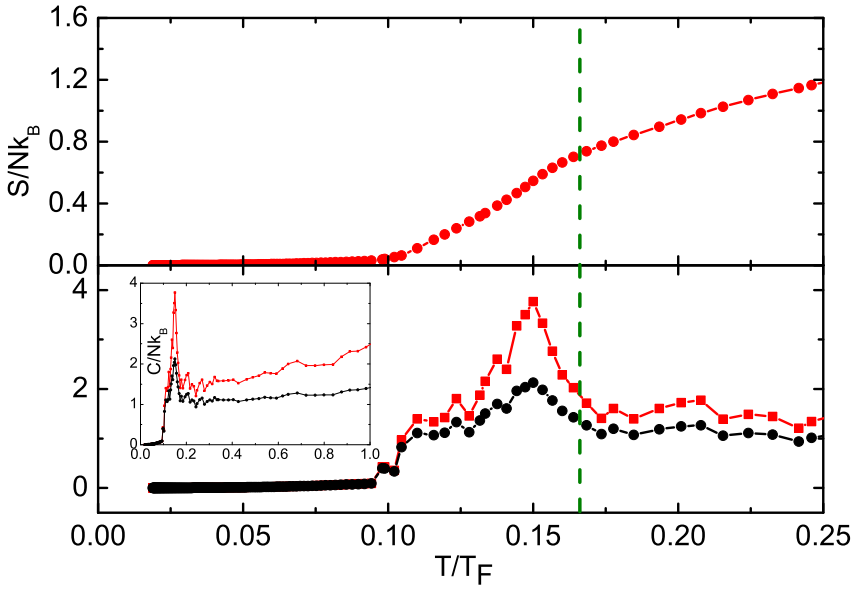

Figure 2.3: Entropy and specific heats per particle in uniform matter, evaluated using Eqs. (2.7)–(2.9). In the lower panel, the red square-guided line corresponds to C_p/Nk_B; the black full-circle-guided line to C_v/Nk_B. The vertical green line indicates the critical temperature.

$$\kappa_s = \frac{1}{n}\left(\frac{\partial n}{\partial P}\right)_{S,N} = \frac{3}{5}\frac{\lambda_T^3}{k_B T f_p}. \tag{2.12}$$

The entropy (s) and the specific heat (c_v, c_p) densities are introduced in Eqs. (2.7)–(2.9).

The scaling function $f_p(x)$ (and hence the various thermodynamic functions) can be determined through microscopic many-body calculations or extracted directly from experiments. In Figs. 2.1 and 2.2 we show, respectively, the equation of state μ/k_BT as a function of T/T_F and the universal functions $f_n(x)$ and $f_p(x)$ as a function of x, determined according to the procedures discussed in the following sections. In Fig. 2.3 we show the relevant thermodynamic functions S/Nk_B, C_V/Nk_B and C_P/Nk_B as a function of T/T_F. The normalized compressibilities κ_T/κ_0 and κ_s/κ_0 are provided in Fig. 2.4 as a function of T/T_F, where $\kappa_0 = \frac{3}{2}\frac{1}{n\epsilon_F}$ is

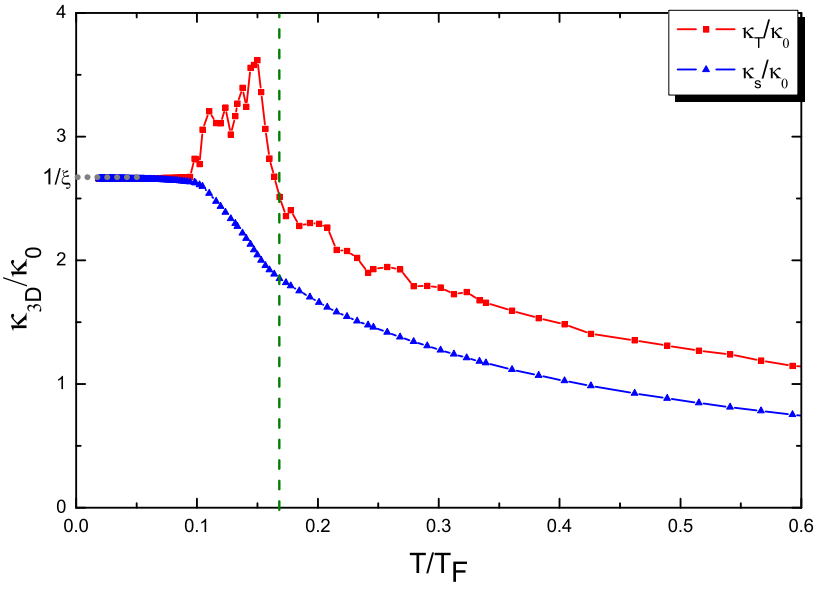

Figure 2.4: Isothermal and isentropic compressibilities in the uniform Fermi gas at unitarity, evaluated using Eqs. (2.11)–(2.12) normalized by the compressibility ($\kappa_0 = \frac{3}{2}\frac{1}{n\epsilon_F}$) of a noninteracting Fermi gas of the same local density at zero temperature. The grey dotted line indicates the zero temperature limit value. The vertical green line indicates the critical temperature.

the compressibility of a noninteracting Fermi gas at the same local density at zero temperature.

Different from the previous thermodynamic quantities, the superfluid density n_s instead requires the knowledge of another independent function. According to dimensional arguments, at unitarity, n_s can be written in terms of a universal function $f_s(x)$ as

$$n_s(T, x) = \frac{1}{\lambda_T^3} f_s(x). \tag{2.13}$$

Its behavior is known at low temperature, in the phonon regime (see Sec. 2.2) [77], and near the critical point where it is predicted to vanish as $n_s \propto (1 - T/T_c)^{2/3}$ [78]. Here T_c is the critical temperature for superfluidity which, at unitarity can be

written in the form,

$$T_c = \alpha_{t_c} T_F, \tag{2.14}$$

with α_{t_c} a dimensionless universal parameter.

2.2 Low temperature regime

At very low temperatures, corresponding to $T \ll T_c$, phonons provide the leading contribution to the thermodynamic behavior of uniform superfluids. In this regime one can easily calculate the relevant thermodynamic functions introduced in the previous section.

Starting from the expression [21],

$$F = E_0 - \frac{V\pi^2 (k_B T)^4}{90(\hbar c)^3}, \tag{2.15}$$

for the free energy associated with the phonon excitations in a uniform 3D superfluid, one can easily evaluate the other thermodynamic functions. In the above equation E_0 is the ground state energy, c is the $T = 0$ value of the sound velocity, while V is the volume occupied by the gas. For the unitary Fermi gas one can write $E_0 = \frac{3}{5} N \xi k_B T_F$ and $mc^2 = \frac{2}{3} \xi k_B T_F$. Here ξ is the so-called universal Bertsch parameter ([79], [24]), accounting for the interaction effects of the unitary Fermi gas. Starting from (2.15) one can calculate the low temperature expansion of the chemical potential $\mu = (\partial F/\partial N)_{T,V}$, pressure $P = -(\partial F/\partial V)_{T,N}$ and entropy $S = -(\partial F/\partial T)_{V,N}$. One finds:

$$\mu = k_B T_F \left[\xi + \frac{\pi^4}{240} \left(\frac{3}{\xi} \right)^{3/2} \left(\frac{T}{T_F} \right)^4 \right], \tag{2.16}$$

$$P = \frac{2}{5} n k_B T_F \left[\xi + \frac{\pi^4}{48} \left(\frac{3}{\xi} \right)^{3/2} \left(\frac{T}{T_F} \right)^4 \right], \tag{2.17}$$

and

$$\frac{S}{N k_B} = \left(\frac{3}{\xi} \right)^{3/2} \frac{\pi^4}{60} \left(\frac{T}{T_F} \right)^3. \tag{2.18}$$

Using Landau equation for the phonon contribution to the normal density one also finds the result (P66 in [21]),

$$\frac{n_n}{n} = \frac{3\sqrt{3}\pi^4}{40\xi^{5/2}} \left(\frac{T}{T_F}\right)^4. \tag{2.19}$$

Using the definition (2.3) together with (2.16)–(2.17) one can also calculate the large x expansion of f_p and hence of f_n. We find

$$f_p(x) = \frac{2}{5}\frac{(4\pi)^{3/2}}{3\pi^2}\left[\xi\left(\frac{x}{\xi}\right)^{5/2} + \frac{\pi^4}{96}\left(\frac{3}{x}\right)^{3/2}\right], \tag{2.20}$$

and

$$f_n(x) = \frac{(4\pi)^{3/2}}{3\pi^2}\left[\left(\frac{x}{\xi}\right)^{3/2} - \frac{\pi^4}{480}\left(\frac{3}{x}\right)^{5/2}\right]. \tag{2.21}$$

The first terms in the expansions determine the $T = 0$ value of the thermodynamic functions, while the second ones account for the first contribution due to the thermal excitation of phonons.

2.3 High temperature regime

Above the Fermi degenerate temperature, virial expansion gives a complete solution of strongly-correlated Fermi gas. Quantum virial expansion, also referred to as quantum cluster expansion, is practically useful for a dilute quantum gas. In general, thermodynamic properties such as the thermodynamic potential can be expanded in terms of the cluster expansion parameter, or fugacity $z = e^{\beta\mu}$, which is a small parameter at large T but increases with decreasing T. By further taking into account the thermodynamic identity $\Omega = -PV$, the expansion for the universal function f_p can be reformulated as:

$$f_p(x) = 2(b_1 e^x + b_2 e^{2x} + ...), \tag{2.22}$$

where b_j are the so-called virial coefficients and the factor '2' comes from spin degeneracy. The determination of the n-th virial coefficient b_n requires full solutions

up to the n-body problem. But Liu and co-workers find that it is sufficient to treat the two-body and the three-body problem ([57] with references therein), that is, the second and third terms in the virial expansion to describe the thermodynamic behaviors down to the Fermi temperature T_F.

The value $b_1 = 1$ is fixed by the classical equation of state, while theoretical calculations have provided the values $b_2 = \frac{3\sqrt{2}}{8}$ [80] and $b_3 = -0.29$ [81] for the second and third coefficients, respectively. These values are consistent with the measurement of the equation of state at high temperatures [28, 76, 55]. By taking the derivative of the pressure (2.22) with respect to x, we obtain, for the function $f_n(x)$, the expansion:

$$f_n(x) = 2(b_1 e^x + 2b_2 e^{2x} + ...). \tag{2.23}$$

2.4 Intermediate temperature regime

In this regime, through high-precision measurements of the local compressibility, density, and pressure, the MIT team measured the universal thermodynamic behavior of the unitary Fermi gas with high accuracy both below and above the critical temperature for superfluidity overcoming, in particular, the problem of the direct measurement of the temperature of the gas [55]. They have been able, in particular, to identify the superfluid phase transition at the temperature $T_c = \alpha_{t_c} T_F$ with $\alpha_{t_c} = 0.167(13)$, corresponding to the value $x_c = \mu_c / k_B T = 2.48$. Also the relevant Bertsch parameter ξ, giving the ground state energy in units of the ideal Fermi gas value, was determined with high accuracy ($\xi = 0.376(4)$). These values are in good agreement with the best theoretical predictions based on accurate many-body calculations ([61, 62, 65, 68]). Concerning the critical temperature it is worth stressing that in [55] its value was identified by exploring the peaked structure exhibited by the specific heat at constant volume near the transition (see Fig. 2.3), by taking explicitly into account finite resolution effects. This yields a value of T_c slightly higher than the value where the measured specific heat exhibits the peak. Figure 2.3 shows that the peak exhibited by the specific heat at constant pressure is even more pronounced, in agreement with the general behavior of the specific heats near a second order phase transition [82]. The difference lies also in the compressibil-

ity. Figure 2.4 reveals that the isothermal compressibility is peaked close to the transition point while the isentropic compressibility looks continuously smooth.

The matching between the values extracted using the MIT data and the predictions provided by phonon thermodynamics discussed above is reasonably good. At high temperatures these experiments also confirm with high accuracy the validity of the virial expansion (see Figs. 2.1 and 2.2) so that, for the goals of the thesis, the equation of state of the unitary Fermi gas can be considered known with reasonably good accuracy at all temperatures. We will adopt the MIT equation of state, together with the low and high temperature behavior discussed above, to implement the calculation of the frequency of the collective oscillations and of the sound velocities within the hydrodynamic formalism in the thesis.

2.5 1D thermodynamic functions

Starting from the above 3D thermodynamic quantities one can calculate the relevant 1D quantities entering the hydrodynamic equations (4.4)–(4.7), whose solution is the main goal of the thesis. In the presence of radial harmonic trapping the chemical potential varies along the radial direction according to the law $\mu(r_\perp) = \mu_1 - (1/2)m\omega_\perp^2 r_\perp^2$ (μ_1 is the chemical potential on the symmetry axis, $r_\perp^2 = x^2 + y^2$, and $\omega_\perp = \sqrt{\omega_x \omega_y}$ characterizes the geometric average of the trapping frequency in the radial direction), predicted by the the local density approximation, so that one can easily reduce the radial integrals to integrals in the variable x [37]. By carrying out the radial integrals of the 3D quantities (2.3, 2.4, and 2.7), one finds the following results for the 1D pressure, density, entropy:

$$P_1(x_1, T) = \int dr_\perp 2\pi r_\perp P = \frac{2\pi}{m\omega_\perp^2} \frac{(k_B T)^2}{\lambda_T^3} f_q(x_1), \tag{2.24}$$

$$n_1(x_1, T) = \int dr_\perp 2\pi r_\perp n = \frac{2\pi}{m\omega_\perp^2} \frac{k_B T}{\lambda_T^3} f_p(x_1)\ , \tag{2.25}$$

$$\frac{s_1(x_1, T)}{k_B} = \int dr_\perp 2\pi r_\perp s = \frac{2\pi}{m\omega_\perp^2} \frac{k_B T}{\lambda_T^3} \left[\frac{7}{2} f_q(x_1) - x_1 f_p(x_1) \right], \tag{2.26}$$

where $x_1 = \mu_1/k_BT$ is the value of the chemical potential, in units of k_BT, calculated on the symmetry axis of the trap. The 1D heat capacity per particle can be derived from the 1D entropy per particle $\bar{s}_1 = s_1/n_1$. One finds:

$$\frac{\bar{c}_{v1}(x_1)}{k_B} = T\left(\frac{\bar{s}_1/k_B}{\partial T}\right)_{n_1} = \frac{35}{4}\frac{f_q(x_1)}{f_p(x_1)} - \frac{25}{4}\frac{f_p(x_1)}{f_n(x_1)}. \tag{2.27}$$

Note that $\bar{c}_{v1}$ doesn't coincide with the radial integral of the bulk specific heat per particle (2.8) as one would expect. For the specific heat at constant pressure, one instead finds the result,

$$\frac{\bar{c}_{p1}(x_1)}{k_B} = T\left(\frac{\partial\bar{s}_1/k_B}{\partial T}\right)_{P_1} = \bar{c}_{v1}(x_1)\frac{7}{5}\frac{f_q(x_1)f_n(x_1)}{f_p^2(x_1)}. \tag{2.28}$$

Since $\bar{s}_1$ depends only on the variable x_1 one finds that the adiabatic derivative of the 1D pressure (2.24) with respect to the 1D density takes the form

$$\left(\frac{\partial P_1}{\partial n_1}\right)_{\bar{s}_1} = \frac{7}{5}\frac{P_1}{n_1}, \tag{2.29}$$

differently from the uniform case where one has, at unitarity, $(\partial P/\partial n)_{\bar{s}} = (5/3)P/n$ with $\bar{s} = S/N$ [37]. From the comparison between Eq. (2.3) and Eq. (2.25) one also finds the relationship

$$n_1 = \frac{2\pi}{m\omega_\perp^2}P(\mathbf{r}_\perp = 0), \tag{2.30}$$

between the 1D density and the pressure calculated at $\mathbf{r}_\perp \equiv x\hat{i} + y\hat{j} = 0$. This relationship holds in the local density approximation for a general fluid radially confined with harmonic trapping [83]. It actually follows directly from the radial integration of the general thermodynamic equation $n = (\partial P/\partial\mu)_T$.

Analogously, in the 1D thermodynamics, we have that the ratio between isobaric heat capacity $\bar{c}_{p1}$ and isochoric heat capacity $\bar{c}_{v1}$ coincides with the ratio between the 1D isothermal (κ_{T1}) and the adiabatic ($\kappa_{\bar{s}_1}$) compressibilities,

$$\frac{\bar{c}_{p1}}{\bar{c}_{v1}} = \frac{\kappa_{T1}}{\kappa_{\bar{s}_1}} = \frac{7}{5}\frac{f_q(x_1)f_n(x_1)}{f_p^2(x_1)}, \tag{2.31}$$

with κ_{T1} and $\kappa_{\bar{s}_1}$ given, respectively, by:

$$\kappa_{T1} = \frac{1}{n_1}\left(\frac{\partial n_1}{\partial P_1}\right)_T = \frac{f_n(x_1)}{\frac{2\pi}{m\omega_\perp^2}\frac{(k_BT)^2}{\lambda_T^3}f_p^2(x_1)}, \tag{2.32}$$

$$\kappa_{\bar{s}_1} = \frac{1}{n_1}\left(\frac{\partial n_1}{\partial P_1}\right)_{\bar{s}_1} = \frac{1}{\frac{7}{5}\frac{2\pi}{m\omega_\perp^2}\frac{(k_BT)^2}{\lambda_T^3} f_q(x_1)}. \tag{2.33}$$

As concerns the 1D superfluid density, starting from Eq. (2.13) we find the expression

$$n_{s1}(x_1, T) = \int dr_\perp 2\pi r_\perp n_s = \frac{2\pi}{m\omega_\perp^2}\frac{k_BT}{\lambda_T^3} f_{s1}(x_1), \tag{2.34}$$

with

$$f_{s1}(x_1) = \int_{-\infty}^{x_1} dx f_s(x). \tag{2.35}$$

An interesting comparison between the 3D and 1D thermodynamic quantities concerns the explicit low T behavior as a consequence of the expansions (2.20–2.21). The 1D entropy (2.26), as well as the 1D specific heats (2.27–2.28) and the 1D normal density $n_{n1} = n_1 - n_{s1}$ (2.34) exhibit a different T dependence as compared to the corresponding bulk quantities (2.18–2.19). In particular they behave like $T^{5/2}$ as $T \to 0$, as can be shown by exploiting the leading behavior at large x. For example the 1D entropy behaves as

$$\frac{s_1(T)}{k_B} = \frac{2\pi(k_BT)^{5/2}}{m\omega_\perp^2}\left(\frac{m}{2\pi\hbar^2}\right)^{3/2}\gamma, \tag{2.36}$$

with $\gamma = \int_{-\infty}^{+\infty} dx' \left[\frac{5}{2} f_p(x') - x' f_n(x')\right]$, the integral being convergent since $(5/2)f_p(x) - x f_n(x)$ decays like $x^{-3/2}$ for large x [84]. Analogously the 1D pressure and the 1D normal density at low temperature behave as

$$P_1(n_1, T) = \frac{2}{7}\xi^{3/5} n_1 k_B T_F^{1D}(n_1) + \frac{4\pi(k_BT)^{7/2}}{7m\omega_\perp^2}\left(\frac{m}{2\pi\hbar^2}\right)^{3/2}\gamma, \tag{2.37}$$

and

$$n_{n1}(T) = \frac{2\pi(k_BT)^{5/2}}{m\omega_\perp^2}\left(\frac{m}{2\pi\hbar^2}\right)^{3/2}\int_{-\infty}^{+\infty} dx \nu_n(x), \tag{2.38}$$

with the quantity $\nu_n(x)$ vanishing as $\frac{\pi^{7/2}}{45}\left(\frac{3}{x}\right)^{5/2}$ at large x, in the phonon regime. The above equations reveal that in order to determine the coefficient of the $T^{5/2}$ law the knowledge of the functions f_n, f_p and f_q are needed for all values of x. This

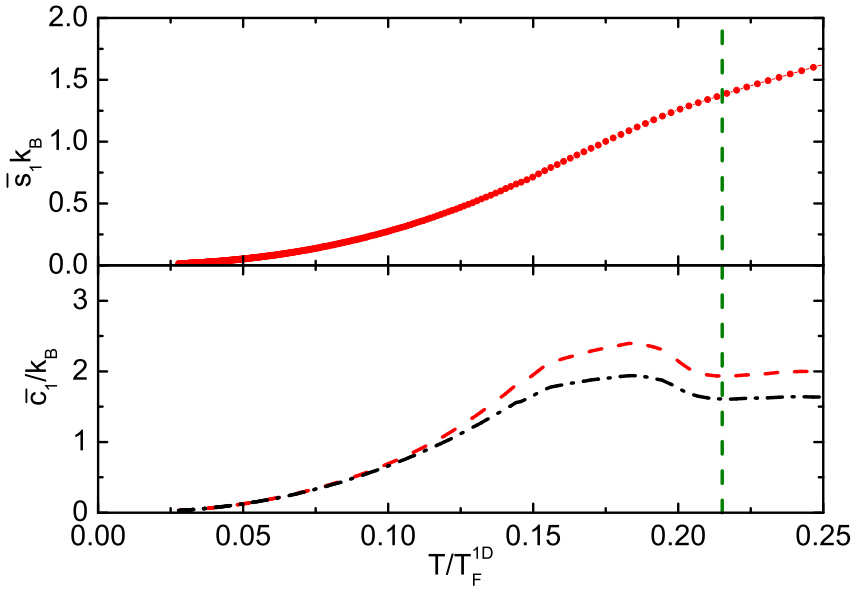

Figure 2.5: The 1D entropy $\bar{s}_1/k_B$ and specific heat $\bar{c}_1/k_B$ evaluated using Eqs. (2.26)–(2.28). In the lower panel, the red dashed line corresponds to $\bar{c}_{p1}/k_B$; the black dash-dotted line to $\bar{c}_{v1}/k_B$. The vertical green line indicates the critical temperature.

is physically due to the fact that in the radial integration the whole range of ratio T/T_F (and not only the large x phonon region) enters the calculation.

It is finally interesting to calculate the low temperature expansion of the 1D chemical potential. Equation (2.30) relates the 1D density to the pressure of the gas calculated on the symmetry axis so that the equation of state $\mu_1(n_1, T)$ corresponds to the equation of state of uniform matter as a function of P and T. We can consequently employ Eqs. (2.16)–(2.17) to derive the low T expansion

$$\mu_1(n_1, T) = k_B T_F^{1D} \left[\xi^{3/5} - \frac{\sqrt{3}\pi^4}{80\xi^{3/10}} \left(\frac{T}{T_F^{1D}}\right)^4 \right]. \tag{2.39}$$

It is worth pointing out that, differently from the case of Eqs. (2.36)–(2.37), the first contribution due to thermal effects to μ_1 is determined by the phonon contribution and exhibits the typical T^4 dependence. It is also interesting to notice the opposite

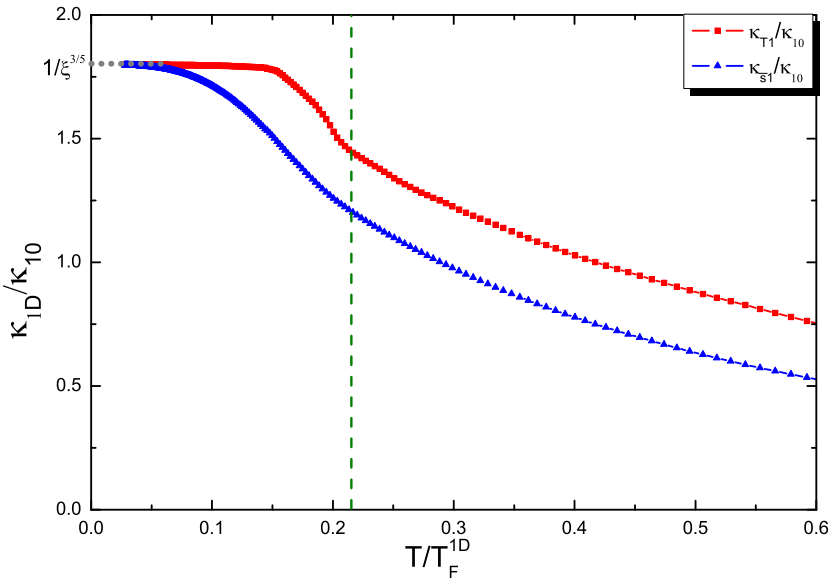

Figure 2.6: The 1D isothermal and isentropic compressibilities evaluated using Eqs. (2.32)–(2.33) normalized by the compressibility ($\kappa_{01} = \frac{5}{2}\frac{1}{n_1\epsilon_F^{1D}}$) of a noninteracting Fermi gas of the same local density at $T = 0$. The grey dotted line indicates the zero temperature limit value. The vertical green line indicates the critical temperature.

sign exhibited by the thermal correction with respect to the bulk Eq. (2.16) which implies that these 1D-like configurations will exhibit a different thermo-mechanical effect as compared to uniform gases [85].

In Figs. 2.5 and 2.6 we show the relevant 1D thermodynamic functions calculated as a function of the ratio

$$\frac{T}{T_F^{1D}} = \left(\frac{16}{15\sqrt{\pi}f_p(x_1)}\right)^{2/5}, \tag{2.40}$$

where,

$$T_F^{1D} = \frac{1}{k_B}\left(\frac{15\pi}{8}\right)^{2/5}(\hbar\omega_\perp)^{4/5}\left(\frac{\hbar^2 n_1^2}{2m}\right)^{1/5}, \tag{2.41}$$

is the natural definition for the Fermi temperature in 1D cylindrical configurations [37]. T_F^{1D} coincides with the usual 3D definition (2.2) of the Fermi temperature if n_1

is calculated for an ideal Fermi gas at zero temperature. If one instead calculates n_1 in the unitary Fermi gas at zero temperature one finds the relationship $T_F^{1D} = \xi^{2/5} T_F$ where ξ is the so-called Bertsch parameter. Figures 2.5 and 2.6 show that the matching between the values extracted using the MIT data and the predictions provided by phonon thermodynamics at low T and virial expansions at high T are remarkably good as concerns the 1D thermodynamic quantities.

From the knowledge of the 1D thermodynamic functions one can also easily calculate the equilibrium properties in the presence of axial harmonic trapping, using the local density approximation $\mu_1(z) = \mu_0 - V_{ext}(z)$ for the chemical potential along the z-th direction, with μ_0 being the chemical potential in the center of the trap and fixed by the normalization condition $\int dz n_1(z) = N$. For example, the 1D density profile is available from Eq. (2.25) by replacing x_1 with $[\mu_0 - (1/2)m\omega_z^2 z^2]/k_B T$. It is then natural to express the value of $x_0 = \mu_0/k_B T$ in terms of the Fermi temperature $T_F^{trap} = (3N)^{1/3}\hbar\bar{\omega}_{ho}/k_B$ of the 3D trapped Fermi gas, where $\bar{\omega}_{ho}$ is the geometrical average of the three oscillator frequencies and N is the total number of atoms. One finds

$$T/T_F^{trap} = \left(\frac{6}{\sqrt{\pi}} \int_{-\infty}^{x_0} dx (x_0 - x)^{1/2} f_n(x) \right)^{-1/3}. \tag{2.42}$$

This temperature scale will be used to discuss the temperature dependence of the discretized frequencies of the elementary excitations in the presence of $3D$ harmonic confinement.

Chapter 3

Two-fluid hydrodynamic theory

This chapter is devoted to reviewing the two-fluid hydrodynamic theory, describing the dynamics of a superfluid at a macroscopic level. Two-fluid hydrodynamics were first developed by Landau in order to describe relevant phenomena of superfluidity in ^{4}He. Nevertheless, the two-fluid hydrodynamic equations, formulated on the basis of fundamental conservation laws, are general and apply to all superfluids despite the different quantum statistics. The differences in the hydrodynamic behavior of different systems are manifested when the specific equation of state, which enters the Landau equations, is taken into account. In Sec. 3.1, we will briefly review Landau's two-fluid hydrodynamic theory developed for ^{4}He and discuss its applications in predicting the dynamic behavior of superfluid helium in Sec. 3.2. Then, we review its applications to ultracold gases, in particular, to the case of weakly interacting Bose gases (Sec. 3.3) and to the case of strongly interacting Fermi gases (Sec. 3.4).

3.1 Landau theory: uniform 3D superfluid

The superfluidity of liquid ^{4}He, below the so-called λ-point, was discovered by Kapitza [1] and, independently, by Allen and Misener [2]. It was soon explained by Landau [5] who showed that, if the spectrum of elementary excitations satisfies suitable criteria, the motion of the fluid cannot give rise to dissipation. In this novel superfluid state several unique properties emerge. The superfluid flow is frictionless (with zero viscosity), carries no entropy and furthermore, is irrotational, in

contrast to the normal fluid, which carries entropy and can have nonzero viscosity and be rotational. Based on these facts, Landau wrote down the famous two-fluid hydrodynamic equations [5, 86]. The classical description of Landau's two-fluid hydrodynamics in superfluid ^{4}He is given in the book by Khalatnikov [86], where dissipation effects are also taken into account. For the goals of our thesis, we will simply present the equations instead of going through detailed derivations:

$$m\partial_t n + \nabla \cdot \mathbf{j} = 0, \tag{3.1}$$

$$\partial_t s + \nabla \cdot (s\mathbf{v_n}) = \nabla \cdot (\frac{\kappa \nabla T}{T}), \tag{3.2}$$

$$m\partial_t \mathbf{v_s} = -\nabla(\mu + V_{ext}), \tag{3.3}$$

$$\partial_t j_i + \partial_i P + n\partial_i V_{ext} = \partial_k(\eta \Gamma_{ik}). \tag{3.4}$$

In the above equations, $\mathbf{j} = m(n_s\mathbf{v}_s + n_n\mathbf{v}_n)$ is the current density, n_s and n_n are the superfluid and normal number densities for a fluid with total particle density $n = n_s + n_n$, $\mathbf{v}_s$ and $\mathbf{v}_n$ are the corresponding velocity fields. The continuity equation in Eq. (3.1) expresses mass conservation and is always valid. The quantity s is the entropy density and κ is the thermal conductivity[1]. Eq. (3.2) assumes that the entropy of the fluid is carried by the normal fluid and a dissipative term, fixed by the thermal conductivity κ, is added to the right-hand side, expressing the increase of entropy in irreversible processes. The quantity μ is the local chemical potential and determined by the uniform equation of state. V_{ext} is the external trapping potential which will be often assumed of harmonic form. Eq. (3.3) implies that the superfluid velocity field is irrotational. P is the local pressure and $\eta\Gamma_{ik} = \eta(\partial_k v_{ni} + \partial_i v_{nk} - 2\delta_{ik}\partial_j v_{nj}/3)$ is the correction to the momentum flux density tensor (or stress tensor) arising from the shear viscosity η. We should emphasize that the inclusion of damping, while giving only higher order corrections in the long wavelength limit in the uniform geometry, can play a crucial role in the presence of

[1]In this thesis we use the notation κ to indicate the thermal conductivity, while κ_T to indicate the isothermal compressibility.

trapping [37], as shown in chapter 4. We have dropped bulk viscosity terms, which give smaller contributions, and omitted terms quadratic in the velocity since we are interested in the linearized solutions around equilibrium.

The Landau two-fluid equations (3.1)–(3.4) are valid in the hydrodynamic regime, where the system can be viewed as in local thermal and mechanical equilibrium, such that well-defined local quantities (n, T, P, s, μ, $\mathbf{v}_n$, $\mathbf{v}_s$...) are allowed and only sufficiently smooth and slow perturbations need to be considered. In general, there are two types of hydrodynamic regimes: the irrotational superfluid hydrodynamic regime that describes the superfluid motion at zero temperature and the collisional hydrodynamic regime that requires fast collisions to drive the system into a state of local equilibrium, characterized by $\omega\tau \ll 1$, where ω is a typical frequency of a collective mode and τ is a mean-collision time. The time τ describes the typical time needed to reach local equilibrium. The two-fluid hydrodynamic equations, at $T = 0$, reduce to the irrotational superfluid hydrodynamic equations and in the dissipationless regime ($\eta = \kappa = 0$) above T_c, to the standard collisional hydrodynamics equations.

3.2 Sound propagation in superfluid ^{4}He

For a uniform liquid, in the dissipationless limit ($\kappa = \eta = 0$), the two-fluid equations (3.1)–(3.4) can be simplified to the standard Landau equations for the uniform sound velocities by assuming a plane wave $e^{i(qz-\omega t)}$ propagating, for example, in the z-direction in the liquid, with $\omega = cq$ [86, 87, 21]. The equation of the sound velocities c takes the form:

$$c^4 - c^2\left[\frac{1}{m}\left(\frac{\partial P}{\partial n}\right)_{\bar{s}} + \frac{1}{m}\frac{n_s T\bar{s}^2}{n_n\bar{c}_v}\right] + \frac{1}{m^2}\frac{n_s T\bar{s}^2}{n_n\bar{c}_v}\left(\frac{\partial P}{\partial n}\right)_T = 0. \tag{3.5}$$

In helium, the temperature expansion coefficient ($\alpha_{3D} = -\frac{1}{n}(\frac{\partial n}{\partial T})_P$) is small and the temperature and pressure fluctuations are essentially uncoupled. Therefore, the isothermal and adiabatic compressibilities are nearly the same, as indicated by the identity (see Sec. 16 of Landau and Lifshitz [82]):

$$\left(\frac{\partial P}{\partial n}\right)_{\bar{s}} = \left(\frac{\partial P}{\partial n}\right)_T + \frac{T}{\bar{c}_v}\frac{1}{n^2}\left(\frac{\partial P}{\partial T}\right)_n^2 = \left(\frac{\partial P}{\partial n}\right)_T + \frac{T}{\bar{c}_v}\alpha_{3D}^2\left(\frac{\partial P}{\partial n}\right)_T^2. \tag{3.6}$$

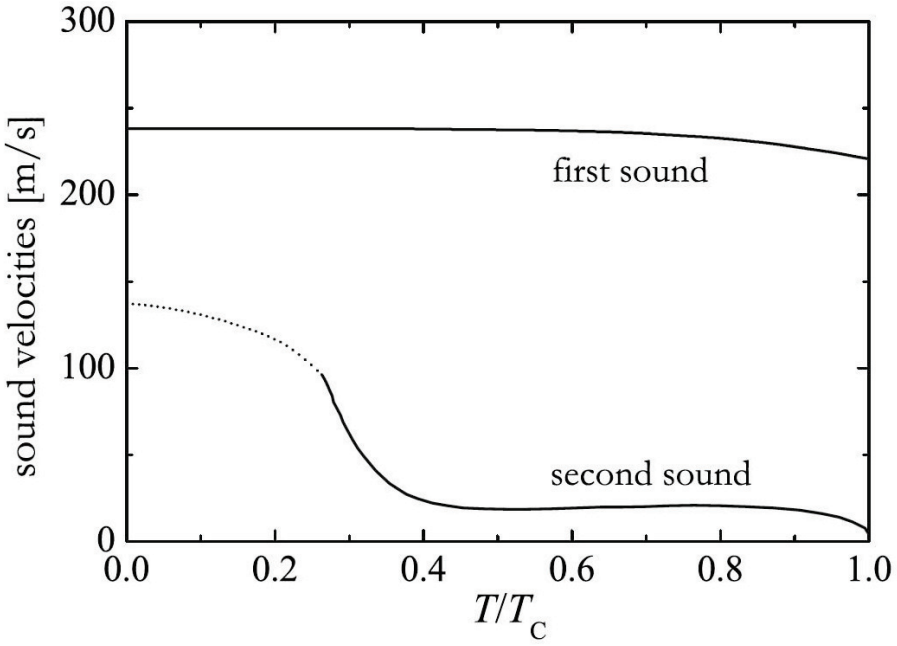

Figure 3.1: Experimental values of first and second sound speeds in superfluid ^{4}He. From Ref. [60].

Equation (3.5) has two non-negative solutions, hence two velocities of sound. One of them is related in the usual way to the compressibility,

$$mc_1^2 = \left(\frac{\partial P}{\partial n}\right)_{\bar{s}}, \tag{3.7}$$

and the other one is the so-called second sound,

$$mc_2^2 = T\frac{\bar{s}^2}{\bar{c}}\frac{n_s}{n_n}, \tag{3.8}$$

where the specific heat $\bar{c}$ can be evaluated equally at either constant volume or pressure, i.e., $\bar{c} \equiv \bar{c}_p \simeq \bar{c}_v$.

The superfluid and normal components move with opposite phase in second sound [5]. In superfluid helium, second sound reduces to a temperature wave, leaving the total density practically unaffected. Differently from first sound, the superfluid density n_s plays a crucial role in the propagation of second sound. The measurement of the second sound velocity in superfluid ^{4}He has actually provided the most

accurate determination of n_s as a function of temperature [6, 7]. The temperature dependence of the two sound velocities are presented in Fig. 3.1. At the λ point, the superfluid density vanishes and the velocity c_2 also goes to zero. At $T \to 0$, the second sound velocity instead tends to the limit $1/\sqrt{3}\ c_1$ [21].

3.3 Sound propagation in weakly interacting Bose gases

Two-fluid hydrodynamic modes have been extensively studied in superfluid helium, providing a deeper understanding of the macroscopic properties of helium. One key question concerning ultracold gases is whether the hydrodynamic conditions that validate the Landau two-fluid description can be achieved. It is crucial to make the interactions or the density large enough to satisfy the local equilibrium criterion.

Two-fluid hydrodynamics in the context of uniform ultracold Bose gases have been discussed in [20, 21, 22]. It is found that in dilute Bose gas, second sound behaves quite differently from the case of strongly interacting superfluids, like ^{4}He. The motion of the condensate and that of the excitations are essentially uncoupled as a result of the weak interactions between the condensate and the thermal cloud. Second sound in dilute Bose gases actually reduces to the oscillation of the condensate in agreement with Tisza's original idea, except at very low temperature in the phonon regime [21] and disappears above T_c; first sound, instead, mainly involves the thermal cloud and reduces to the usual hydrodynamic sound above T_c [88, 89]. A schematic representation of the velocity of first and second sound in a dilute Bose gas as a function of temperature is shown in Fig. 3.2.

In non uniform media sound waves can propagate if the wavelength is smaller than size of the condensate. The propagation of sound in a magnetically trapped dilute Bose-Einstein condensate near zero temperature was first reported by MIT group [26] and shows quite satisfying agreement with Bogiubov theory [29]. Attempts to excite the relative motion between the condensate and the thermal components of a harmonically trapped Bose gas were first carried out in [32] and more recently in [33] where the use of denser samples permitted to explore collisional damping effects. The propagation of second sound waves in dilute Bose gases was

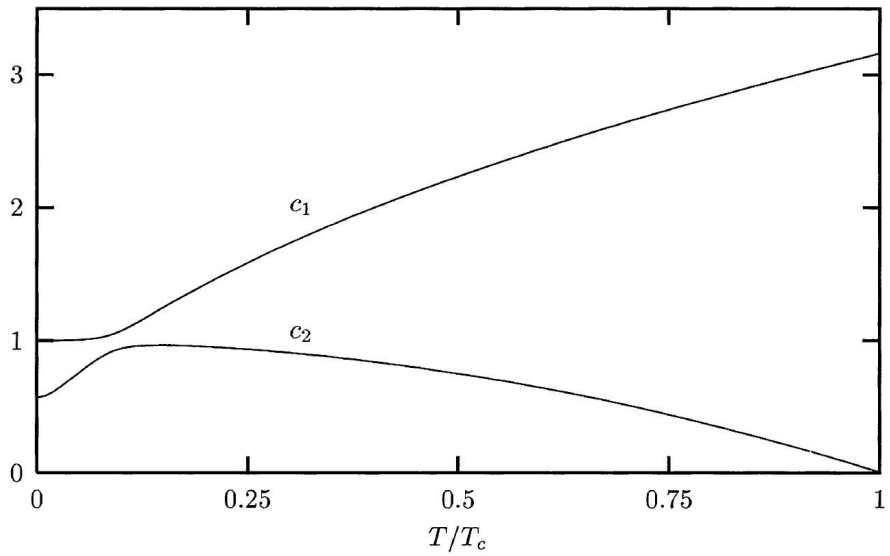

Figure 3.2: Velocities of first and second sound in a dilute Bose gas as a function of temperature. The figure points out the effect of hybridization between the two modes taking place at low temperature. Above T_c only first sound survives. From Ref. [21].

recently measured in [34].

3.4 Sound propagation in unitary Fermi gases

Unitary Fermi gases are characterized by strong interaction effects. In such systems, the normal component behaves in a deeply hydrodynamic way over a wide range of temperatures, as manifested in recent experiments [50, 51, 52, 53, 54], and the spatial overlap between the normal and the superfluid components can be very large also in the presence of harmonic trapping. This provides a new system where we can look for first and second sound hydrodynamic oscillations. In this situation, Landau's two-fluid theory can be readily applied.

The propagation of first sound waves near zero temperature across the BEC-BCS crossover in very elongated traps was recently measured [27], in good agreement with

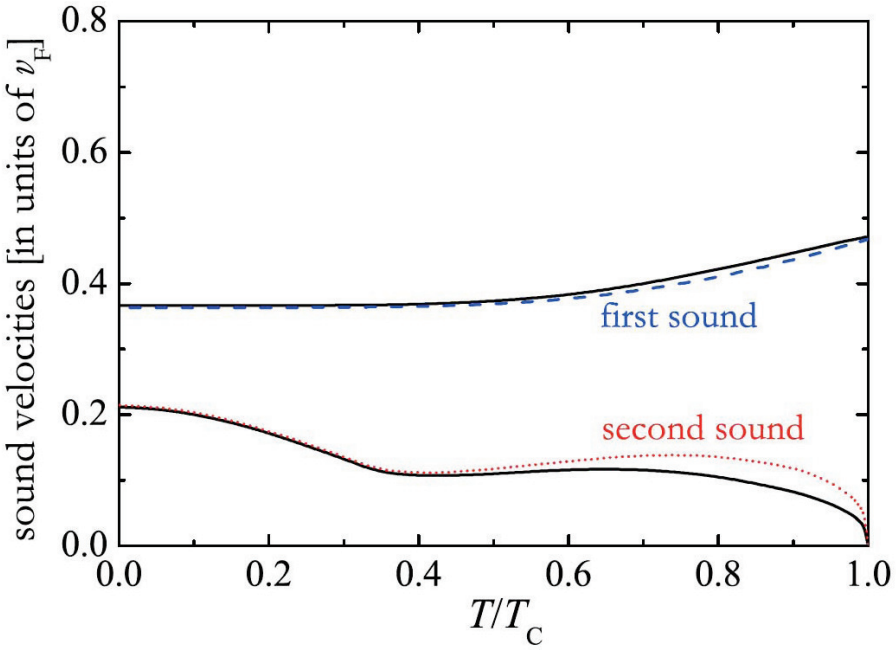

Figure 3.3: Two-fluid sound speeds in a uniform superfluid gas of ultracold Fermi atoms at unitarity. From Ref. [60].

the hydrodynamic prediction [30] at unitarity. The search for second sound in the unitary Fermi gas has been already the object of numerous theoretical investigations [58, 60, 90, 91, 92] in uniform geometries (see Fig. 3.3) and, more recently, in cylindrical configurations [37]. However, one major problem is that the thermodynamic functions which enter the hydrodynamic equations are quite complicated and difficult to derive, so that accurate predictions for the dynamic behaviors represent a challenging task for theorists. Nevertheless, these theoretical works have suggested that second sound in strongly interacting Fermi gases is rather similar to that in superfluid ^{4}He, namely, the two components are out of phase in an almost pure temperature oscillation. In the next chapter, we will discuss explicitly the sound propagations in the experimentally favorable elongated harmonic traps and draw some final conclusions about second sound in strongly interacting fluids.

Chapter 4

From 3D to 1D

In this chapter we will concentrate on the unitary Fermi gas in highly elongated harmonic traps. These configurations are well suited for the experimental excitation and detection of sound waves [26, 27, 28, 36]. It turns out that there are important differences with respect to the case of homogeneous systems, depending on geometry and dissipative effects [37, 53, 93, 36]. We start by reviewing the quasi-1D hydrodynamic theory [94] and, in particular, its conditions of validity [37, 95]. Then we discuss the sound propagations in a strongly interacting Fermi gas in the cylindrical geometry. This problem was first investigated by G. Bertaina et al [37] by numerically solving the two-fluid hydrodynamic equations. We will revisit the problem by employing more accurate thermodynamic ingredients, now available experimentally. Furthermore, by grasping the essential features of the two sound propagations, we will derive an analytic expression to describe the second sound velocity, which permits to extract the superfluid fraction from the knowledge of the second sound velocity. This is actually the procedure employed in the experiment of Ref. [36] based on the measurement of the second sound velocity. Finally, we will discuss the behavior of the superfluid fraction in superfluid Fermi gases.

4.1 Quasi-1D hydrodynamics

We consider atomic gases confined by a harmonic potential of the form

$$V_{ext} = \frac{1}{2}m\omega_\perp^2 r_\perp^2 + \frac{1}{2}m\omega_z^2 z^2, \tag{4.1}$$

and we will assume highly elongated configurations with trapping frequency satisfying the condition $\omega_z \ll \omega_\perp$, while m is the atomic mass. Our aim in this chapter is to investigate the propagation of sound in the cylindrical geometry ($\omega_z = 0$). The discretized solutions with frequency of order ω_z will be discussed in chapter 5. To derive simplified 1D hydrodynamic equations we start from the usual two-fluid Landau hydrodynamic equations defined in 3D [86]. We will consider the usual hydrodynamic regime $l \ll \lambda$ with the geometrical condition of tight radial confinement $R_\perp \ll \lambda$, where $R_\perp$ is the radial size of the sample, l is the mean free path and λ is the wavelength of the sound wave. We will assume the Thomas Fermi regime along the radial direction. Furthermore, we require that the viscous penetration depth δ satisfies the condition, $\delta = \sqrt{\eta/mn_n\omega} \gg R_\perp$, where η is the shear viscosity coefficient, n_n is the normal density and ω is the frequency of the sound wave. The penetration depth is the typical distance from a surface at which an oscillation becomes attenuated due to shear viscosity [87]. In the case of a uniform fluid confined by the hard walls of a tube, the condition $\delta \gg R_\perp$, imposes the uniformity of the normal velocity field as a function of the radial coordinate. Since friction between the normal part of the fluid and the walls further requires that the normal velocity be zero on the walls, the normal part cannot move at all along the tube. This interesting mode is known as 4th sound where it involves only the motion of the superfluid [96]. In the presence of harmonic trapping the condition $\delta \gg R_\perp$ of large viscous penetration depth is equivalent to requiring the low frequency condition $\omega \ll \omega_\perp^2\tau$, where τ is a typical collisional time to characterize the effects of viscosity. This can be obtained by estimating, as usual, $\eta \approx \tau\bar{v}^2 mn$, where $\bar{v}$ is the average velocity of the particles, of the order of the Fermi velocity $\sim v_F$. In the case of a harmonically trapped gas the effect of viscosity exhibits new features. In fact, the uniformity of the velocity field does not stop the motion of the normal component, as shown later on.

In the presence of axial trapping, we are interested in the low energy solutions of the order of ω_z for the hydrodynamic equations satisfying the condition $\omega \ll \omega_\perp$.

As a consequence of the tight radial confinement, Eq. (3.4) for the current implies the important condition

$$\nabla_\perp P + \nabla_\perp V_{ext} = 0 \tag{4.2}$$

of mechanical equilibrium along the radial direction. Violation of this condition would in fact result in frequencies of the order of $\omega_\perp$ rather than ω_z. Due to the same reason, the superfluid velocity is uniform in the radial direction as indicated by Eq. (3.3). The tight radial confinement also implies that the radial component of the velocity field must be much smaller than the longitudinal one. Excluding the superfluid velocity from Eqs. (3.3) and (3.4) and using the Gibbs-Duhem identity $dP = sdT + nd\mu$ one can write the equation for the relevant z component of the velocity field of the normal component in the form,

$$mn_n\partial_t v_n^z + n_n\partial_z(\delta\mu) + s\partial_z(\delta T) = \nabla\cdot(\eta\nabla v_n^z), \tag{4.3}$$

where terms containing the small radial components of the velocity field are ignored.

The presence of viscosity in Eq. (4.3) results in the independence of v_n^z on the radial coordinate $r_\perp$. In fact violation of such a behavior would be incompatible with the low frequency condition $\omega \ll \omega_\perp^2\tau$. As already anticipated, it is worth noticing that, differently from the case of the tube with hard walls, for harmonic trapping the normal component can move. Here we assume that the collisional times responsible for viscosity and thermal conductivity are comparable so, analogously, the presence of thermal conductivity in Eq. (3.2) for the entropy results in the independence of the temperature fluctuations on the radial coordinate in the same low frequency limit. This in turns implies that also the fluctuations of the chemical potential will be independent of the radial coordinate. This follows from the radial mechanical equilibrium condition and the use of the thermodynamic identity $dP = sdT + nd\mu$, namely, $0 = \nabla_\perp P + n\nabla_\perp V_{ext} = s\nabla_\perp T + n\nabla_\perp(\mu_0 + \delta\mu)$. Thus in the low frequency limit both the fluctuations δT and $\delta\mu$ are independent of the radial coordinates. In a word, due to the crucial roles played by the shear viscosity and by the thermal conductivity in the case of tight radial confinement, the velocity fields are independent of the radial position and a thermal equilibrium in the radial direction is achieved. This is the reason why we call this regime a 1D regime,

despite the fact that the system satisfies the radial Thomas Fermi conditions and is consequently 3D from a local point of view.

By radial integration of the 3D hydrodynamic equations, and following the procedure described in [37, 95], one obtains the following 1D hydrodynamic equations:

$$m\partial_t n_1 + \partial_z j_z = 0, \tag{4.4}$$

$$\partial_t s_1 + \partial_z (s_1 v_n^z) = 0, \tag{4.5}$$

$$m\partial_t v_s^z = -\partial_z(\mu_1(z) + V_{ext}(z)), \tag{4.6}$$

$$\partial_t j_z = -\partial_z P_1 - n_1 \partial_z V_{ext}(z), \tag{4.7}$$

where the terms n_1, s_1, P_1 are the radial integrals of their 3D counterparts, namely the particle density, the entropy density and the local pressure, the integration accounting for the inhomogeneity caused by the radial component of the trapping potential (4.1). In the above equations $j_z = m(n_{n1}v_n^z + n_{s1}v_s^z)$ is the current density, n_{s1} and n_{n1} are the superfluid and normal number densities respectively with $n_1 = n_{s1} + n_{n1}$ while v_s^z and v_n^z are the corresponding velocity fields. $\mu_1 = \mu(T, n(\mathbf{r}_\perp = 0, z))$ is the chemical potential calculated on the symmetry axis of the trapped gas and is determined by the equation of state of uniform matter. Here and in the following we assume that the system is large enough to safely carry out the radial integrals using the local density approximation.

4.2 First sound and second sound in the cylindrical trap

In the following we will assume $\omega_z = 0$ (cylindrical geometry) in order to calculate the velocity of the sound waves propagating along the axial direction. We will limit ourselves to the description of small-amplitude oscillations. So the equations of motion for both fluids (4.4)–(4.7) have to be linearized and all the thermodynamic variables are expanded around their equilibrium values, e.g., $n_1(z,t) = n_{10} + \delta n_1(z,t)$. In

addition, the equilibrium values of the velocities v_{n0}^z and v_{s0}^z are zero. The linearized hydrodynamic equations take the form:

$$m\partial_t \delta n_1 + \partial_z \delta j_z = 0, \quad (\delta j_z = m n_{n1}^0 v_n^z + m n_{s1}^0 v_s^z) \tag{4.8}$$

$$\partial_t \delta s_1 + \partial_z (s_1^0 v_n^z) = 0, \tag{4.9}$$

$$m\partial_t v_s^z = -\partial_z \delta\mu, \tag{4.10}$$

$$\partial_t \delta j_z = -\partial_z \delta P_1. \tag{4.11}$$

Hereafter, we use v_n^z, v_s^z to denote the out-of-equilibrium velocity fields. The thermodynamic quantities entering the above equations are not independent and, in the linear regime, obey the thermodynamic relation $\delta P_1 = s_1 \delta T + n_1 \delta\mu$.

By excluding δj_z from Eqs. (4.8) and (4.11) one obtains the important equation,

$$m\frac{\partial^2 \delta n_1}{\partial t^2} = \nabla_z^2 \delta P_1, \tag{4.12}$$

relating the time and space variations of the density and of the pressure, respectively. Our purpose now is to derive an equation relating the time and space variations of the temperature and the entropy. To achieve this it is convenient to have the entropy conservation equation given by (4.5) written in terms of the local entropy per particle with its linearized form given by

$$\partial_t \delta \bar{s}_1 = \frac{\bar{s}_1^0}{n_1^0} n_{s1}^0 \partial_z (v_s^z - v_n^z). \tag{4.13}$$

In getting this expression, we have used the mass and entropy continuity equations, and we have assumed homogeneity along the z-direction. It is worth noticing that in the normal phase, where the superfluid density is zero, or in the superfluid phase, when the two fluid velocity fields are identical, the 1D entropy per particle $\bar{s}_1$ is conserved. This shows that an in-phase motion of first sound nature corresponds to an isentropic oscillation.

Using the Gibbs-Duhem relation and the equation for the superfluid velocity field (4.6) and the current (4.7), we find,

$$n_{n1}^0 \partial_t (v_s^z - v_n^z) = \bar{s}_1^0 n_1^0 \partial_z \delta T, \tag{4.14}$$

which, combined with Eq. (4.13), yields the required equation

$$m\frac{\partial^2\delta\bar{s}_1}{\partial t^2} = \frac{n^0_{s1}}{n^0_{n1}}\bar{s}_1^{02}\nabla_z^2\delta T. \tag{4.15}$$

It's worth mentioning that Eq. (4.14) implies that $\partial_z\delta T = 0$ for an in-phase mode with $v_s^z = v_n^z$. This means that in the superfluid phase an isentropic mode is also an isothermal mode. Hereafter we refer $v_s^z = v_n^z$ as the first sound ansatz, corresponding to a pure density oscillation.

Equations (4.12) and (4.15) are coupled via the following thermodynamic identities,

$$\delta P_1 = (\frac{\partial P_1}{\partial n_1})_{\bar{s}_1}\delta n_1 + (\frac{\partial P_1}{\partial \bar{s}_1})_{n_1}\delta\bar{s}_1, \tag{4.16}$$

$$\delta T = (\frac{\partial T}{\partial n_1})_{\bar{s}_1}\delta n_1 + (\frac{\partial T}{\partial \bar{s}_1})_{n_1}\delta\bar{s}_1. \tag{4.17}$$

Inserting the above two equations into (4.12) and (4.15) we obtain the following two coupled wave equations for the density and entropy fluctuations,

$$m\frac{\partial^2\delta n_1}{\partial t^2} = (\frac{\partial P_1}{\partial n_1})_{\bar{s}_1}\nabla_z^2\delta n_1 + (\frac{\partial P_1}{\partial \bar{s}_1})_{n_1}\nabla_z^2\delta\bar{s}_1, \tag{4.18}$$

$$m\frac{\partial^2\delta\bar{s}_1}{\partial t^2} = \frac{n^0_{s1}}{n^0_{n1}}\bar{s}_1^0\left[(\frac{\partial T}{\partial n_1})_{\bar{s}_1}\nabla_z^2\delta n_1 + (\frac{\partial T}{\partial \bar{s}_1})_{n_1}\nabla_z^2\delta\bar{s}_1\right]. \tag{4.19}$$

By looking for plane wave solutions varying in time and space like $\propto e^{i(qz-\omega t)}$ with $\omega = cq$, we obtain:

$$mc^2\delta n_1 = (\frac{\partial P_1}{\partial n_1})_{\bar{s}_1}\delta n_1 + (\frac{\partial P_1}{\partial \bar{s}_1})_{n_1}\delta\bar{s}_1, \tag{4.20}$$

$$mc^2\delta\bar{s}_1 = \frac{n^0_{s1}}{n^0_{n1}}\bar{s}_1^0\left[(\frac{\partial T}{\partial n_1})_{\bar{s}_1}\delta n_1 + (\frac{\partial T}{\partial \bar{s}_1})_{n_1}\delta\bar{s}_1\right]. \tag{4.21}$$

Thereby, if the thermodynamic function $\frac{1}{n_1^0}(\frac{\partial P_1}{\partial \bar{s}_1})_{n_1} = n_1^0(\frac{\partial T}{\partial n_1})_{\bar{s}_1}$ in Eqs. (4.20) and (4.21) is equal to zero, or alternatively, if the isothermal compressibility coincides

with the isentropic compressibility, we get a pure density wave with an adiabatic sound velocity,

$$mc_1^2 = \left(\frac{\partial P_1}{\partial n_1}\right)_{\bar{s}_1}, \tag{4.22}$$

and a pure entropy wave with the sound velocity given by,

$$mc_2^2 = T\frac{\bar{s}_1^{02}}{\bar{c}_{v_1}^0}\frac{n_{s1}^0}{n_{n1}^0}, \tag{4.23}$$

involving an out-of-phase motion of the two components with the total mass current of the liquid remaining at rest, as indicated by Eq. (4.8). Hereafter, we refer to the condition $n_{s1}^0 v_s^z + n_{n1}^0 v_n^z = 0$ as the second sound ansatz, corresponding to a pure entropy oscillation. A nonzero value of the thermal expansion coefficient leads to a coupling between density and temperature oscillations.

Using straightforward thermodynamic relations for the solutions of the two coupled equations (4.20) and (4.21), we obtain the following equation for the sound velocity[2]:

$$c^4 - c^2\left[\frac{1}{m}\left(\frac{\partial P_1}{\partial n_1}\right)_{\bar{s}1} + \frac{1}{m}\frac{n_{s1}T\bar{s}_1^2}{n_{n1}\bar{c}_{v1}}\right] + \frac{1}{m^2}\frac{n_{s1}T\bar{s}_1^2}{n_{n1}\bar{c}_{v1}}\left(\frac{\partial P_1}{\partial n_1}\right)_T = 0, \tag{4.24}$$

which generalizes the well known Landau equation (3.5) [5, 86] for the first and second sound velocities to the case of a cylindrically trapped gas.

In the normal phase the superfluid vanishes ($n_{s1} = 0$), Eq. (4.24) admits only one solution with velocity different from zero, namely, the adiabatic sound (4.22). In the superfluid phase, Eq. (4.24) gives rise to two distinct sound velocities as a consequence of the coexistence of two fluids. Unlike in helium, where the temperature and pressure fluctuations are essentially uncoupled and Eq. (4.23) holds, the situation in interacting Fermi gases is different. In this case $\left(\frac{\partial P_1}{\partial n_1}\right)_{\bar{s}_1} \neq \left(\frac{\partial P_1}{\partial n_1}\right)_T$ or $\bar{c}_{v1} \neq \bar{c}_{p1}$ except at very low temperature, as shown in Figs. 2.5 and 2.6. The second sound solution emerging from Eq. (4.24) will be different from Eq. (4.23) due to the coupling with first sound. The coupling can be important to better understand the

[2]Hereafter, we drop the superscript '0' to denote the equilibrium quantities and pick it up only when necessary.

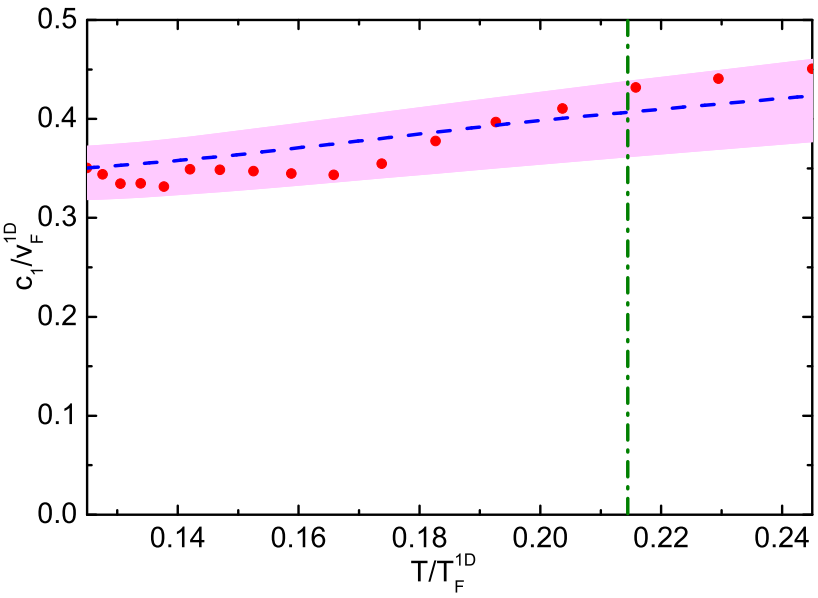

Figure 4.1: 1D first sound velocity in units of v_F^{1D} calculated using Eq. (4.26) (blue dashed line). The experiment data (red dots) for the first sound in the shaded region are taken from [36]. The shaded area indicates the uncertainty range of experimental data. The vertical green line indicates the critical temperature.

nature of second sound propagation which is a crucial ingredient for its experimental detection. Taking into account the relation between the ratio of specific heats and compressibilities given by (2.31), Eq. (4.24) can be rewritten as:

$$c^4 - c^2\left[\frac{1}{m}\left(\frac{\partial P_1}{\partial n_1}\right)_{\bar{s}_1} + \frac{1}{m}\frac{n_{s1}T\bar{s}_1^2}{n_{n1}\bar{c}_{v1}}\right] + \frac{1}{m^2}\frac{n_{s1}T\bar{s}_1^2}{n_{n1}\bar{c}_{p1}}\left(\frac{\partial P_1}{\partial n_1}\right)_{\bar{s}_1} = 0. \tag{4.25}$$

For the in-phase motion of the two fluids (first sound), we expect that oscillation is basically isentropic and we take Eq. (4.22) as the zero order approximation for the first sound velocity. By inserting Eq. (2.29) into Eq. (4.22), we obtain the speed of isentropic sound waves,

$$mc_{10}^2 = \frac{7}{5}\frac{P_1}{n_1}. \tag{4.26}$$

This differs from the sound velocity in uniform Fermi gases at unitarity, given by $mc^2 = (5/3)P/n$ [37], the difference being caused by the 1D nature of our configurations generated by the radial trapping which gives rise to a different condition of adiabaticity. In Fig. 4.1 we show the value of the first sound velocity c_1 as a function of T/T_F^{1D} using the thermodynamic results for P_1/n_1 discussed in Sec. 2.5. Using the expansion (2.37) for the 1D pressure one finds that at $T = 0$ the first sound velocity approaches the value $c_1 = \sqrt{\xi^{3/5}(v_F^{1D})^2/5} = \sqrt{\xi v_F^2/5}$ where $v_F^{1D} = \sqrt{2k_B T_F^{1D}/m}$ and $v_F = \sqrt{2k_B T_F/m}$ are, respectively, the 1D and 3D Fermi velocities. The quenching of the sound velocity by the factor $\sqrt{3/5}$ with respect to the bulk value $\sqrt{\xi v_F^2/3}$ was first pointed out in [30], in analogy with a similar behavior exhibited by Bose-Einstein condensed gases [29].

In order to get access to the second sound velocity, it is crucial to know the behavior of the superfluid density. At present the theoretical knowledge of n_s is rather poor in the unitary Fermi gases. In the following we will make use of simple ansatz for n_s in order to provide a first estimate of the speed of the second sound oscillation. We use two different models for n_s. The first model employs the formula,

$$n_s/n = (1 - T/T_c)^{2/3}, \tag{4.27}$$

accounting for the correct critical exponent 2/3 characterizing the vanishing of n_s near the critical point. A second model employs the phenomenological expression

$$n_s/n = 1 - (T/T_c)^4, \tag{4.28}$$

which also vanishes at $T = T_c$ and exhibits, at low temperature the correct T^4 behavior, although the coefficient of the T^4 law is about 8 times larger than the one predicted by the phonon contribution to the normal density (see Eq. (2.19)). The second sound velocity depends in a crucial way on the choice of the model for n_s so that the measurement of c_2 is expected to provide useful information on its temperature dependence.

For the out-of-phase motion of the two fluids, we find (see discussions below) that a better description of the velocity is given by the expression,

$$mc_{20}^2 = T\frac{n_{s1}}{n_{n1}}\frac{\bar{s}_1^2}{\bar{c}_{p1}}. \tag{4.29}$$

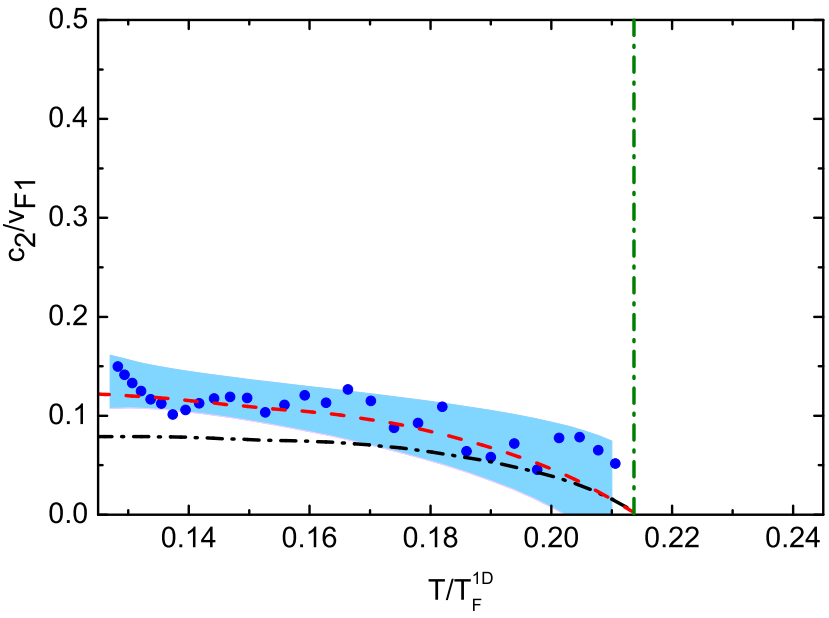

Figure 4.2: 1D second sound velocity, calculated using Eq. (4.29) and two different models for the superfluid density: the phenomenological ansatz: $n_s/n = 1-(T/T_c)^4$ (the red dashed-line) and $n_s/n = (1-T/T_c)^{2/3}$ (the black dash-dotted-line). The scattered blue circles are the experimental data [36]. At low temperature the 1D second sound velocity is expected to vanish like $\sqrt{T}$. The shaded area indicates the uncertainty range of experimental data. The vertical green line indicates the critical temperature.

This expression for the velocity differs from Eq. (4.23) because of the presence of the specific heat at constant pressure rather than at constant density. The two specific heats actually exhibit a different behavior for temperatures close to T_c (see Fig. 2.5). When $T \to 0$ the specific heat at constant pressure and at constant volume instead coincide and, as a consequence of the temperature dependence of the 1D thermodynamic functions in the low temperature regime (see Sec. 2.5), the second sound velocity vanishes like $\sqrt{T}$, differently from what happens in the bulk where it approaches a constant value [21]. In Fig. 4.2 we show the prediction for the second sound velocity (4.29), with the two ansatz (4.27) and (4.28) for the superfluid

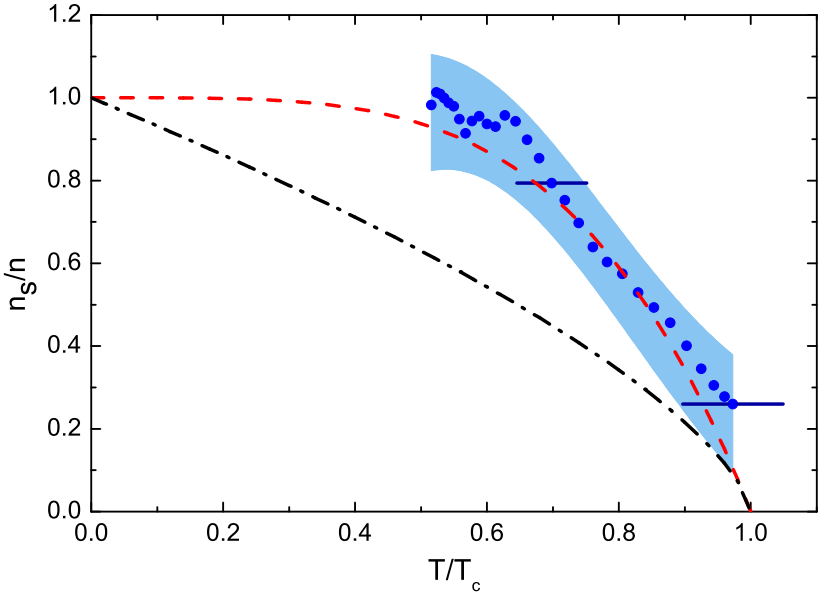

Figure 4.3: Uniform superfluid density: the red dashed-line corresponds to the phenomenological ansatz: $n_s/n = 1 - (T/T_c)^4$ while the black dash-dotted-line to the choice: $n_s/n = (1 - T/T_c)^{2/3}$. The blue dots are the experimental data [36]. The shaded area indicates the uncertainty range of experimental data.

fraction (see Fig. 4.3).

We have checked the accuracy of (4.29) by considering the next order correction. In terms of c_{10}^2 and c_{20}^2 we can write the exact equation (4.25) as:

$$c^4 - c^2[c_{10}^2 + c_{20}^2 \frac{\bar{c}_{p1}}{\bar{c}_{v1}}] + c_{10}^2 c_{20}^2 = 0. \tag{4.30}$$

As the first approximation we assume:

$$c_1^2 = c_{10}^2(1 + o_1), c_2^2 = c_{20}^2(1 + o_2), |o_1| \ll 1, |o_2| \ll 1. \tag{4.31}$$

A simple calculation shows that the first order corrections are given by,

$$o_1 = -o_2 = \frac{\frac{c_{20}^2}{c_{10}^2}(\frac{\bar{c}_{p1}}{\bar{c}_{v1}} - 1)}{1 - \frac{c_{20}^2}{c_{10}^2}}. \tag{4.32}$$

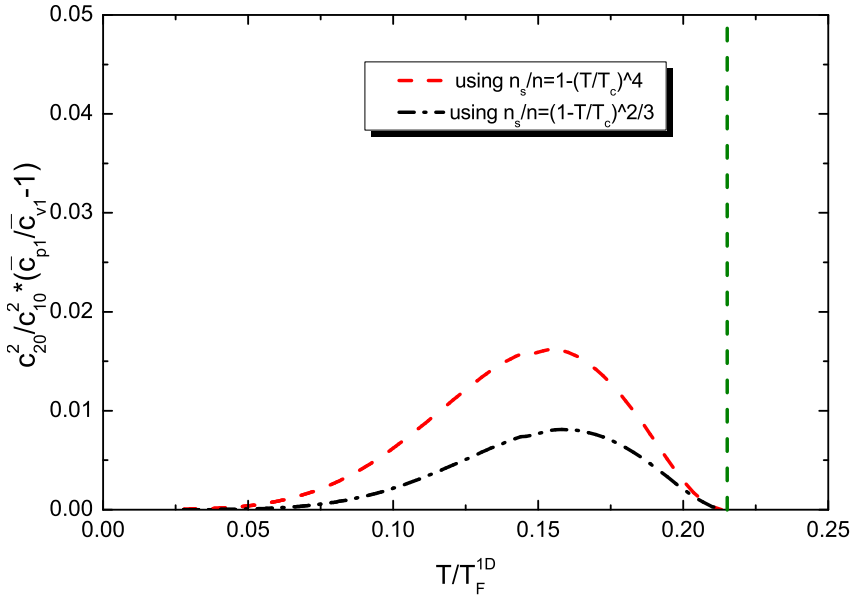

Figure 4.4: First order correction (4.33) to the ansatz (4.29) for the second sound velocity. The vertical green line indicates the critical temperature.

Thus the expressions (4.29) can accurately describe the sound velocities under the condition,

$$\frac{c_{20}^2}{c_{10}^2}\frac{\bar{c}_{p1}-\bar{c}_{v1}}{\bar{c}_{v1}} \ll 1, \tag{4.33}$$

where we have dropped the higher order terms of $\frac{c_{20}^2}{c_{10}^2}$. It turns out that the condition (4.33) is well satisfied for all temperatures as shown in Fig. 4.4, thereby proving that the expression (4.29) is very accurate in reproducing the lower solution of (4.25) as confirmed by Fig. 4.5. The solutions from the exact numerical method for both sounds are compared with the solutions from the two approximations given by Eqs. (4.22) and (4.29). The figure shows that the first sound velocity is actually independent of the different ansatz for the superfluid density and that expression (4.26) is essentially accurate. On the other hand, it shows that the second sound velocity crucially depends on the ansatz for the superfluid density. For both ansatz the expression (4.29) turns out to be very accurate. The inset of the figure 4.5

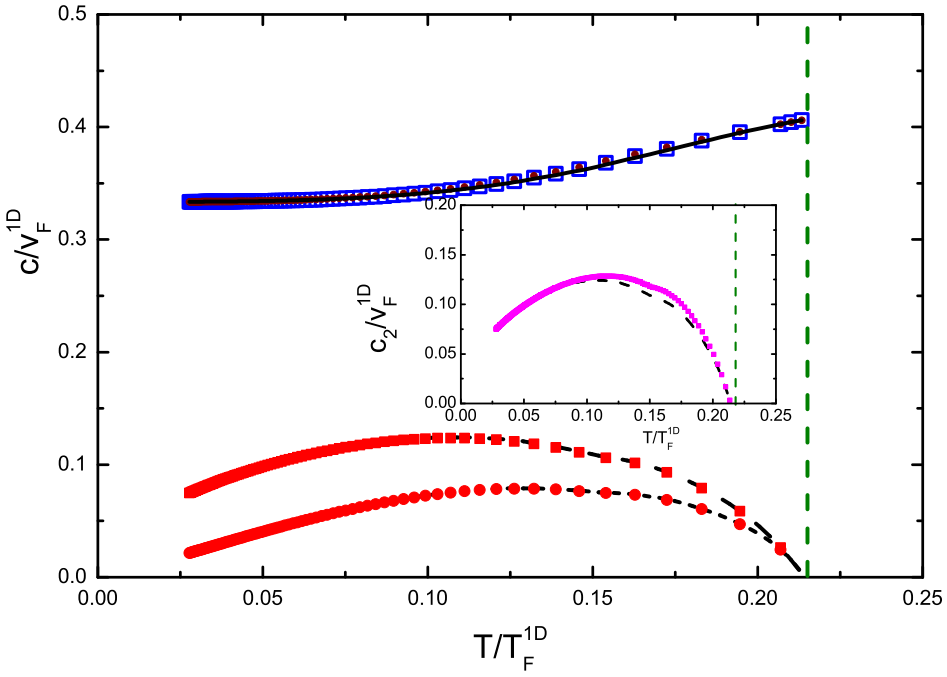

Figure 4.5: 1D first and second sound velocity in units of v_F^{1D}. Upper branch (first sound): numerical solution of Eq. (4.25) for the first sound by using the superfluid fraction as $n_s/n = (1 - T/T_c)^{2/3}$ (blue open squares) and $n_s/n = 1 - (T/T_c)^4$ (dark-red filled circles); The black solid line corresponds to the approximate adiabatic sound solution (4.26). Lower branch (second sound): numerical solution of Eq. (4.25) for the second sound by using the superfluid fraction as $n_s/n = (1 - T/T_c)^{2/3}$ (red filled circles) and $n_s/n = 1 - (T/T_c)^4$ (red squares); the black short-dashed line and the dashed line correspond to the approximation (4.29) with the superfluid fraction ansatz being, $n_s/n = (1 - T/T_c)^{2/3}$ and $n_s/n = 1 - (T/T_c)^4$, respectively. The vertical green line indicates the critical temperature. In the inset, the second sound velocity is calculated under the ansatz $n_s/n = 1 - (T/T_c)^4$ using Eqs. (4.23) (pink squares) and (4.29) (black dashed line), based, respectively, on the specific heat at constant volume and constant pressure.

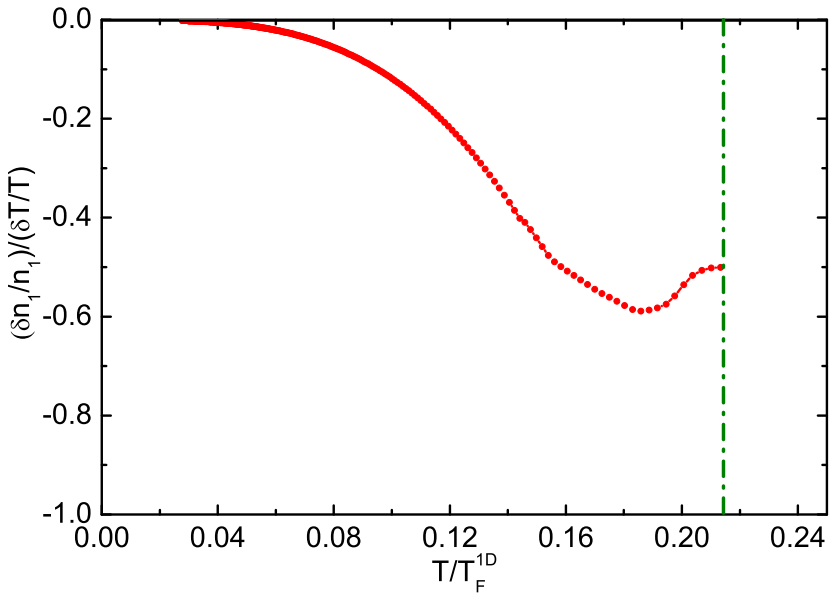

Figure 4.6: Ratio (4.35) between the relative density and temperature fluctuations calculated for 1D second sound. The vertical green line indicates the critical temperature.

shows that the two expressions (4.23) and (4.29) differ, at maximum, by 10%. In 3D, the maximum difference is significantly larger (33%). The relative difference in the second sound velocities is defined with respect to the expression (4.29).

Second sound can be actually regarded as an oscillating wave at constant pressure, rather than at constant density, as previously assumed in the derivation of (4.23). In fact, by a lengthy but straightforward calculation using the equations for the density and entropy fluctuations given by (4.20) and (4.21), we can get the ratio between the relative density and temperature fluctuations,

$$\frac{\delta n_1/n_1}{\delta T/T} = \frac{-\frac{T}{n_1}\left(\frac{\partial n_1}{\partial T}\right)_{P_1}}{\frac{c^2}{c_{10}^2}\frac{\bar{c}_{p1}}{\bar{c}_{v1}} - 1}, \tag{4.34}$$

holding for both the first sound ($c = c_1$) and second sound ($c = c_2$). Under the condition $c_{20} \ll c_{10}$, the ratio between the relative density and temperature fluctuations

for second sound takes the simple expression,

$$\frac{\delta n_1/n_1}{\delta T/T} = \frac{T}{n_1}\left(\frac{\partial n_1}{\partial T}\right)_{p1} = \frac{5}{2} - \frac{7}{2}\frac{f_n f_q}{f_p^2}, \tag{4.35}$$

where we have used the expression $\alpha_1 = -\frac{1}{n_1}(\frac{\partial n_1}{\partial T})_{P_1} = \frac{5}{2T}(\frac{\bar{c}_{p1}}{\bar{c}_{v1}} - 1)$ for the 1D thermal expansion coefficient at unitarity. The ratio (4.35) turns out to be negative [97] and is shown in Fig. 4.6. It should be compared with the result $\frac{\delta n_1/n_1}{\delta T/T} = \frac{T}{n_1}\left(\frac{\partial n_1}{\partial T}\right)_{\bar{s}1} = \frac{5}{2}$ characterizing the propagation of first sound, where the derivative is calculated at constant entropy rather than at constant pressure. It is remarkable that the ratio (4.35) is significantly large in a useful range of temperatures, thereby revealing that second sound can be observed by looking at the density fluctuations of the propagating signal [91, 92, 36].

4.3 Experimental excitation and observations

In ultracold atomic gases, below the critical temperature for superfluidity, the propagation of sound has been the object of extensive experimental work in recent years. In the case of highly elongated configurations, it is possible to investigate directly the propagation of sound waves, by generating a perturbation in the center of the trap and subsequently investigating the time and space propagation of the resulting signal along the long axis. Detections of propagation of sound along the axial direction in the cigar-shaped trap have been reported both for the Bose-Einstein condensate [26] and for Fermi gases along the BEC-BCS crossover [27, 28] at zero temperature. The propagation of second sound waves in dilute Bose gases was explored in [34]. In dilute Bose gas, however, second sound actually reduces to the oscillation of the condensate except at very low temperature in the phonon regime [21], exhibiting quite different behaviors from the case of strongly interacting superfluids, like ^{4}He. Differently from dilute Bose gases, Fermi gases at unitarity behave like strongly interacting fluids and, in this respect, are more similar to liquid ^{4}He, despite the different statistics. Thanks to the accurate experiment carried out by the Innsbruck team, the long-standing goal of observation of second sound in superfluid fermions has been recently achieved [36].

We summarize here the key features of the experiment of Ref. [36]. Experimentally, an ultracold, resonantly interacting Fermi gas can be prepared by evaporating a two-component spin mixture of fermionic ^{6}Li in an optical dipole trap [98]. The sample consists of $N = 3.0 \times 10^5$ atoms in a balanced mixture of the two lowest-spin states. The axial and radial trap frequencies are $\omega_z = 2\pi \times 22.46(7)$ Hz and $\omega_\perp = 2\pi \times 539.4(8)$ Hz, respectively. The corresponding Fermi temperature is $T_F^{trap} \sim 0.9\mu K$. The magnetic field is set to 834 Gauss, right on top of the well-known broad Feshbach resonance [18]. The relevant temperature range for the present experiment is between $0.11T_F^{trap}$ and $0.15T_F^{trap}$. The schemes to excite the first and second sound are illustrated in Fig. 4.7.

First sound is excited by suddenly turning on the repulsive laser that perpendicularly intercepts the trapped sample at its center, which induces local reduction in the trapping potential. The actions caused by the potential variations acts on the superfluid and normal components in the same way and creates a small hump in the axial density distribution, which then propagates along the axis. Second sound is excited by locally heating the cloud through a fast modulation of the power of the green beam ($2\omega_\perp \sim 3\omega_\perp$) for a certain period of time and observed through a density pulse, due to the sizeable thermal expansion as discussed in the previous section, propagating across the atomic cloud. The signal, however, travels at a slower speed than that of the first sound and disappears at the superfluid boundary, in clear contrast to the first sound pulse, as shown in Fig. 4.7.

To detect sound propagation, the axial density profile, $n_1(z,t)$ is recorded for various time delays, t, after the excitation pulse. The density pulse signal is obtained by subtracting a background profile (average of the profiles over all measured delay times). Then the speed of sound is extracted by taking the derivative of density pulse with respect to time. The temperature dependence of the sound speeds is determined by converting local linear density into its corresponding local Fermi temperature defined by (2.40), without changing the global temperature, T, of the trapped sample. The corresponding experimental results are shown in Figs. 4.1 and 4.2. The good agreement between the experimental results (red dots) and the theoretical prediction (dashed line) based on the isentropic expression (4.26) in Fig. 4.1 shows that first sound in strongly interacting fermions is a wave that propagates with constant entropy per particle (adiabatic oscillation). The measured speed of

second sound (Fig. 4.2, blue points) is instead observed to decrease with increasing temperature and becomes zero at the critical point, in contrast to first sound. The 1D superfluid fraction, n_{s1}/n_1 is extracted from the data set of Fig. 4.2 using the isobaric expression (4.29). The temperature dependence of the superfluid fraction in the uniform geometry can be obtained by taking the derivative of the 1D superfluid fraction [36]. The result for the superfluid fraction is presented in Fig. 4.8. A comparison with Fig. 4.3 shows that the ansatz $n_s/n = 1 - (T/T_c)^4$ provides a much better description of the measured data in the relevant temperature regime explored in this experiment. Of course the experiment cannot explore the critical behavior of the superfluid density near T_c.

4.4 Superfluid fraction

In this section, we discuss the behavior of the superfluid density. Several papers have provided theoretical predictions for the temperature dependence of the superfluid fraction of the interacting Fermi gas at unitarity. A comprehensive discussion is contained in the paper by Taylor et al. [59]. However, these calculations predict values of the critical temperature which are in general significantly higher than the experimental value so that the comparison in the relevant region, where the fraction n_s/n significantly deviates from unity, is not particularly useful. Theoretical predictions in the lower temperature region, corresponding to $T < 0.5T_c$, and accounting for the effects of fermionic excitations in addition to the leading phonon contribution, have been also reported [99, 100], but this regime, cannot be resolved in the experiment of Ref. [36]. On the other hand, the most reliable quantum many-body calculations providing accurate values for the critical value for the superfluid transition [61, 62, 68] have not yet provided predictions for the temperature dependence of the superfluid fraction.

The experimental investigation of second sound, which is particularly sensitive to the behavior of the superfluid density, has provided the first access to this quantity of fundamental interest [36]. The results (Fig. 4.8) turn out to be rather close to those for liquid helium II [101] (solid line). In particular, the gas is almost completely superfluid below $0.6T_c$. This behaviour is quite different from that exhibited by a

weakly interacting Bose gas, whose superfluid fraction is significantly smaller, as a function of temperature, than the fraction represented by the data points in Fig. 4.8 and is well approximated by the condensate fraction of the ideal Bose gas (dashed line). The recent experiment of Ref. [36] has already stimulated new calculations of the superfluid fraction (see, for instance, [102] and [103]).

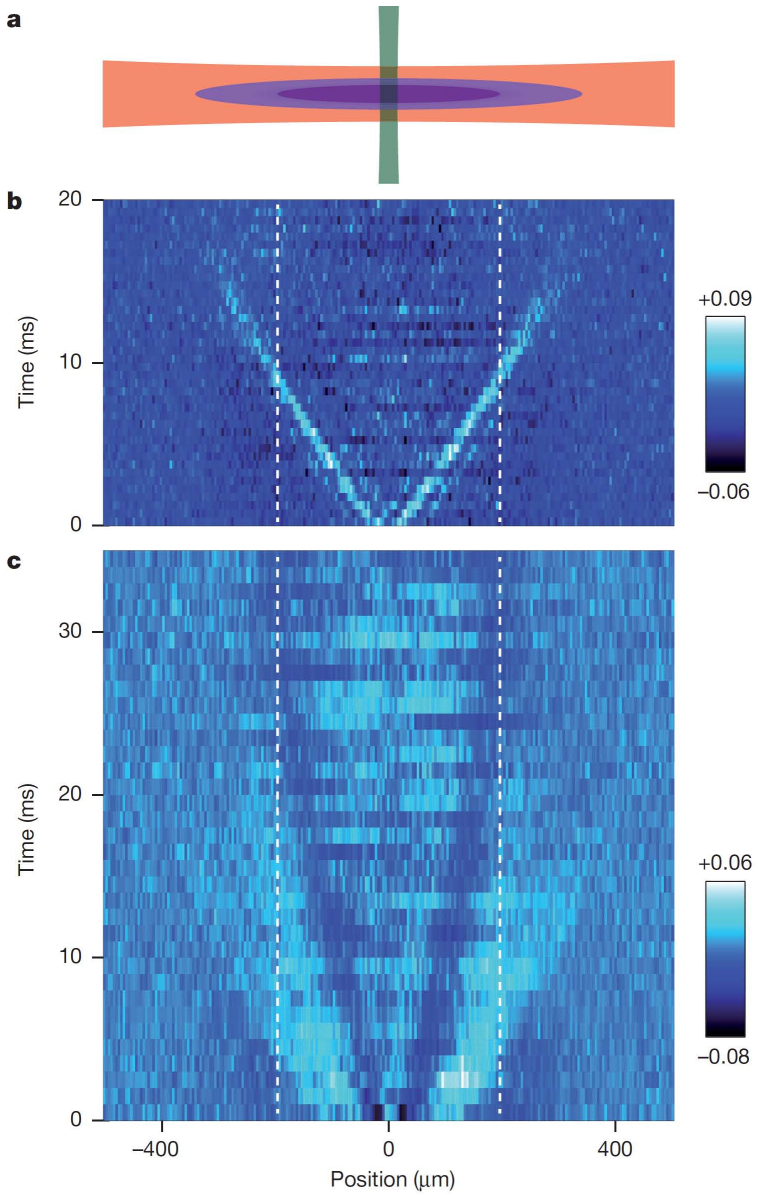

Figure 4.7: Exciting and observing the propagation of first and second sound. a, the basic geometry of exciting the optically trapped cloud with a weak, power-modulated repulsive laser beam (green), which perpendicularly intersects the trapping beam (red). The trapped cloud has a superfluid core ($|z| < 190\mu m$), surrounded by a normal region (about 1.5 times larger). b, c, normalized differential axial density profiles, $\delta n_1(z,t)/n_{1,max}$ (colour scale), measured for variable delay times after the excitation show the propagation of first sound (local density increase, bright) and second sound (local decrease, dark). The temperature of the atomic cloud is $0.135(10)T_F^{trap}$. The vertical dashed lines indicate the axial region where superfluid is expected to exist according to the recent determination of the critical temperature. From Ref. [36].

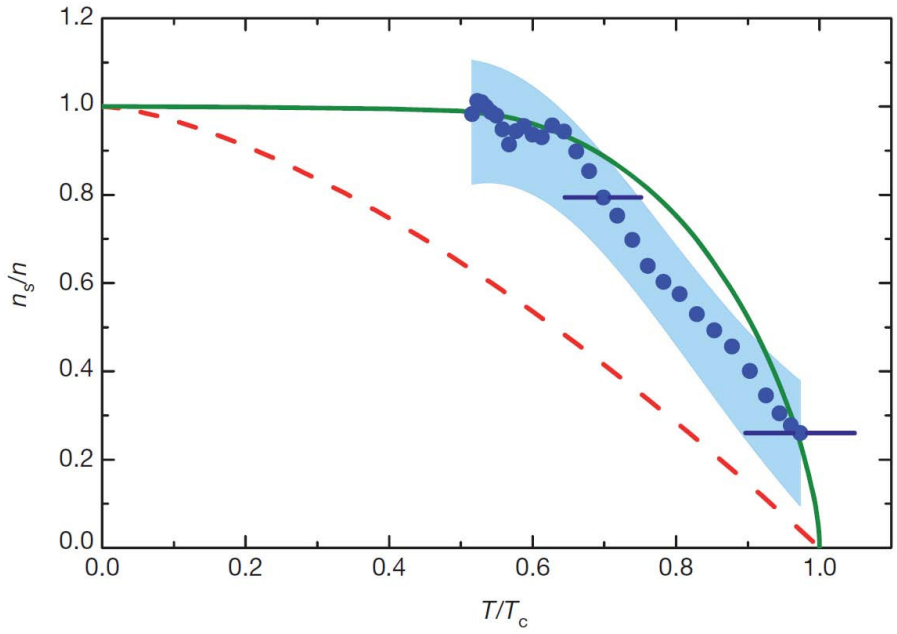

Figure 4.8: Superfluid fraction for the homogeneous case. The data points and the corresponding uncertainty range (shaded region) show the superfluid fraction for a uniform, resonantly interacting Fermi gas, reconstructed from its 1D counterpart, as a function of T/T_c. The two horizontal error bars indicate the systematic uncertainties resulting from the limited knowledge of the critical temperature T_c. For comparison, we show the fraction for helium II [101] (solid line) and the textbook expression $1 - (T/T_c)^{3/2}$ for the Bose-Einstein condensed fraction of the ideal Bose gas (dashed line). From Ref. [36].

Chapter 5

Discretized collective oscillations in a harmonic trap

While in uniform systems it is straightforward to solve the linearized Landau two-fluid equations since the solutions are plane waves (see chapter 4), for trapped gases it is not easy to solve these differential equations since the coefficients are position-dependent. An exception is the zero temperature case, where the chemical potential has a power law dependence on the density, allowing for analytic solutions. In Sec. 5.1, we will review the well-established results of hydrodynamic theory on the dynamic behavior of the unitary Fermi gas at zero temperature, like, the expansion and the collective oscillations. In Sec. 5.2 we show that in the regime of small amplitude oscillations the two-fluid Landau hydrodynamic equations, when applied to the unitary gas in the presence of harmonic trapping, admit exact scaling solutions of compressional and surface nature characterized by the linear spatial dependence of the velocity field and temperature independent frequencies. This is the consequence of the universal scaling behavior exhibited by the unitary Fermi gas at all temperatures. When the velocity field is no longer characterized by the linear spatial dependence, the frequency of the collective oscillations exhibits a temperature dependence. This is the case of the so-called higher-nodal modes, for which no analytic solutions exist. In Sec. 5.3, we build the so-called quasi-1D hydrodynamic formalism by generating the variational approach developed by E. Taylor et al [58, 59, 60]. This variational approach is equivalent to the Landau two-fluid hydrodynamic the-

ory but permits an easier and rather accurate estimate for the higher-order modes. As a specific application, in Sec. 5.4, we search for the discrete collective modes under the first sound ansatz (assuming that the two components move with the same velocity field). We present the comparison of theoretical predictions with the experimental observations in Sec. 5.5 and show that the agreement is remarkably good, thus confirming the validity of our 1D hydrodynamic approach. In the last section 5.6, we discuss the discretized modes of second sound nature, and in particular, the coupling of the second sound dipole mode with the first sound mode of the same parity.

5.1 Hydrodynamic behavior at zero temperature

At zero temperature, the hydrodynamic equations of superfluid consist of coupled and closed equations for the density and the velocity field. Actually, due to the absence of the normal component, the superfluid density coincides with the total density and the superfluid current with the total current. At $T = 0$ the equations for entropy identically vanishes and Euler equation coincides with the equation for the superfluid velocity. In this limit the Landau two-fluid equations then reduce to two coupled equations for the density and the velocity field, first applied to the case of a nonuniform dilute Bose gas in [40]. The same equations were employed to discuss beyond mean field corrections in [104].

While in the case of normal fluid the hydrodynamic description requires fast collisions to ensure local equilibrium, the hydrodynamic is always guaranteed at $T = 0$. The hydrodynamic formalism at $T = 0$ has been also extensively employed to describe the anisotropic expansions of the superfluid gas after releasing of the confining trap. The agreement between theory and experiment is very good in both Fermi and Bose superfluids [24, 20]. See Fig. 5.1 as an example of the anisotropic expansion of fermions at unitarity.

In the following of this section, we will seek for the zero temperature hydrodynamic solutions in the quasi-1D geometry. At $T = 0$, there is no normal component ($n_{s1} = n_1$ and $v_s^z = v_z$) and entropy is zero. So the reduced quasi-1D superfluid

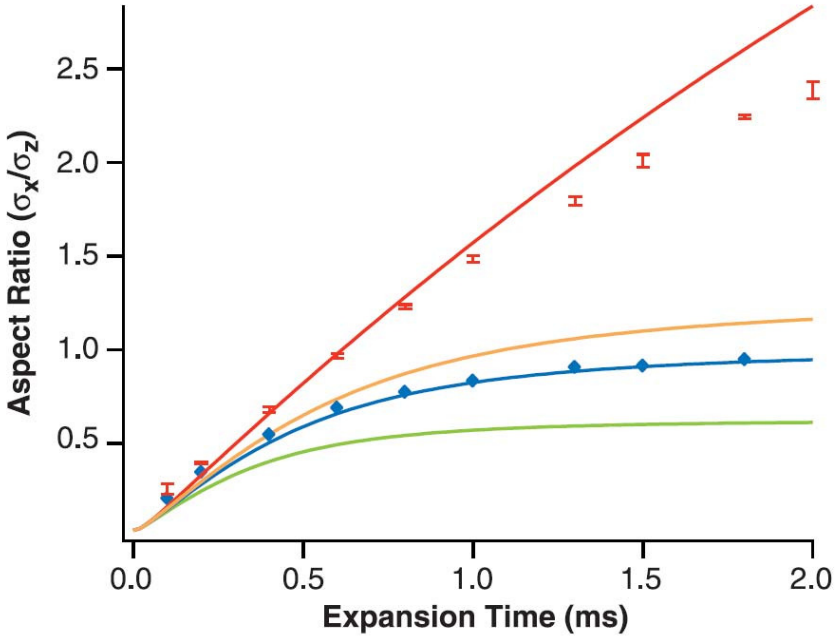

Figure 5.1: Aspect ratio of the cloud as a function of time after release. The dots indicate experimental data at unitarity (red) and in the absence of interactions (blue). The solid curves show theoretical predictions with no adjustable parameters (red, hydrodynamic; blue, ballistic; green, attractive mean field; orange, repulsive mean field). From Ref. [17].

hydrodynamic equations (see section 4.1) are:

$$\partial_t \delta n_1 + \partial_z (n_1 v_z) = 0, \tag{5.1}$$

$$m \partial_t v_z = -\partial_z (\mu + V_{ext}) = -\partial_z \delta\mu. \tag{5.2}$$

It's worth noticing that the above equations hold both for Bose and Fermi superfluids but its solutions depend on the equation of state. By taking the second time derivative of Eq. (5.1) and inserting the Euler equation Eq. (5.2), the hydrodynamic equations at zero temperature take the following form in the linear regime:

$$\partial_t^2 \delta n_1 = \partial_z \left[\frac{n_1}{m} \partial_z \left(\frac{\partial \mu}{\partial n_1} \delta n_1 \right) \right]. \tag{5.3}$$

The key ingredient needed for the above equation is the EOS, or more specifically, the $\partial\mu/\partial n_1$. We assume that the chemical potential has a power law dependence $\mu \propto n^\gamma$ on the density in uniform matter [105]; then the Thomas-Fermi equilibrium profiles take the analytic form:

$$n = C\mu^{1/\gamma} = C\left(\mu_0 - V_{ext}(\mathbf{r}_\perp, z)\right)^{1/\gamma}, \tag{5.4}$$

where C is a constant independent of coordinates and μ_0 is the chemical potential in the center of the trap. By carrying out the radial integral of the bulk density we get the 1D density profile:

$$n_1 = \int d\mathbf{r}_\perp n(\mathbf{r}_\perp, z) \quad = \frac{2\pi C}{m\omega_\perp^2}\frac{\gamma}{\gamma+1}\mu_1^{(\gamma+1)/\gamma}, \tag{5.5}$$

where μ_1 is the chemical potential along the symmetry axis. Therefore $\mu_1 \propto n_1^{\gamma/(\gamma+1)}$, yielding a density dependence of the chemical potential different from the 3D case.

Let us assume that the density oscillation has a harmonic time dependence and a spatial dependence of a form determined by the expression $\delta\mu = \frac{\partial\mu}{\partial n_1}\delta n_1 = \sum c_l z^l$. Multiplying Eq. (5.3) by $\frac{\partial\mu}{\partial n_1}$ and using the identity $(\partial\mu/\partial n_1)\nabla n_1 = -\nabla V_{ext}(z)$ holding at $T = 0$ for the density profile at equilibrium, we find solutions that obey the following dispersion law:

$$\omega^2 = \frac{\gamma l^2 + (\gamma+2)l}{2\gamma+2}\omega_z^2, \tag{5.6}$$

where $l = 1, 2...$ represents the order of the polynomial. According to Kohn's theorem, the dipole oscillation ($l = 1$ mode), which can be excited by a sudden shift of the confining harmonic trap, has the same frequency as the trap frequency, independent of statistics and interactions. This is the consequence of the translational invariance of the two-body force and is confirmed by Eq. (5.6). For the breathing mode ($l = 2$) we instead find $\omega^2 = \frac{3\gamma+2}{\gamma+1}\omega_z^2$ [105]. For fermions at unitary, the equation of state is characterized by the power law coefficient $\gamma = 2/3$, and the corresponding frequency is $\omega^2 = 12/5\omega_z^2$. The frequency of the breathing mode for dilute Bose gas ($\gamma = 1$) is instead $\omega^2 = 5/2\omega_z^2$. Those results are consistent with the literature [40, 106, 41] in the elongated limit $\omega_z \ll \omega_\perp$. If we focus on the unitary Fermi gas and take $\gamma = 2/3$, the exact zero temperature dispersion relation is given

by:

$$\omega^2 = \frac{k^2 + 6k + 5}{5}\omega_z^2, \tag{5.7}$$

where we use the integer value, $k = l - 1$ counting from '0' for later convenience.

An alternative way to derive the equation of motion for the collective modes at zero temperature is to take the time derivative of Eq. (5.2) and substitute the time derivative of density fluctuation by Eq. (5.1), leading to the following expression:

$$m\partial_t^2 v_z = -\nabla_z(\frac{\partial \mu_1}{\partial n_1}\partial_t \delta n_1) = \nabla_z(\frac{\partial \mu_1}{\partial z}v_z + n_1\frac{\partial \mu_1}{\partial n_1}\frac{\partial v_z}{\partial z}). \tag{5.8}$$

By assuming that the velocity oscillates with $v_z \propto e^{-i\omega t}$, Eq. (5.8) can be rewritten as:

$$m\omega^2 v_z = \nabla_z^2 V_{ext} v_z - \frac{1}{n_1}\nabla_z[n_1(\frac{dP_1}{dn_1})\nabla_z v_z], \tag{5.9}$$

where the pressure enters through the identity $n_1\frac{\partial \mu}{\partial n_1} = \frac{dP_1}{dn_1}$ holding at zero temperature and the mechanical equilibrium condition, $\nabla_z \mu_1 = -\nabla_z V_{ext}$, is used to replace the chemical potential with the external harmonic trap. Inserting the polytropic equation of state, namely, $P_1 \propto n_1^{\gamma+1}$ into the above equation, we reproduce the same results as the solutions from Eq. (5.3). Furthermore, as will be demonstrated in Sec. 5.4, if $\frac{dP_1}{dn_1}$ is replaced by $(\frac{\partial P_1}{\partial n_1})_{\bar{s}_1}$, Eq. (5.9) can be generalized to the case of finite temperature.

5.2 Exact Scaling solutions at finite temperature

In this section, we prove that the two-fluid Landau hydrodynamic equations, when applied to unitary gas in the presence of harmonic trapping, admit exact scaling solutions of mixed compressional and surface nature. These solutions are characterized by a linear dependence of the velocity field on the spatial coordinates and a temperature independent frequency which is calculated in terms of the parameters of the trap. Our results are derived in the regime of small amplitude oscillations and hold both below and above the superfluid phase transition. They apply to isotropic

as well as to deformed configurations, thereby providing a generalization of Castin's theorem [107] holding for isotropic trapping. Our predictions agree with the experimental findings in resonantly interacting atomic Fermi gases. The breathing scaling solution, in the presence of isotropic trapping, is also used to prove the vanishing of two bulk viscosity coefficients in the superfluid phase in the end of this section.

In Ref. [107] Castin has shown that exact scaling solutions for the time evolution of a unitary quantum gas are available if the system is trapped by an isotropic three-dimensional harmonic potential. A remarkable example is the occurrence of an undamped radial breathing mode oscillating at the frequency $2\omega_{ho}$, where ω_{ho} is the oscillator frequency of the harmonic potential. This result is remarkable because it concerns a strongly interacting system and its validity is not restricted to small amplitude oscillations. Furthermore it holds exactly at all temperatures irrespective of the collisional regime and the value of the mean free path. It can be regarded as the strongly interacting and quantum analog of the most famous classical result derived by Boltzmann for an ideal gas trapped by an isotropic harmonic potential [108].

Similarly to the case of the Boltzmann gas, the universality of the scaling oscillation breaks down in the presence of a deformed harmonic trap. In this case no general exact result is available, unless one considers the collisional hydrodynamic regime characterized by the occurrence of fast collisions. This is the case considered in this section where we prove the existence of a class of scaling solutions describing small amplitude oscillations of the gas around equilibrium, characterized by a temperature independent value of the collective frequency. These solutions have been already identified in the literature at zero temperature (see Sec. 5.1). Their existence is proven here at all temperatures, both below and above the critical temperature for superfluidity. For simplicity we consider the axially symmetric trapping potential given in Eq. (4.1), but our proof can be easily generalized to the more general case of tri-axial trapping.

We start from the two-fluid hydrodynamic equations given in chapter 3 but in the dissipationless case ($\kappa = \eta = 0$)[3]. In the following, we prove the existence of exact solutions of the hydrodynamic equations, corresponding to the first sound like

[3]For the scaling modes, when we refer to the Landau two-fluid hydrodynamic equations, we focus only on the dissipationless regime, namely, setting $\kappa = \eta = 0$ in (3.2) and (3.4).

ansatz $\mathbf{v}_n = \mathbf{v}_s \equiv \mathbf{v}$ for the velocity field of the normal and superfluid components. Firstly, we consider a velocity flow with symmetric behavior in the x and y directions, corresponding to excitations carrying angular momentum along the z-th direction $\ell_z = 0$, namely:

$$\mathbf{v} = \beta(t)\mathbf{r}_\perp + \delta(t)\mathbf{z} \ . \tag{5.10}$$

Above T_c, where the superfluid density is absent, the same anstaz applies to the velocity field of the fluid. The generalization of the formalism to scaling excitations carrying angular momentum $\ell_z = \pm 1$ and $\ell_z = \pm 2$ is straightforward and will be given later in this section.

The choice (5.10) is accompanied by the following scaling transformations for the density

$$n(\mathbf{r}, t) = e^{2\alpha(t)+\gamma(t)} n_0(\mathbf{r}'), \tag{5.11}$$

and for the entropy density

$$s(\mathbf{r}, t) = e^{2\alpha(t)+\gamma(t)} s_0(\mathbf{r}'), \tag{5.12}$$

where $\mathbf{r}' \equiv (e^{\alpha(t)}x, e^{\alpha(t)}y, e^{\gamma(t)}z)$ is the scaled spatial variable and n_0 and s_0 are the particle density and entropy density calculated at equilibrium. The prefactor $e^{2\alpha(t)+\gamma(t)}$ in the above equations ensures the normalization condition for the density and the conservation of total entropy. At unitary the entropy density can be written in the form $s(n, T) = n f_e(T/T_F(n))$ where T_F is the Fermi temperature, proportional to $n^{2/3}$, and f_e is a universal function that can be derived from the knowledge of the equation of state (see chapter 2), but whose explicit form is irrelevant for the proof of our theorem. The ansatz (5.12) then requires that the ratio $T/T_F(n)$ should be conserved by the scaling transformation. This implies that the temperature should exhibit the position independent scaling law

$$T(t) = e^{(2\alpha(t)+\gamma(t))2/3} T_0, \tag{5.13}$$

where T_0 is the temperature of the gas at equilibrium. Finally the chemical potential, which due to dimensionality arguments can be written in the form $\mu =$

$T_F(n) f_\mu(T/T_F(n))$ where f_μ is a dimensionless function, exhibits the following scaling behavior

$$\mu(\mathbf{r}, t) = e^{(2\alpha(t)+\gamma(t))2/3} \mu_0(n_0(\mathbf{r}')), \tag{5.14}$$

with μ_0 calculated at the equilibrium temperature T_0. The fact that temperature fluctuations associated with the scaling solutions are uniform in space represents a peculiar feature of these collective oscillations. It implies, in particular, that as a consequence of the thermodynamic relationship $\nabla P = s\nabla T + n\nabla\mu$ and of the ansatz (5.10), the equations (3.3) and (3.4) for the superfluid velocity and for the current are exactly equivalent[3].

We now prove that the above scaling ansatz actually corresponds to an exact solution of the hydrodynamic equations. From the equation of continuity one finds the following relationship

$$[(2\dot{\alpha} + \dot{\gamma}) + (2\beta + \delta)]n_0 + (\beta + \dot{\alpha})\mathbf{r}_\perp \cdot \nabla_\perp n_0 + (\delta + \dot{\gamma}) z \nabla_z n_0 = 0, \tag{5.15}$$

which implies the identities

$$\dot{\alpha} = -\beta, \qquad \dot{\gamma} = -\delta. \tag{5.16}$$

The same conditions permit to satisfy the equation for the entropy density.

Since at equilibrium the chemical potential satisfies the condition $\nabla\mu_0(\mathbf{r}) = -m\omega_\perp^2 \mathbf{r}_\perp - m\omega_z^2 \mathbf{z}$ (see Eq. (3.3)), the equation for the superfluid velocity (or, equivalently, the equation for the total current) takes the simplified form

$$\dot{\beta}\mathbf{r}_\perp + \dot{\delta}\mathbf{z} \;=\; (e^{2\alpha+(2\alpha+\gamma)2/3} - 1)\omega_\perp^2 \mathbf{r}_\perp + (e^{2\gamma+(2\alpha+\gamma)2/3} - 1)\omega_z^2 \mathbf{z}. \tag{5.17}$$

By looking for time dependent solutions proportional to $e^{-i\omega t}$ and expanding the exponentials of Eq. (5.17) up to terms linear in α and γ, one finally derives the coupled equations

$$\omega^2 \alpha = \left(\frac{10}{3}\alpha + \frac{2}{3}\gamma\right)\omega_\perp^2, \tag{5.18}$$

and

$$\omega^2 \gamma = \left(\frac{4}{3}\alpha + \frac{8}{3}\gamma\right)\omega_z^2, \tag{5.19}$$

yielding the temperature independent result

$$\omega^2 = \left(\frac{5}{3} + \frac{4}{3}\lambda^2 \pm \frac{1}{3}\sqrt{16\lambda^4 - 32\lambda^2 + 25}\right)\omega_\perp^2, \tag{5.20}$$

for the collective frequencies, where $\lambda = \omega_z/\omega_\perp$ is the aspect ratio of the trap.

For isotropic trapping ($\lambda = 1$, i.e. $\omega_\perp = \omega_z \equiv \omega_{ho}$) the corresponding modes are the uncoupled monopole (breathing) mode with $\omega = 2\omega_{ho}$ and the surface quadrupole mode with $\omega = \sqrt{2}\omega_{ho}$. For highly elongated traps ($\lambda \ll 1$, i.e. $\omega_z \ll \omega_\perp$) the two solutions are instead $\omega = \sqrt{10/3}\omega_\perp$ and $\omega = \sqrt{12/5}\omega_z$, in agreement with the results already derived in the literature at zero temperature (see for example [106, 41]).

The above results provide a generalization of the theorem of [107], where it was shown that for isotropic trapping the monopole breathing mode of the unitary Fermi gas oscillates with frequency $\omega = 2\omega_{ho}$, independent of temperature. Differently from the case of [107] our results hold, however, only in the dissipationless hydrodynamic regime and in the limit of small amplitude oscillations. The temperature independence of the frequency of the scaling solutions of the unitary Fermi gas has been already confirmed in experiments [49, 53].

Let us also mention that the proof of the temperature independence of the frequency of the scaling solutions can be derived also for the $\ell_z = \pm 1$ and $\ell_z = \pm 2$ excitations, respectively. The velocity field corresponding to the excitation of the $\ell_z = \pm 1$ modes is characterized by velocity field proportional to $\nabla(zx)$, namely,

$$\mathbf{v} = \beta(t) z\hat{i} + \beta(t) x\hat{j} \ . \tag{5.21}$$

The corresponding scaling transformations for the density is:

$$n(x, y, z, t) = n_0(x + \alpha(t)z, y, z + \alpha(t)x) \ , \tag{5.22}$$

which satisfies the normalization condition of the density. The local entropy has the same scaling form as the density while the chemical potential exhibits the following scaling behavior independent of the specific equation of state:

$$\mu(x, y, z, t) = \mu_0(x + \alpha(t)z, y, z + \alpha(t)x) \ . \tag{5.23}$$

The above scaling ansatz is shown to be an exact solution of the hydrodynamic equations below. In view of the previous arguments, the independent equations are the continuity equation (3.1) and the velocity field equation (3.3) under the first sound ansatz. Inserting the Taylor expansion till the first order of the time evolution of the density and the chemical potential into Eqs. (3.1) and (3.3), respectively, we can get the following relationships:

$$\dot{\alpha} + \beta = 0, \quad \dot{\beta} = \alpha(\omega_\perp^2 + \omega_z^2), \tag{5.24}$$

yielding the temperature independent value

$$\omega = \sqrt{\omega_\perp^2 + \omega_z^2}, \tag{5.25}$$

for the collective frequency corresponding to the excitation of the combination of the $l_z = \pm 1$ modes. And analogously for the velocity field $v = \beta(t)\nabla(x^2 - y^2)$ of the excitation of the $l_z = \pm 2$ modes, the scaling transformation for the density is defined by:

$$n(x, y, z, t) = n_0(xe^{\alpha(t)}, ye^{-\alpha(t)}, z) \ , \tag{5.26}$$

obeying the normalization condition of the density. Hence the scaling behavior for the chemical potential is:

$$\mu(x, y, z, t) = \mu_0(xe^{\alpha(t)}, ye^{-\alpha(t)}, z) \ . \tag{5.27}$$

Following the similar strategy as the $l_z = \pm 1$ modes, we get the temperature independent frequency as below:

$$\omega = \sqrt{2}\omega_\perp. \tag{5.28}$$

Differently from the $\ell_z = 0$ solutions discussed above the results for the $\ell_z = \pm 1$ and $\ell_z = \pm 2$ are not restricted to the unitary Fermi gas, but simply require the applicability of the hydrodynamic equations, being solutions characterized by divergency free velocity fields (surface excitations). They hold in particular for both Fermi and Bose gases in the presence of harmonic trapping.

Furthermore, in the 1D geometry (considered in the thesis), there exists an exact scaling solution as well. In this geometry the velocity field of the breathing mode linearly depends on the axial coordinate. In the following, we show that the frequency for the breathing mode is invariant at different temperatures by applying proper scaling transformations. We know that for 3D Fermi gases at unitarity, one has $\mu = Tf(\frac{T}{n^{2/3}})$, so that the equilibrium density profile under the local density approximation is: $n(r_\perp, z) = T^{3/2}\left(f^{-1}(\frac{\mu_1(z)}{T} - \frac{m\omega_\perp^2 r_\perp^2}{2T})\right)^{-3/2}$, where f^{-1} denotes the inverse of the dimensionless function f and $\mu_1(z) = \mu_0^0 - m\omega_z^2 z^2/2$ with μ_0^0 being the chemical potential in the center of the trap. The 1D density profile is defined by:

$$n_1(z) = \int d\vec{r}_\perp n = T^{5/2} h(\frac{\mu_1(z)}{T}), \tag{5.29}$$

whose inversion gives the following expression for the chemical potential along the axial direction:

$$\mu_1(z) = n_1^{2/5} h^{-1}\left(\frac{n_1(z)}{T^{5/2}}\right). \tag{5.30}$$

For the axial breathing mode we make the scaling ansatz:

$$n_1(z,t) = e^{\alpha(t)} n_1^0(e^{\alpha(t)} z), \tag{5.31}$$

where the coefficient $e^{\alpha(t)}$ comes from the normalization condition, n_1^0 is the equilibrium density and

$$T(t) = T_0 e^{2/5\alpha(t)}, \tag{5.32}$$

where T_0 is the equilibrium temperature. The entropy has the same scaling transformation as density:

$$s_1(z,t) = e^{\alpha(t)} s_1^0(e^{\alpha(t)} z). \tag{5.33}$$

The velocity field of the axial breathing mode takes the form:

$$v_z = \beta(t) z. \tag{5.34}$$

Following the same strategy as the 3D case, we get an equation for the scaling parameters by substituting the scaled density into Eq. (4.4):

$$\dot{\alpha} + \beta = 0. \tag{5.35}$$

Concerning the velocity field equation (4.6), we need the 1D EOS for further simplification, in particular, the scaling form for the chemical potential. From Eq. (5.30) and the scaling ansatz for 1D density (5.31) and temperature (5.32) we obtain

$$\mu_1(z,t) = e^{2\alpha(t)/5}\mu_{10}(e^{\alpha(t)}z). \tag{5.36}$$

Following the similar procedure as in 3D case, we get from Eq. (4.6) the following:

$$\dot{\beta} - \frac{12}{5}\alpha\omega_z^2 = 0. \tag{5.37}$$

Taking into account Eq. (5.35), we get the result $\omega = \sqrt{\frac{12}{5}}\omega_z$.

The scaling solutions of the 3D configurations discussed above are characterized by temperature variations and by an axial velocity field v_z independent of the radial coordinates x and y. These are the conditions required, in general, to apply the 1D hydrodynamic equations in highly elongated configurations (see chapter 4) which have been recently successfully applied to describe the experimental results of [53, 36]. In general these 1D like conditions are ensured by the effective roles of the thermal conductivity and of the viscosity which cause the absence of gradients in the radial direction and are favored by the presence of a tight radial confinement as shown in chapter 4. In the case of the low frequency oscillations considered in the present work the absence of radial gradients is automatically ensured by the form of the scaling transformation. This explains, in particular, why the frequency $\omega = \sqrt{12/5}\omega_z$ of the axial breathing mode, here derived in a 3D framework in the highly elongated limit $\omega_z \ll \omega_\perp$, coincides with the predictions of the 1D hydrodynamic equations.

Let us finally discuss a non trivial implication of the scaling solutions concerning the behavior of the bulk viscosity coefficients. According to Khalatnikov [86] the entropy production per unit volume associated with a hydrodynamic flow is R/T, where R is the so-called dissipative function in the superfluid phase, defined by

$$\begin{aligned} R \;=\; & \frac{1}{2}\eta\left(\partial_k v_{ni} + \partial_i v_{nk} - \frac{2}{3}\delta_{ik}\nabla\cdot\mathbf{v}_n\right)^2 \\ & + 2\zeta_1 \nabla\cdot\mathbf{v}_n \nabla\cdot mn_s\left(\mathbf{v}_s - \mathbf{v}_n\right) + \\ & + \zeta_2\left(\nabla\cdot\mathbf{v}_n\right)^2 + \zeta_3\left[\nabla\cdot mn_s\left(\mathbf{v}_s - \mathbf{v}_n\right)\right]^2 \\ & + \left(\kappa/T\right)\left(\nabla T\right)^2 \ . \end{aligned} \tag{5.38}$$

Here the Einstein convention is used for the summation.

In the above equation η is the shear viscosity, ζ_1, ζ_2 and ζ_3 are the three bulk viscosity coefficients appearing in the superfluid phase, while κ is the thermal conductivity. For the scaling modes discussed in the present paper $\nabla T = 0$ and the velocity fields for the normal and superfluid components coincide. Furthermore, for the monopole breathing mode in an isotropic trap one has $\mathbf{v}_n = \mathbf{v}_s = \beta\mathbf{r}$ and the first term, proportional to the shear viscosity, identically vanishes. It follows that in this case only the term with ζ_2 survives. However, according to Castin's theorem [107] the dissipation associated with the breathing oscillation must be zero and we then conclude that $\zeta_2 = 0$. On the other hand the positiveness of R implies that $\zeta_1^2 \leq \zeta_2\zeta_3$. Thus also ζ_1 must vanish, the only surviving bulk viscosity coefficient being ζ_3. Above T_c, where one can introduce only one bulk viscosity term, the viscosity coefficient ζ should be also zero in order to ensure the absence of dissipation. The same results, concerning the value of the bulk viscosity coefficients, were previously derived by Son [109] using different considerations. Actually, our derivation provides a simple foundation to Son's heuristic argumentation.

5.3 Variational procedures for higher nodal collective modes

In the previous sections we have shown that at zero temperature the superfluid hydrodynamic equations (Sec. 5.1) can be solved exactly in the elongated harmonic trap for the collective modes. At finite temperatures one can identify the exact temperature-independent solutions only for the scaling modes characterized by a linear dependence of the velocity field on the spatial coordinates (Sec. 5.2). The solutions for the higher collective modes at finite temperatures are instead more difficult due to the complex thermodynamics of the strongly interacting fermions and the inhomogeneity induced by the trap. Easy solutions are available in the classical limit where only the normal fluid exists and $P = nk_BT$. Starting from the hydrodynamic equations in the normal phase regime:

$$\partial_t n_1 + \partial_z(n_1 v_z) = 0, \tag{5.39}$$

$$mn_1\partial_t v_z + \partial_z P + n_1\partial_z V_{ext} = 0, \tag{5.40}$$

$$\partial_t s_1 + \partial_z(s_1 v_z) = 0, \tag{5.41}$$

and taking the second derivative of Eq.(5.40), we get:

$$mn_1\partial_t^2 v_z + \partial_z\partial_t P + \partial_t n_1\partial_z V_{ext} = 0. \tag{5.42}$$

Using the EOS for classical gas and Eq.(5.39), we finally find

$$mn_1\partial_t^2 v_z - T\partial_z^2(n_1 v_z) + \partial_z(n_1\partial_t T) - \partial_z(n_1 v_z)\partial_z V_{ext} = 0. \tag{5.43}$$

To further simplify the velocity field equation (5.43), we need to know the time evolution behavior of the temperature. We find that $\partial_t T$ can be written in the form:

$$\frac{\partial T}{\partial t} = -n_1\left(\frac{\partial T}{\partial n_1}\right)_{\bar{s}_1}\frac{\partial v_z}{\partial z}. \tag{5.44}$$

In fact, by choosing the density and entropy per particle as independent variable, we have,

$$\partial_t T = (\partial T/\partial n_1)_{\bar{s}_1}\partial_t n_1 + (\partial T/\partial \bar{s}_1)_{n_1}\partial_t \bar{s}_1. \tag{5.45}$$

Recalling equations (5.39) and (5.41) for n_1 and s_1 we can write,

$$\partial_t T = -v_z\left[(\partial T/\partial n_1)_{\bar{s}_1}\nabla_z n_1 + (\partial T/\partial \bar{s}_1)_{n_1}\nabla_z \bar{s}_1\right] - n_1(\partial T/\partial n_1)_{\bar{s}_1} T\nabla_z v_z. \tag{5.46}$$

The term in the square brackets is zero since it corresponds to $\nabla_z T$ evaluated at equilibrium so that the final result for the temperature fluctuations reduces to Eq. (5.44). For a classical gas, Eq. (5.44) becomes,

$$\frac{\partial T}{\partial t} = -\frac{2}{5}T^0\frac{\partial v_z}{\partial z}, \tag{5.47}$$

where we have used the 1D adiabatic equation (2.29).

At unitarity (for all temperatures) the adiabatic derivative $n_1(\partial T/\partial n_1)_{\bar{s}_1}$ is equal to $2/3T$ in 3D and to $2/5T$ in 1D. It is worth noticing that result (5.44) is valid in general, not only for the unitary Fermi gas, for example it is valid along the BEC-BCS crossover although in this case the adiabatic derivative cannot be calculated in an easy way.

The gradient of the 1D density profile for the classical gas at equilibrium is readily available by adopting the classical EOS $P_1 = n_1 k_B T$ and applying the mechanical equilibrium condition within the local density approximation, i.e., $\nabla_z P_1 = -n_1 \nabla_z V_{ext}(z)$. Hence we have

$$\partial_z n_1 = \frac{\partial_z P_1}{k_B T} = -\frac{n_1}{k_B T} \partial_z V_{ext}(z). \tag{5.48}$$

Substituting Eq. (5.47) and Eq. (5.48) into Eq. (5.43), we get the equation of motion for the collective modes in terms of the velocity field for small deviations from the equilibrium state:

$$\begin{aligned} m\partial_t^2 v_z &= \frac{7}{5} k_B T \partial_z^2 v_z - \frac{7}{5} \partial_z V_{ext} \partial_z v_z - \partial_z^2 V_{ext} v_z \\ &= -\partial_z^2 V_{ext} v_z + \frac{1}{n_1} \partial_z \left[n_1 \left(\frac{\partial P_1}{\partial n_1} \right)_{\bar{s}_1} \partial_z v_z \right], \end{aligned} \tag{5.49}$$

holding for a classical gas. It's worth mentioning that Eq. (5.49) has a similar form as Eq. (5.9), suggesting the existence of a general equation of motion for the collective modes in terms of the velocity field. Taking the polynomial ansatz for the spatial dependence of the velocity field, i.e., $v_z(z,t) = e^{-i\omega t} \sum_k a_k z^k + a_{k-2} z^{k-2} + ...$, we get the following iteration relation:

$$\frac{a_{k+2}}{a_k} = \frac{7k + 5 - 5(\omega^2/\omega_z^2)}{7(k+1)(k+2)} \frac{m\omega_z^2}{k_B T}. \tag{5.50}$$

By truncating the polynomials to the k_{th} term in order to avoid nonphysical divergent solutions, we get the dispersion law:

$$\omega^2 = \frac{7k+5}{5} \omega_z^2. \tag{5.51}$$

At $k = 0$, $v_z(z) = a_0$, we find $\omega = \omega_z$. The result for the $k = 0$ mode follows from the universality of the center-of-mass oscillation in the presence of harmonic trapping. At $k = 1$, $v_z(z) = a_1 z$, $\omega^2 = \frac{12}{5}\omega_z^2$, consistent with the temperature independent result of the breathing mode. The fact that the frequency of the lowest axial breathing oscillation does not depend on temperature is a peculiarity of the unitary Fermi gas as discussed in Sec. 5.2. It is worth noting that Eqs. (5.7)

and (5.51) coincide for the dipole mode and the lowest axial breathing mode. The $k \geq 2$ results instead differ in the two limits revealing that these modes are more interesting because of the temperature dependence.

Though there exist exact solutions in the zero temperature limit and in the classical limit, for the higher modes ($k \geq 2$) solving Landau's two-fluid equations for trapped gases in general is difficult due to the inhomogeneity of the equilibrium thermodynamic quantities entering the equations, making a reliable 'brute force' numerical calculation very challenging [110, 90]. An alternate variational approach was developed by E. Taylor et al [58, 59, 60]. In this method, the involved quantities are the spatial integral of the thermodynamic quantities, making it simpler and more reliable than directly solving the differential two-fluid equations for trapped gases. We do not review the details of this technique, referring the reader to the Ph.D thesis of E. Taylor [111], where the variational approach to solve the two-fluid hydrodynamic equations in the trapped Fermi gases is described in an explicit way. The main idea is to derive an action $S_0^{(2)}$ to describe the fluctuations in the displacement fields $\mathbf{u}_s$, $\mathbf{u}_n$ defined by $\mathbf{v}_s \equiv \dot{\mathbf{u}}_s$ and $\mathrm{v}_n \equiv \dot{\mathbf{u}}_n$. By adopting physically reasonable ansatz for the displacement fields, the action can be written in terms of the variational parameters involved in the ansatz. The stationary condition for the action then gives the solutions of the linearized Landau two-fluid differential equations. The frequencies ω corresponding to the solutions of the two-fluid hydrodynamic equations (3.1)–(3.4) without dissipation, with time dependence proportional to $e^{-i\omega t}$, can then be derived using the variational procedure

$$\delta\omega^2/\delta\mathbf{u}_n = \delta\omega^2/\delta\mathbf{u}_s = 0, \tag{5.52}$$

where [60]:

$$\omega^2 = \frac{\int d\mathbf{r}\left[\frac{1}{n_0}(\frac{\partial P}{\partial n})_{\bar{s}}(\delta n)^2 + 2n_0(\frac{\partial T}{\partial n})_{\bar{s}}\delta n\delta\bar{s} + n_0(\frac{\partial T}{\partial \bar{s}})_n(\delta\bar{s})^2\right]}{m\int d\mathbf{r}\left[n_{s0}\mathbf{u}_s^2(\mathbf{r}) + n_{n0}\mathbf{u}_n^2(\mathbf{r})\right]} \tag{5.53}$$

and the displacement fields $\mathbf{u}_s$ and $\mathbf{u}_n$ are characterized by the density and entropy fluctuations according to $\delta n = -\nabla\cdot[n_{s0}\mathbf{u}_s + n_{n0}\mathbf{u}_n]$ and $\delta\bar{s} = -\mathbf{u}_n\cdot\nabla\bar{s}_0 + (\bar{s}_0/n_0)\nabla\cdot[n_{s0}(\mathbf{u}_s - \mathbf{u}_n)]$. The densities for the superfluid and normal fluid in the equilibrium state are denoted by n_{s0} and n_{n0}, respectively. As already anticipated, an approximate expression for the collective frequencies can be obtained within a variational

approach by adopting a simplified form of Rayleigh-Ritz method and make ansatz for the displacement fields of the form: $\mathbf{u}_s(\mathbf{r}) = a_{si} f_i(\mathbf{r})$, $\mathbf{u}_n(\mathbf{r}) = a_{ni} g_i(\mathbf{r})$, where the constant coefficients a_{si} and a_{ni} are the variational parameters. Inserting this ansatz into Eq. (5.53) and equating to zero the variation of the resulting expression with respect to these parameters, one can obtain approximate results for the collective modes.

The scheme above was developed for a 3D system and can be generalized to a 1D configurations. The 1D counterpart of Eq. (5.53) takes the form:

$$\omega^2 = \frac{\int dz \left[\frac{1}{n_1} \left(\frac{\partial P_1}{\partial n_1} \right)_{\bar{s}_1} (\delta n_1)^2 + 2 n_1 \left(\frac{\partial T}{\partial n_1} \right)_{\bar{s}_1} \delta n_1 \delta \bar{s}_1 + n_1 \left(\frac{\partial T}{\partial \bar{s}_1} \right)_{n_1} (\delta \bar{s}_1)^2 \right]}{m \int dz \, [n_{s1} u_s^2 + n_{n1} u_n^2]}, \tag{5.54}$$

and the hydrodynamic solutions are derived imposing the variational conditions,

$$\delta\omega^2/\delta u_n = 0, \quad \delta\omega^2/\delta u_s = 0. \tag{5.55}$$

Keeping $\bar{s}_1$ constant in the derivatives of Eq. (5.54) corresponds to considering 1D isentropic transformations. The density and entropy fluctuations δn_1 and $\delta \bar{s}_1$ with respect to equilibrium are given, in terms of the displacement fields $u_n(z)$ and $u_s(z)$, by $\delta n_1 = -\partial_z [n_{s1} u_s + n_{n1} u_n]$ and $\delta \bar{s}_1 = -u_n \partial_z \bar{s}_1 + (\bar{s}_1/n_1) \partial_z [n_{s1}(u_s - u_n)]$. We have dropped the superscript '0' to denote the equilibrium quantities. The 1D quantities with subscript '1' are obtained by radial integral of their corresponding 3D quantities within the local density approximation (see chapter 2). In App. A, repeating the 3D derivations, we actually show that the 1D variational equations (5.54)–(5.55) are exactly equivalent to the 1D two-fluid hydrodynamic equations (4.4)–(4.7). Equations (5.54)–(5.55) hold both in uniform and in trapped configurations. Actually for a uniform superfluid, it can be proved that the variational equations are identical to the standard Landau quadratic equations for the velocities c_i^2 of first and second sound given by Eq. (4.25), by adopting a plane wave ansatz for the displacement fields, namely $u_s(z) = a_s e^{iqz}$ and $u_n(z) = a_n e^{iqz}$ and taking the variational procedure with respect to the variational parameters a_s and a_n, respectively. The advantage of the variational methods is that it allows to get the approximate analytic sound solutions under suitable ansatz for the velocity field of the fluid, therefore revealing the physical nature of the solutions.

Let us now discuss the behavior of the discretized collective oscillations in the presence of axial harmonic trapping. The effect of the trapping potential enters through the position dependent thermodynamic functions at equilibrium. The use of the variational procedure is particularly convenient in trapped configurations where analytic solutions of the full hydrodynamic equations are not available. In analogy with the 3D strategy, we can get approximate expressions by making the following ansatz for the displacement fields:

$$u_s(z) = \sum_{l=0} a_l^s z^l, \quad u_n(z) = \sum_{l=0} a_l^n z^l, \tag{5.56}$$

where l is a non-negative integer and the constant coefficients a_l^s and a_l^n are the variational parameters. Inserting this ansatz into Eq. (5.54) and equating to zero the variation of the resulting expression with respect to these parameters, i.e., setting $\partial\omega^2/\partial a_l^s = 0, \partial\omega^2/\partial a_l^n = 0$, we can obtain explicit solutions for the collective frequencies.

We will implement the variational approach in Secs. 5.4 and 5.6, where we provide results for the discretized first and second sound modes, respectively. In particular in Sec. 5.4 we calculate the discretized frequencies which have been recently measured in [53, 54] as discussed in Sec. 5.5, while in Sec. 5.6 we discuss the behavior of the second sound solutions in the case of axially trapped configurations. The coupling between the two modes will be discussed in detail as well.

5.4 Higher-nodal collective modes of first sound nature at finite temperatures

In this section, we will illustrate the variational formalism under the so-called first sound ansatz, a simplified case, by assuming that the superfluid and the normal fluid move in phase with equal displacement fields i.e.,

$$u_s = u_n \equiv u. \tag{5.57}$$

This condition, which is exact for the scaling solutions as discussed in Sec. 5.2, will provide approximate predictions in the case of higher-nodal modes. Employing the

first sound ansatz (5.57), the expressions for the density fluctuations and the entropy fluctuations to be used in the variational calculation take the simplified form

$$\delta n_1 = -\partial_z \left[n_1 u \right], \tag{5.58}$$

$$\delta \bar{s}_1 = -u \partial_z \bar{s}_1. \tag{5.59}$$

Inserting the above two equations into Eq. (5.54), the expression for the integrals entering in the variational calculation can be simplified and after combining the terms in a proper way (App. B.1), takes the form:

$$\omega^2 = \frac{\int dz n_1 \left(\frac{\partial P_1}{\partial n_1} \right)_{\bar{s}_1} \left(\frac{\partial u}{\partial z} \right)^2}{\int dz m n_1 u^2} + \omega_z^2. \tag{5.60}$$

In the unitary Fermi gas, where the 1D thermodynamic relation $(\partial P_1/\partial n_1)_{\bar{s}_1} = 7/5\,(P_1/n_1)$ holds, Eq. (5.60) is further simplified to the following form:

$$\omega^2 = \frac{7}{5} \frac{\int dz P_1 \left(\frac{\partial u}{\partial z} \right)^2}{\int dz m n_1 u^2} + \omega_z^2. \tag{5.61}$$

In order to provide a simple quantitative prediction for the temperature dependence of the higher nodal collective modes, we implement the variational strategy developed in Sec. 5.3. Since the displacement field has the dimension of length, we take the following ansatz:

$$u = R_z \sum_l X_l z'^l, \tag{5.62}$$

where $z' = z/R_z$ and l takes either odd values: 1, 3,... or even values: 0, 2,... in view of the parity of the displacement field and $R_z \equiv \sqrt{\frac{2k_B T}{m\omega_z^2}}$ at finite temperature to achieve dimensionless equations (in the case of zero temperature, see App. B.2). Carrying out the variation with respect to the parameters X_k characterizing the displacement fields, after a lengthy but straightforward algebra (see App. B.2) we find the following equation:

$$\sum_l [(\frac{\omega^2}{\omega_z^2} - \frac{7k+5}{5}) \frac{2}{k+l+1} M_{k+l} + \frac{7k(k-1)}{5} \frac{1}{k+l-1} H_{k+l}] X_l = 0, \tag{5.63}$$

where,

$$M_{k+l} = \int_{-\infty}^{\beta\mu_0} dx(\beta\mu_0 - x)^{\frac{k+l+1}{2}} f_n(x), \tag{5.64}$$

and

$$H_{k+l} = \int_{-\infty}^{\beta\mu_0} dx(\beta\mu_0 - x)^{\frac{k+l-1}{2}} f_p(x), \tag{5.65}$$

with the universal functions $f_n(x)$ and $f_p(x)$ defined in chapter 2. Since $f_p'(x) = f_n(x)$ at constant temperature, we get the recursion relation between M_{k+l} and H_{k+l} by applying partial integration to (5.65):

$$M_{k+l} = \frac{k+l+1}{2} H_{k+l}. \tag{5.66}$$

Equation (5.63) is a matrix equation of the form: $\sum_l C_l(\omega/\omega_z)X_l = 0$, with $C_l(\omega/\omega_z)$ representing the coefficient vectors as a function of the frequency. By requiring the determinant of the coefficient matrix be zero, we obtain the eigenfrequency ω; from the vectors X_l we get the density fluctuation according to Eqs. (5.58) and (5.62) as will be shown in the followings. One can see that when $k = l = 0$, corresponding to $u = const$, we recover the frequency for dipole mode ($\omega = \omega_z$); when $k = l = 1$, corresponding to $u \propto z$, we recover the frequency for axial breathing mode ($\omega^2 = \frac{12}{5}\omega_z^2$). For the higher modes, it is hard to solve exactly in general we can test the validity of the Eq. (5.63) in both the $T = 0$ limit (Sec. 5.1) and high T limit (in the beginning of Sec. 5.3) where we already know the exact results.

Let us now calculate the moments of the density which are crucial ingredient of Eq. (5.63). As indicated by Eq. (2.21), **at zero temperature**, we already know the universal function of $f_n(x) = \frac{(4\pi/\xi)^{3/2}}{3\pi^2} x^{3/2}$ for $x > 0$ and zero elsewhere. Inserting it into Eq. (5.63), we get:

$$\begin{aligned} M^0_{k+l} &= \frac{(4\pi/\xi)^{3/2}}{3\pi^2} \int_0^1 dx'(1-x')^{\frac{k+l+1}{2}} x'^{\frac{3}{2}} \\ &= \frac{k+l+1}{2} \frac{(4\pi/\xi)^{3/2}}{3\pi^2} \frac{\Gamma(\frac{5}{2})\Gamma(\frac{k+l+1}{2})}{\Gamma(4+\frac{k+l}{2})}, \end{aligned} \tag{5.67}$$

suggesting (according to Eq. (5.66)),

$$H^0_{k+l} = \frac{(4\pi/\xi)^{3/2}}{3\pi^2} \frac{\Gamma(\frac{5}{2})\Gamma(\frac{k+l+1}{2})}{\Gamma(4+\frac{k+l}{2})}, \tag{5.68}$$

where $x' = x/(\mu_0/k_BT)$ and M^0_{k+l}, H^0_{k+l} are the corresponding moments at zero temperature (see App. B.2). Taking these two expressions into account, the general sum terms in Eq. (5.63) can be rewritten as:

$$(\frac{\omega^2}{\omega_z^2} - \frac{7k+5}{5} - \frac{k(k-1)}{5})H^0_{k+l} + \frac{k(k-1)}{5}H^0_{k+l-2}. \tag{5.69}$$

Since according to the property of a determinant, whenever two columns (or rows) of a matrix are identical, or more generally some column (or row) can be expressed as a linear combination of the other columns, its determinant is 0, we require that $\frac{\omega^2}{\omega_z^2} - \frac{7k+5}{5} - \frac{k(k-1)}{5} = 0$ in order to make the determinant of the coefficient matrix be zero. Therefore, the variational solution at zero temperature reproduces exactly the frequencies (5.7) in the $T = 0$ limit.

In the classical limit, we know, from Eq. (2.23), the expression for the universal function: $f_n(x) = 2e^x$ (we will discuss the contributions from higher order virial terms later in this section). Analogously, we get the moments

$$\begin{aligned} M_{k+l} &= \int_{-\infty}^{x_0} dx(x_0 - x)^{\frac{k+l+1}{2}} 2e^x \\ &= \frac{k+l+1}{2} 2e^{x_0}\Gamma(\frac{k+l+1}{2}), \end{aligned} \tag{5.70}$$

and

$$H_{k+l} = 2e^{x_0}\Gamma(\frac{k+l+1}{2}). \tag{5.71}$$

Therefore, in the classical limit, the general sum terms in Eq. (5.63) can be rewritten as:

$$(\frac{\omega^2}{\omega_z^2} - \frac{7k+5}{5})H_{k+l} + \frac{7}{10}k(k-1)H_{k+l-2}, \tag{5.72}$$

and the determinant of the coefficients is zero when $\frac{\omega^2}{\omega_z^2} = \frac{7k+5}{5}$, reproducing exactly the frequencies (5.51) in the high T limit.

In the intermediate temperature regime, there are no simple analytical solutions to the higher mode frequency and the displacement field since the universal functions $f_n(x)$ and $f_p(x)$ are not simple analytic functions. In order to provide a simple quantitative prediction for the temperature dependence of the frequencies we

adopt the variational approach discussed above and we will focus on the $k = 2$ and $k = 3$ modes in the followings.

For the $k = 2$ mode, we assume a displacement field of the form $u = R_z(X_0 + X_2 z'^2)$, i.e., we truncate the polynomial expansion (5.62) up to the second order, namely, the integers $k, l = 0, 2$. We show that our prediction for the frequency is practically not sensitive to the the inclusion of higher order terms in the polynomial expansion for the velocity field in Apps. C and D. Under this approximation, Eq. (5.63) turns out to be:

$$\begin{bmatrix} (\frac{\omega^2}{\omega_z^2} - 1)M_0 & \frac{1}{3}(\frac{\omega^2}{\omega_z^2} - 1)M_2 \\ \frac{1}{3}(\frac{\omega^2}{\omega_z^2} - 1)M_2 & \frac{1}{5}(\frac{\omega^2}{\omega_z^2} - \frac{43}{15})M_4 \end{bmatrix} \begin{bmatrix} X_0 \\ X_2 \end{bmatrix} = 0, \tag{5.73}$$

where we have used the recursion relation (5.66) to replace the moments of pressure by the moments of the density. One trivial solution for the above equation is $\frac{\omega^2}{\omega_z^2} = 1$, $X_2 = 0$, corresponding to the dipole mode. The nontrivial solution is given by:

$$\omega_{k=2}^2 = \frac{129t_2 - 25}{45t_2 - 25}\omega_z^2, \tag{5.74}$$

$$\frac{X_0}{X_2} = -\frac{M_2}{3M_0}, \tag{5.75}$$

where $t_2 \equiv M_0 M_4 / M_2^2$. In the zero temperature and in the classical limits, we get $t_2 = 4/3,\ 5/3$, available from Eq. (5.67) and Eq. (5.70), respectively. This ansatz reproduces exactly the frequencies in both the $T = 0$ (5.7) and high T (5.51) limits. Similarly, for the $k = 3$ mode, we take the assumption $u = R_z(X_1 z' + X_3 z'^3)$ for the displacement field and the corresponding solutions are given by:

$$\omega_{k=3}^2 = \frac{440t_3 - 252}{5(25t_3 - 21)}\omega_z^2, \tag{5.76}$$

$$\frac{X_1}{X_3} = -\frac{3}{5}\frac{M_4}{M_2}, \tag{5.77}$$

where $t_3 \equiv M_2 M_6 / M_4^2$. In the zero temperature and the classical limits, we get $t_3 = 7/6,\ 7/5$, respectively, therefore reproduce also in this case the frequencies in both the $T = 0$ (5.7) and high T (5.51) limits for the $k = 3$ mode.

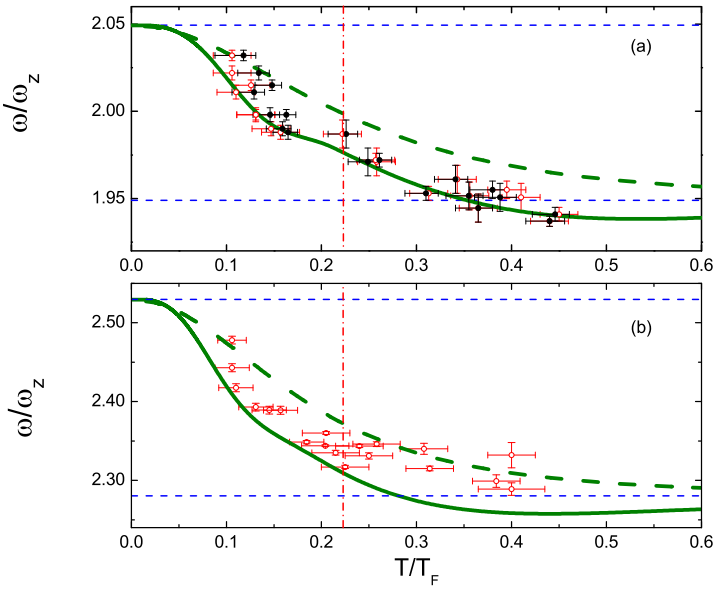

Figure 5.2: Frequency for the $k = 2$ (upper panel) and $k = 3$ (lower panel) first sound collective modes. Experiment data are from [53, 54]. The green lines are the theoretical predictions based on Eqs. (5.74) and (5.76) using the equation of state of the unitary (solid) and ideal (dashed) Fermi gas. The thin horizontal dashed lines mark the zero-T superfluid limit (5.7) and the classical hydrodynamic limit (5.51), respectively. The red dash-dot vertical lines in (a) and (b) indicate the critical temperature. In this figure and Fig. 5.3 the Fermi temperature corresponds to the definition $T_F^{trap} = (3N)^{1/3}\hbar\bar{\omega}_{ho}/k_B$ introduced in the text.

At finite temperature, for simplicity, we express the moments of density as

$$M_l = \int_{-\infty}^{x_0} dx (x_0 - x)^{\frac{l+1}{2}} f_n(x), \tag{5.78}$$

where x_0 is related to the value of T/T_F^{trap} by Eq. (2.42). The integrals can be calculated using the data for the thermodynamic function $f_n(x)$ discussed in chapter 2 which include the proper interpolation between the experimental data from [55], the low temperature phonon regime as well as the classical regime, relevant to describe the low density region on the tails. The resulting predictions for the temperature dependence of the frequencies are shown in Fig. 5.2 and are denoted by the green solid line, together with the asymptotic zero temperature and classical values

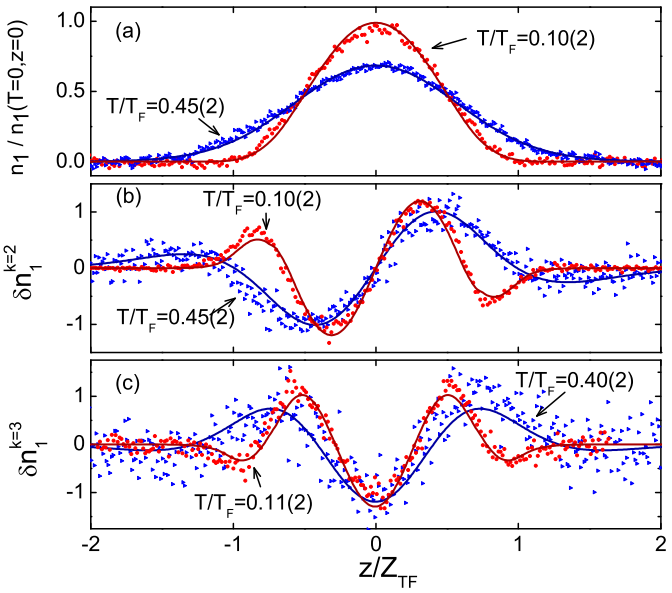

Figure 5.3: Equilibrium profiles (upper figure) and density oscillations for the $k = 2$ (middle figure) and the $k = 3$ (lower figure) first sound collective modes at different temperatures. See Fig. 5.2 for the definition of the Fermi temperature. From Ref. [54].

marked by the thin horizontal dashed lines. The results are plotted as a function of T/T_F^{trap}.

Using the same ansatz for the velocity field determined by Eqs. (5.75) and (5.77) and the equation of continuity we can also calculate **the density fluctuations** of each mode given by $\delta n_1 = -\partial_z[n_1 u]$. Since the 1D density profile $n_1(z)$ is related to the pressure at point $(\mathbf{r}_\perp = 0, z)$ by Eq. (2.25) and the normalized displacement field for the $k = 2$ mode is given by $u \propto (1 - \frac{3M_0(x_0)}{M_2(x_0)} z'^2)$, the mode profile for the $k = 2$ mode can be obtained as:

$$\delta n_{k=2} = -\partial_z[n_1 u] \propto \frac{\partial f_p}{\partial z'} u + \frac{\partial u}{\partial z'} f_p \propto 3\frac{M_0}{M_2} z'^3 f_n - (f_n + 3\frac{M_0}{M_2} f_p) z', \tag{5.79}$$

where the moments M_l are given by Eq. (5.78). Similarly, the mode profile of the $k = 3$ mode can be shown to be

$$\delta n_{k=3} \propto \frac{10}{3}\frac{M_2}{M_4} f_n z'^4 - (2f_n + 5\frac{M_2}{M_4}) z'^4 + f_p. \tag{5.80}$$

The normalized 1D profile of a unitary Fermi gas is given by

$$\frac{n_1(z')}{n_1(z'=0,T=0)} = \frac{15\pi^{1/2}}{8}\xi^{1/4}(\frac{T}{T_F^{trap}})^{5/2} f_p(x_0 - z'^2). \tag{5.81}$$

Here the 1D density profile is normalized by the zero-temperature density of the unitary Fermi gas with the same number of atoms: $n_1(z'=0,T=0) = \frac{8N}{5\pi Z_{TF}}$, where Z_{TF} is the Thomas Fermi radius for the unitary Fermi gas[4]. In Fig. 5.3 we show the density profile and the density fluctuations of the $k=2$ and the $k=3$ modes. As shown, the higher mode has richer nodal structure than the elementary modes of the same parity. We will discuss the comparison with the experimental observations later in section 5.5. In addition to the density fluctuations, we can get the temperature fluctuations of first sound solutions as well. They are given by $\partial_t T = -n_1(\partial T/\partial n_1)_{\bar{s}_1}\nabla_z v_z$ (see Eq. (5.44)) already discussed in Sec. 5.3.

Virial correction As shown in Fig. 5.2, the temperature dependence of the frequencies in the higher temperature region exhibits non monotonic behavior. In the followings, we show that this is caused by the presence of the higher virial corrections into the equation of state at lower temperatures below the classical limit. In general, the phase-space density can be expanded in terms of the fugacity as given in Eq. (2.23),

$$f_n(x) = 2\sum_{j=1}^{\infty} j b_j e^{jx}. \tag{5.82}$$

Hence the moment of density is:

$$M_l = 2\sum_{j=1}^{\infty} j b_j \int_{-\infty}^{x_0} dx (x_0 - x)^{\frac{l+1}{2}} e^{jx} = 2\sum_{j=1}^{\infty} b_j j^{-\frac{l+1}{2}} \mathsf{z}_0^j \Gamma(1 + \frac{l+1}{2}), \tag{5.83}$$

where z_0 is the fugacity in the trap center. In the high temperature regions, $x = \mu/k_B T$ is very large and negative, making the fugacity $\mathsf{z} \equiv e^x \ll 1$. So in deriving Eqs. (5.70)–(5.72), we keep only the first order virial terms. When the temperature

[4]For convenience, we use the Thomas Fermi radius for the unitary Fermi gas $Z_{TF} = \sqrt{\frac{2\xi^{1/2}\epsilon_F^{trap}}{m\omega_z^2}}$ or its finite temperature analogue' $R_z = \sqrt{\frac{2k_B T}{m\omega_z^2}}$ as *Length* scales. They are related to each other by $\frac{R_z}{Z_{TF}} = \frac{1}{\xi^{1/4}}\sqrt{\frac{T}{T_F^{trap}}}$ at finite temperature.

is lowered, higher order terms should be included [69]. In general, the ratio of the moments entering the $k = 2$ mode is:

$$\begin{aligned} t_2 &= \frac{M_0 M_4}{M_2^2} \\ &= \frac{5}{3}\frac{(\sum_{j=1}^{\infty} b_j j^{-\frac{1}{2}} z_0^{j-1})(\sum_{j=1}^{\infty} b_j j^{-\frac{5}{2}} z_0^{j-1})}{(\sum_{j=1}^{\infty} b_j j^{-\frac{3}{2}} z_0^{j-1})^2}. \end{aligned} \tag{5.84}$$

Let us first take into account up to the second virial terms and keep only the leading term of the fugacity in the expansion of t_2:

$$\begin{aligned} t_2 &= \frac{5}{3}\frac{(1 + b_2 2^{-\frac{1}{2}} z_0)(1 + b_2 2^{-\frac{5}{2}} z_0)}{(1 + b_2 2^{-\frac{3}{2}} z_0)^2} \simeq \frac{5}{3}(1 + \frac{b_2 z_0}{4\sqrt{2}}) \\ &= \frac{5}{3}(1 + \Delta t_2). \end{aligned} \tag{5.85}$$

The first term comes from the first order virial expansion and the second term $\Delta t_2 = \frac{b_2 z_0}{4\sqrt{2}}$ is the correction due to the second order terms. Correspondingly, the frequency of the $k = 2$ mode is modified as below:

$$\frac{\omega_{k=2}^2}{\omega_z^2} = \frac{129 t_2 - 25}{45 t_2 - 25} \simeq \frac{19}{5} - \frac{7}{5}\frac{b_2 z_0}{4\sqrt{2}}. \tag{5.86}$$

As can be seen, due to the second order correction, the frequency is reduced below the classical value $\frac{\omega_{k=2}^2}{\omega_z^2} = \frac{19}{5}$ as T decreases ($b_2 = \frac{3\sqrt{2}}{8} > 0$ [80]).

Working to the third order and keeping the corresponding leading terms of the fugacity in the expansion of t_2, we have

$$\begin{aligned} t_2 &= \frac{5}{3}\frac{(1 + b_2 2^{-\frac{1}{2}} z_0 + b_3 3^{-\frac{1}{2}} z_0^2)(1 + b_2 2^{-\frac{5}{2}} z_0 + b_3 3^{-\frac{5}{2}} z_0^2)}{(1 + b_2 2^{-\frac{3}{2}} z_0 + b_3 3^{-\frac{3}{2}} z_0^2)^2} \\ &\simeq \frac{5}{3}(1 + \frac{b_2 z_0}{4\sqrt{2}} + (\frac{4 b_3}{9\sqrt{3}} - \frac{b_2^2}{8}) z_0^2) \\ &= \frac{5}{3}(1 + \Delta t_2 + \Delta t_3), \end{aligned} \tag{5.87}$$

where, $\Delta t_3 = (\frac{4 b_3}{9\sqrt{3}} - \frac{b_2^2}{8}) z_0^2$. The first term comes from the first order virial expansion and the second and the third terms are the second and the third correction, respectively. Therefore, the corresponding frequency is

$$\frac{\omega_{k=2}^2}{\omega_z^2} \simeq \frac{19}{5} - \frac{7}{5}\left[\frac{b_2 z_0}{4\sqrt{2}} - (\frac{-4 b_3}{9\sqrt{3}} + \frac{b_2^2}{8}) z_0^2\right]. \tag{5.88}$$

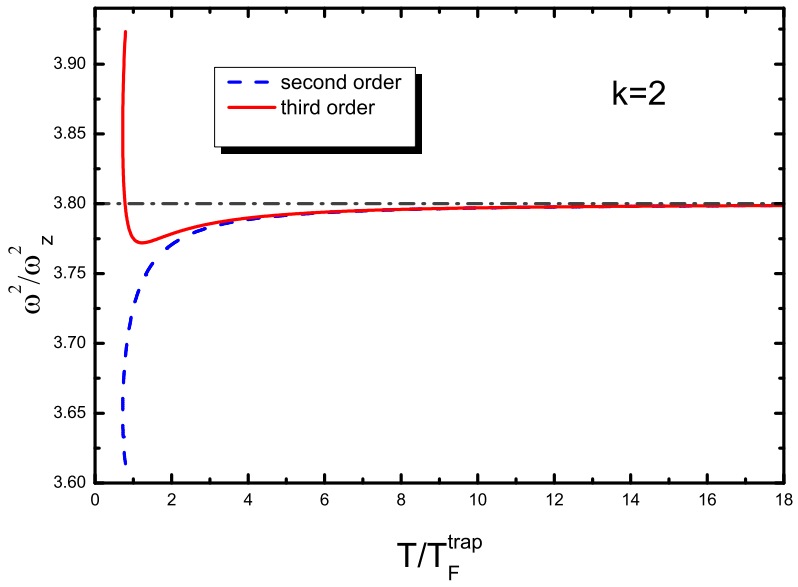

Figure 5.4: The square frequency for the $k = 2$ mode given by the 2×2 matrix in the high T regime by considering the higher order virial corrections. The dashed line corresponds to the second order correction. The solid line includes the third order correction. In the high temperature regime, the frequency is reduced below its classical value 19/5 (indicated by the dash-dotted line) as the temperature decreases.

We denote the square frequency shift due to the higher virial correction as $\delta\epsilon \equiv -\frac{7}{5}[\frac{b_2 z_0}{4\sqrt{2}} - (\frac{-4b_3}{9\sqrt{3}} + \frac{b_2^2}{8})z_0^2]$. It's known that $b_2 = \frac{3\sqrt{2}}{8} > 0$ [80] and $b_3 = -0.29 < 0$ [81], so the second and the third order virial correction compete, but as shown in Fig. 5.4, for small values of the fugacity, i.e., at high temperature, the second order correction of course dominates. $\delta\epsilon < 0$ due to the second order correction, the frequency is reduced below the classical value as T decreases within the range of small fugacity. The same scenario holds for the $k = 3$ mode as shown in Fig. 5.5.

The variational procedure $\delta\omega^2/\delta u = 0$, under the first sound ansatz, yields the following equation for the displacement field:

$$m\omega^2 u = \nabla_z^2 V_{ext} u - \frac{1}{n_1}\nabla_z \left[n_1 \left(\frac{\partial P_1}{\partial n_1} \right)_{\bar{s}_1} \nabla_z u \right], \tag{5.89}$$

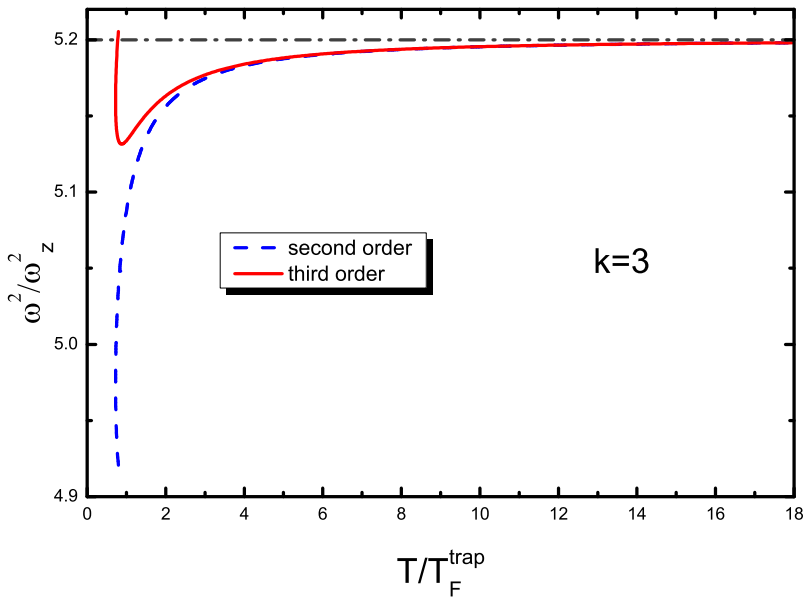

Figure 5.5: The square frequency for the $k = 3$ mode given by the 2×2 matrix in the high T regime by considering the higher order virial corrections. The dashed line corresponds to the second order correction. The solid line includes the third order correction. Its classical value (26/5) is represented by the dash-dotted line.

a generalized form for the equation of motion in the $T = 0$ (5.9) and the classical limit (5.49). In both cases, it is immediate to find the polynomial solutions of the hydrodynamic equation (5.89). Actually, starting from this equation, we can recover the previous results concerning the in-phase motion of the two-fluid. For instance, for axially uniform configurations, we recover the adiabatic expression of first sound $mc_1^2 = \frac{7}{5}\frac{P_1}{n_1}$ (4.26) discussed in Sec. 4.2 by setting $\omega_z = 0$ in Eq. (5.89). In the presence of axial harmonic trapping, exact numerical solutions of Eq. (5.89) for the temperature dependence of the frequency of the $k = 2$ and the $k = 3$ modes are presented in App. D [112] and turn out practically indistinguishable from the approximate results obtained in this section.

5.5 Experimental excitation and observations

In this section, first, we briefly describe the experimental procedures carried out by the Innsbruck team [53, 54] and then compare the experimental results with the main theoretical predictions for the two different higher-nodal modes. Experiment is carried out on a mixture of fermionic ^6Li atoms in two hyperfine states trapped in an elongated harmonic potential. The atoms are cooled well below degeneracy on top of the broad Feshbach resonance at 834 Gauss where the scattering length diverges. The lowest temperature achieved in the experiment is around $0.1T_F^{trap}$ (deep in the superfluid regime) and the highest temperature explored in the experiment is around $0.45T_F^{trap}$, corresponding to rather closely the classical hydrodynamic case. An almost perfect harmonic confinement along the long trap axis (z axis) is ensured by the magnetic trapping that results from the curvature of the magnetic field used for the Feshbach tuning [98]; Also, anharmonicities in the radial confinement remain negligibly small, indicating that the experimental setup and the theoretical conditions match well with each other. The thermometry is also under control. In the experiment, two methods have been adopted, i.e., the wing-fit method and the potential-energy method to fit the temperature ([53, 54]), which, in general showed satisfying agreement with each other.

The higher-nodal modes ($k = 2$ and $k = 3$ modes) could be efficiently excited using a resonant local excitation scheme. A repulsive 532-nm laser beam perpendicularly intersects the trapping beam, with its position and size chosen in a way to provide best mode matching. The power, length, and shape of the excitation pulse are optimized in order to resonantly drive the desired small amplitude oscillation. The one-dimensional axial density profiles $n_1(z)$ are recorded by near in situ absorption imaging and sensitively analyzed by a Fourier transformation of the detected time evolution of the axial density profile. The experimental results are given in Fig. 5.2. For the $k = 2$ mode, the comparison between the theoretical predictions and the corresponding experimental data remarkably agree with each other. The excellent agreement of the experimentally observed mode frequencies with the theoretical predictions provides a stringent test for the validity of this 1D approach and provides an independent confirmation of the recently measured EOS [55] of the resonantly interacting Fermi gas. At the lowest temperature realized in

the experiment ($T/T_F^{trap} \approx 0.1$), the frequency lies close to the $T = 0$ superfluid limit ($\omega_{k=2}/\omega_z = 2.049$), but already shows a significant down-shift amounting to almost 1%. This illustrates the high sensitivity of the mode frequency to finite-temperature effects. At the highest temperatures ($T/T_F^{trap} \approx 0.45$) the experimental data show a clear trend to go below the asymptotic high-temperature value ($\omega_{k=2}/\omega_z = 1.949$), which corresponds to the classical hydrodynamic case. This non-monotonic temperature dependence is consistent with the higher-order virial expansions discussed above. For the $k = 3$ mode, the general behavior is very similar to the $k = 2$ mode, with the main difference that the relative frequency change from superfluid to collisional hydrodynamics ($\omega_{k=2}/\omega_z = 2.530$ and 2.280, respectively) is about two times larger. For temperatures below $0.2T_F$ the agreement is similarly good as in the $k = 2$ case. However, for higher temperatures there is a significant trend to lie above the predicted frequencies. This discrepancy is most likely due to dissipative effects, which manifest themselves in mode damping and we will be discuss damping effects in chapter 6.

5.6 Discretized collective modes of second sound nature

Second sound corresponds to an out-of-phase oscillation of the normal and superfluid components of the fluid. The out-of-phase oscillations, which are the analogue in trapped gases of second sound in uniform superfluids, have so far not been observed in strongly interacting Fermi gases, although there are some theoretical proposals to observe these modes via two-phonon Bragg scattering or by density perturbations (the spectrum of the Bragg scattering is related to the imaginary part of density response function) [60].

We will discuss our predictions using the quasi-1D hydrodynamic formalism in the experimentally-favored geometry. As a first ansatz for the second sound discrete modes, we assume that the total current be zero ($j_z = mn_{n1}v_n^z + mn_{s1}v_s^z = 0$), which implies that the oscillation corresponds to a pure temperature (or entropy) oscillation, without any fluctuation of the density. The coupling of this mode with the first sound solutions discussed in the previous sections will be discussed in detail

later. Under the assumption that the total current vanishes, the expression (5.54) for the frequency of second sound to be used in the variational calculation takes the simplified form:

$$\omega^2 = \frac{\int dz \left(\frac{\partial T}{\partial s_1}\right)_{n_1} \left[\frac{\partial}{\partial z}\left(\frac{u_s s_1 n_{s1}}{n_{n1}}\right)\right]^2}{\int dz m \frac{n_{s1} n_1}{n_{n1}} u_s^2}, \tag{5.90}$$

and the variational condition $\delta\omega^2/\delta u_s = 0$ yields the following equation for the displacement field of the superfluid component:

$$\omega^2 u_s = -\frac{s_1}{m n_1^2}\frac{\partial}{\partial z}\left[\left(\frac{\partial T}{\partial \bar{s}_1}\right)_{n_1}\frac{\partial}{\partial z}\left(\frac{s_1 n_{s1} u_s}{n_{n1}}\right)\right]. \tag{5.91}$$

The above equations reveal that the key thermodynamic quantities characterizing the propagation of second sound are the 1D density, entropy, specific heat and superfluid density. The presence of axial trapping is indirectly present through the value of the equilibrium quantities. As discussed in Sec. 4.4, at present, the theoretical knowledge of n_s is rather poor in the unitary Fermi gas. In the following we will make use of simple ansatz for n_s (4.27) and (4.28) in order to provide a first estimate of the frequency of the second sound oscillations.

From Eq. (5.91) one immediately recovers the second sound velocity for an axially uniform system by considering a plane wave solution of the form e^{iqz} for u_s. One finds $\omega = c_2 q$ with $m c_2^2 = T \frac{\bar{s}_1^2}{\bar{c}_{v_1}} \frac{n_{s1}}{n_{n1}}$, consistent with Eq. (4.23).

In the presence of harmonic trapping along the z-th direction, the second sound modes are discretized. In principle, it's possible to solve the differential equation (5.91) numerically. However, this involves non trivial thermodynamic quantities. In particular, the appearance of the unavoidable derivative of the specific heat (in some sense, the derivative of the MIT experiment data [55] is required) makes the control of the ingredients of the equations challenging. So we resort to the variational approach (5.90), whose solution requires no numerical derivatives of the specific heat, to obtain first estimates for the collective frequencies by assuming the polynomial ansatz for the superfluid displacement field:

$$u_s = \sum_l a_{sl} z^l. \tag{5.92}$$

Then the normal fluid velocity field is given by

$$u_n = -\frac{n_{s1}}{n_{n1}} u_s = -\sum_l a_{sl} \frac{n_{s1}}{n_{n1}} z^l, \tag{5.93}$$

where l takes either even $(0, 2, ...)$ or odd values $(1, 3, ...)$. Minimizing the frequency by taking variation with respect to a_{sk}, we get:

$$\sum_l [\omega^2 A_{k,l} - B_{k,l} - \frac{k+l}{2} C_{k,l} - klD_{k,l}] a_{sl} = 0, \tag{5.94}$$

where

$$A_{k,l} = m \int dz n_1 \frac{n_{s1}}{n_{n1}} z^{k+l}, \tag{5.95}$$

$$B_{k,l} = \int dz (\frac{\partial T}{\partial s_1})_{n_1} (\frac{\partial s_1 n_{s1}/n_{n1}}{\partial z})^2 z^{k+l}, \tag{5.96}$$

$$C_{k,l} = \int dz (\frac{\partial T}{\partial s_1})_{n_1} \frac{\partial}{\partial z} (s_1 n_{s1}/n_{n1})^2 z^{k+l-1}, \tag{5.97}$$

$$D_{k,l} = \int dz (\frac{\partial T}{\partial s_1})_{n_1} (s_1 \frac{n_{s1}}{n_{n1}})^2 z^{k+l-2}, \tag{5.98}$$

which can be expressed in terms of the dimensionless chemical potential $x = \beta\mu_0 - \frac{\beta}{2} m\omega_z^2 z^2$ within local density approximation in order to make direct use of the universal thermodynamic functions investigated in chapter 2.

The lowest frequency mode of second sound nature is expected to be of dipolar nature for which we make the simplifying assumption that the displacement field u_s of the superfluid component is constant in space and u_n is fixed by the condition $n_s u_s + n_n u_n = 0$ of vanishing total current. Including only the term $l = k = 0$ in Eq. (5.94), we obtain the simplest expression $\omega^2 = B_{0,0}/A_{0,0}$. In Fig. 5.6 we show the resulting prediction for the temperature dependence of the lowest second sound mode, using the two models for the superfluid density given by Eqs. (4.27) and (4.28). We have checked that the inclusion of higher order terms in the polynomial ansatz for u_s introduces minor corrections (less than 10 %, see Fig. 5.7). However,

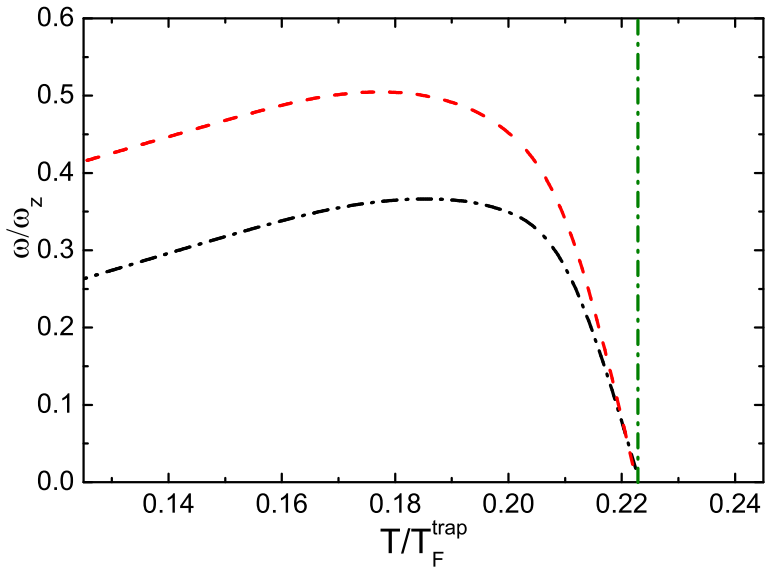

Figure 5.6: Frequency for the lowest discretized second sound mode in an axially trapped configuration with $\omega_z \ll \omega_\perp$. Two different models for the superfluid density are used: the phenomenological ansatz: $n_s/n = 1 - (T/T_c)^4$ (the red dashed-line) and $n_s/n = (1 - T/T_c)^{2/3}$ (the black dash-dotted-line). The vertical green line indicates the critical temperature.

we have checked that the convergence of higher order modes of second sound nature is not as good as for the dipole mode.

Notice that in Fig. 5.6, an important feature of the second sound frequency is that it vanishes when the temperature approaches the critical value, as a consequence of the vanishing of the superfluid density at T_c. This result differs from the one predicted in 3D isotropic configurations [60, 90] and can be understood noticing that an estimate for the discretized frequency can be obtained using the expression $\omega \sim c_2 q$ with $q \sim 1/R_{s,z}$ where $R_{s,z}$ is the size of the superfluid along the z-th direction. On the other hand the main temperature dependence of the second sound velocity, as $T \to T_c$, is given by the the 1D superfluid velocity that behaves like $\sqrt{n_{s1}} \sim \sqrt{n_s R_{s,\perp}^2}$ and is hence proportional to the square root of the bulk superfluid density calculated in the center of the trap and the size of the superfluid

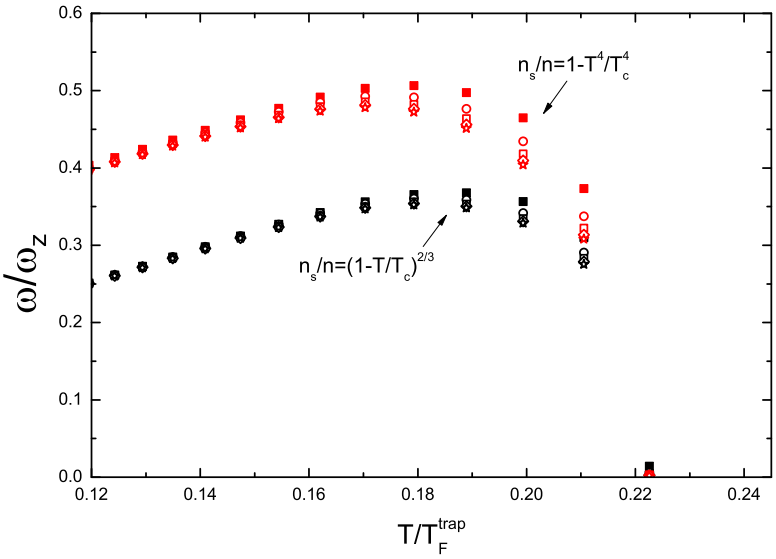

Figure 5.7: Convergence of the out-of-phase dipole mode. From top to bottom, the orders of the polynomials for the superfluid displacement field are: $0, 2, 4, 6, 8$.

along the radial direction. Since the ratio $R_{s,\perp}/R_{s,z}$ in the LDA is given by $\frac{\omega_z}{\omega_\perp}$ and n_s vanishes as one approaches the transition temperature, the second sound frequencies will vanish too.

We can estimate the temperature fluctuations under the second sound ansatz. For the entropy fluctuation (4.5), we have:

$$\frac{\partial \delta s_1}{\partial t} = -\partial_z(s_1^0 v_n^z) = \partial_z(v_s \frac{s_1^0 n_{s1}}{n_{n1}}). \tag{5.99}$$

So the temperature-fluctuation is determined by:

$$\frac{\partial T}{\partial t} = (\frac{\partial T}{\partial n_1})_{s_1}\frac{\partial n_1}{\partial t} + (\frac{\partial T}{\partial s_1})_{n_1}\frac{\partial s_1}{\partial t} = (\frac{\partial T}{\partial s_1})_{n_1}\partial_z(\frac{s_1 n_{s1}}{n_{n1}}u_s), \tag{5.100}$$

where we have imposed the condition $\frac{\partial n_1}{\partial t} = 0$. As a simple application, we can get the rough temperature fluctuation mode corresponding to the second sound 'dipole' mode assuming that the displacement field can be well approximated by $u_s = const.$ In contrast to the dipole mode of first sound nature, where the temperature is

uniform in space and time (indicated by Eq. (5.44)), the temperature fluctuations of the 'dipole' mode of second sound nature exhibits a spatial-dependence structure.

Let us point out that the discretized second sound oscillations discussed above are expected to be more damped than the first sound ones discussed in the previous section. The reason is that the thermal conductivity in the normal phase tends to infinity near the transition point [113] and is consequently large near the boundary between the superfluid and the normal phases. This is expected to result in the penetration of the temperature fluctuations into the normal phase, resulting in an increase of damping.

Next, we discuss the coupling between the two modes. This can be estimated using a variational approach. To this purpose we will look for solutions of the variational hydrodynamic equations in the form $u_s = au^{(1)}+u_s^{(2)}$ and $u_n = au^{(1)}+u_n^{(2)}$ for the superfluid (u_s) and normal (u_n) displacement fields, respectively. Here $u_n^{(1)} = u_s^{(1)} \equiv u^{(1)}$ corresponds to the velocity field of the first sound solutions discussed in Sec. 5.4, while $u_n^{(2)}$ and $u_s^{(2)}$ are the velocity fields of the uncoupled second sound solutions satisfying the condition of vanishing total current. By inserting the ansatz into Eq. (5.54) we find, after a straightforward calculation, the expression

$$\omega^2 = \frac{a^2\omega_1^2 + \omega_2^2\frac{K_2}{K_1} - a\frac{U_{1,2}}{K_1}}{a^2 + \frac{K_2}{K_1}}, \tag{5.101}$$

for the collective frequency as a function of the variational parameter a, where $K_1 = \frac{1}{2}\int dz m n_1 u_1^2$, $K_2 = \frac{1}{2}\int dz \frac{m(u_s^{(2)})^2 n_{1} n_{s1}}{n_{n1}}$ and $U_{1,2} = \frac{1}{2}T\int dz \frac{\partial u_1}{\partial z}\frac{\partial s_1 n_{s1} u_s^{(2)}/n_{n1}}{\partial z}$ and we have used the identity $n_1(\frac{\partial T}{\partial n_1})_{\bar{s}_1} = \frac{2}{5}T$ holding at unitarity. By imposing the variational condition $\delta\omega^2/\delta a = 0$ we find the result

$$\omega^2 = \frac{\omega_1^2 + \omega_2^2 \pm \sqrt{(\omega_1^2-\omega_2^2)^2 + \frac{U_{1,2}^2}{K_1K_2}}}{2}, \tag{5.102}$$

for the frequency of the two coupled modes. The corresponding solution for the coupling parameter is:

$$a = -\frac{(\omega_1^2-\omega_2^2) \pm \sqrt{(\omega_1^2-\omega_2^2)^2 + \frac{U_{1,2}^2}{K_1K_2}}}{\frac{U_{1,2}}{K_2}}. \tag{5.103}$$

When applied to uniform matter, using result (4.22) and (4.23) for the uncoupled

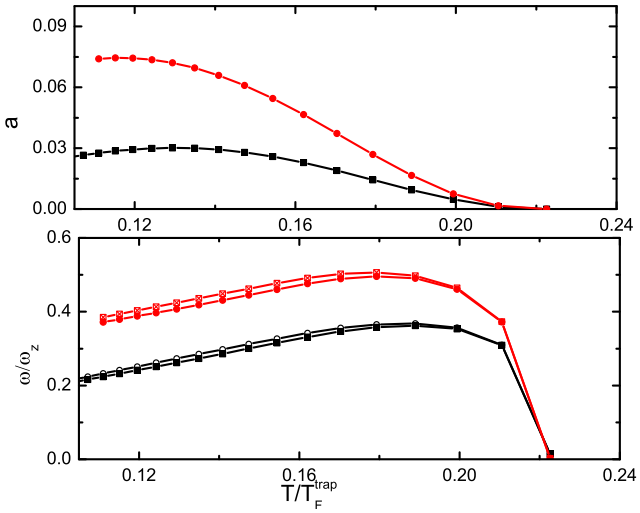

Figure 5.8: The upper panel shows the coupling strength (5.103) between the second sound dipole mode and the $k = 2$ first sound mode using two different ansatz for the superfluid density as indicated in the captions. In the lower panel, the frequency of the second sound dipole mode calculated with (denoted by filled symbols) and without (denoted by empty symbols) coupling with the first sound mode. In both panels, the superfluid density ansatz $n_s/n = 1-(T/T_c)^4$ (upper branch) and $n_s/n = (1 - T/T_c)^{2/3}$ (lower branch) are used.

first (ω_1) sound and second (ω_2) frequencies, the above procedure reproduces exactly the two decoupled solutions given by the roots of Eq. (4.25). As an example of application in the presence of harmonic trapping we have considered the coupling between the dipole second sound solution discussed above and the $k = 2$ first sound solution discussed in Sec. 5.4. The $k = 2$ mode is actually the lowest first sound mode that can be coupled to the dipole second sound mode, being characterized by the same parity symmetry. The $k = 0$ (dipole) first sound mode is in fact an exact solution of the two-fluid hydrodynamic equations and cannot exhibit any coupling with other modes. The numerical calculation shows that the changes in the value of the second sound frequency caused by the coupling are very small (see Fig. 5.8).

Chapter 6

Damping mechanisms

In the previous chapters we have applied the quasi-1D two-fluid hydrodynamic theory to investigate the sound propagations (chapter 4) and discretized oscillations (chapter 5) of the unitary Fermi gas in the highly elongated configuration. In this chapter, we will discuss the applicability of the 1D approximation employed in the thesis. To this purpose we will apply the two-fluid hydrodynamic equations to calculate the damping of the sound waves, induced by a violation of the 1D condition, i.e., by the presence of radial gradients in the normal velocity field and in the temperature fluctuations.

The damping behavior of the higher-node modes in the elongated unitrary Fermi gas has been investigated experimentally in Ref. [54]. There, it is found that the damping rate increases with the order of the mode investigated. A better understanding of damping is very important to understand the limitations of the theoretical approach applied to describe these modes. As discussed in Sec. 4.1, under suitable conditions of radial trapping, it is possible to derive simplified 1D hydrodynamic equations from the usual two-fluid Landau hydrodynamic equations starting from a 3D description [86]. The basic point of such a derivation is the requirement that both the normal velocity field along the long z-th axis and the temperature oscillations during the propagation of sound do not depend on the radial coordinates. This requirement is justified in the case of tight radial confinement and is a direct consequence of the effects of viscosity and of thermal conductivity. The condition

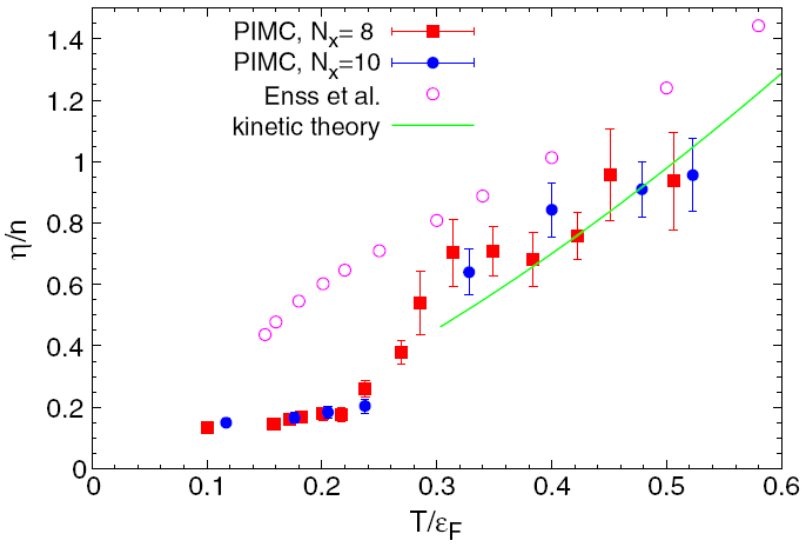

Figure 6.1: Theoretical calculation of the shear viscosity. From Ref. [114].

can be formulated in a simple form:

$$\eta \gg m n_{n1} \omega, \tag{6.1}$$

(As we will see below, actually there is a small prefactor in the right side of the inequality (6.1)). An analogous condition holds for the thermal conductivity. Indeed the relatively small damping shown by the experiment [54] in the case of the $k = 2$ mode confirms that the main assumption $m n_{n1} \omega / \eta \ll 1$ needed to derive the 1D hydrodynamic equations is reasonably well satisfied. One can estimate the correctness of (6.1) using the available data for the density and the shear viscosity [55, 114].

To this purpose, Eq. (6.1) is rewritten in the following form:

$$\begin{aligned} \frac{\eta}{n\hbar} &\gg \frac{m n_{n1} \omega}{n\hbar} \\ &= 2\pi (3N)^{1/3} \left(\frac{\omega_z}{\omega_\perp}\right)^{4/3} \frac{T}{T_F^{trap}} \frac{f_p}{f_n} \frac{\omega}{\omega_z}. \end{aligned} \tag{6.2}$$

In achieving the above expression, we have adopted the universal functions discussed in chapter 2 and replaced the normal 1D density by the total 1D density as we will concentrate on the estimate in the normal phase. The quantity on the right-hand side can be readily calculated by using the EOS discussed in chapter 2 together with the experimental parameters: $N = 3\times10^5$, $\omega_z = 2\pi\times22.52Hz$ and $\omega_\perp = 2\pi\times473Hz$ (for lowest T); $\omega_z = 2\pi\times23.31Hz$ and $\omega_\perp = 2\pi\times1226Hz$ (for highest T) adopted by the Innsbruck team [54, 53]. The corresponding value of the Fermi temperature ranges from $T_F^{trap} \simeq 0.8\mu K$ to $T_F^{trap} \simeq 1.5\mu K$. The quantity on the left-hand side of Eq. (6.2) is the shear viscosity divided by the density, whose value is accessible from the recent theoretical estimates [114]. By comparing the values of the left- and right-hand sides of Eq. (6.2) (see Figs. 6.1 and 6.2), we find that the condition (6.2) is actually violated for the experimental conditions of [53, 36, 54]. However, a more careful investigation shows the occurrence of a small numerical coefficient in the right-hand side of the inequality, as will be discussed below.

To produce more quantitative estimates, one should calculate the first correction to some observable quantity and confirm that the correction is small. We will actually calculate the first correction $\delta c/c$ to the velocity of sound, propagating in the z-th direction in the absence of axial trapping. The calculations are cumbersome and we consider here only the case of unitary Fermi gas above the transition temperature. It is easy to show that the first correction is imaginary and corresponds to damping. Thus it is more convenient to calculate the correction through the energy dissipation due to the radial gradients of the velocity field v and of the temperature fluctuations δT.

The dissipation of the energy of the oscillation due to the shear viscosity (we keep only the leading term) is given by (see §49 in [87])

$$\dot{E}_{osc} = -\int_0^\infty \eta(r_\perp)\left(\partial_{r_\perp} v\right)^2 2\pi r_\perp dr_\perp \ . \tag{6.3}$$

The correction we are looking for is

$$\frac{|\delta c|}{c} = \frac{\left|\dot{E}_{osc}\right|}{2\omega E_{osc}}, \tag{6.4}$$

where $E_{osc} = 2E_{osc}^{kin} = mn_1v^2$. The relevant hydrodynamic equation, needed to calculate $\partial_{r_\perp} v$, is the equation of momentum conservation along the z-th direction

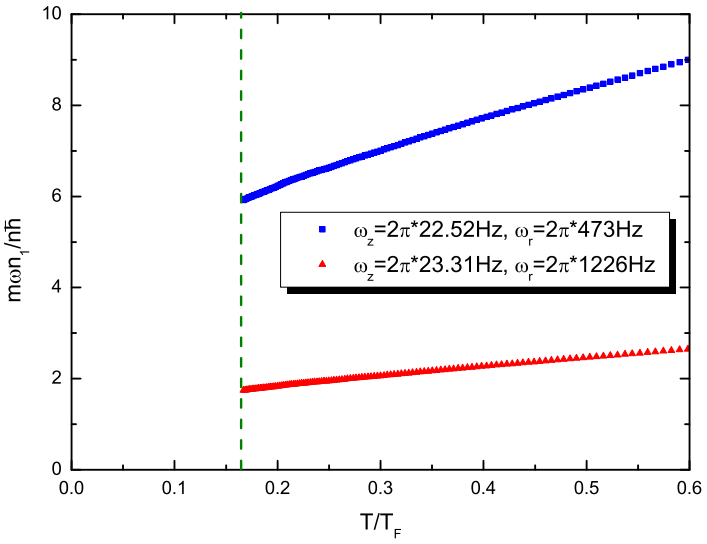

Figure 6.2: Value of $\frac{mn_1\omega}{n\hbar}$ for the $k = 2$ mode with larger (blue data) and smaller (red data) aspect ratio, respectively. The total number of particles is 3×10^5. The green line indicates the critical point.

given, with proper accuracy, by:

$$\frac{1}{r_\perp}\partial_{r_\perp}\left[r_\perp\left(\eta\partial_{r_\perp}v\right)\right] = -i\omega\left(mnv - \delta P/c\right), \tag{6.5}$$

where, to the lowest order, the velocity v in the right-hand side can be considered $r_\perp$-independent and the pressure changes δP can be evaluated in terms of v using Eqs. (3.1)–(3.4). The proper solution is given by:

$$\partial_{r_\perp}v\left(r_\perp\right) = -v\frac{1}{\eta(r_\perp)r_\perp}\int_r^\infty F(r_\perp)r_\perp dr_\perp, \tag{6.6}$$

where, for the unitary gas, the function F can be expressed through the universal functions introduced in Sec. 2.1 as:

$$F(r_\perp) = i\omega\frac{k_BT}{c^2\lambda_T^3}\left[\frac{2}{5}\left(x_1 - x\right)f_n - \frac{mc^2}{T}f_n + f_p\right], \tag{6.7}$$

with $x = x_1 - r_\perp^2/R_\perp^2$ and $R_\perp^2 \equiv 2k_BT/m\omega_\perp^2$. The correction to the speed of sound is finally given by

$$\frac{|\delta c|}{c} = \frac{\pi}{\omega m n_1}\int_0^\infty \left(\int_r^\infty F(r_\perp) r_\perp dr_\perp\right)^2 \frac{dr_\perp}{\eta\,(r_\perp)\, r_\perp}. \tag{6.8}$$

Further calculations demand the knowledge of the viscosity. It is reasonable to assume that, in the relevant region around the critical temperature, the value of the shear viscosity is close to the "minimal quantum value" [115] $\eta_Q = \hbar s/4\pi k_B$. Experimental data on the shear viscosity by [116, 117] confirms this ansatz. Actually the measured values of η turn out to be larger than η_Q, which makes the correction $\frac{|\delta c|}{c}$ even smaller. A simple calculation then gives the result,

$$\frac{|\delta c|}{c} \leq \left(\frac{|\delta c|}{c}\right)_Q = \frac{A}{8\times 49\pi}\frac{m n_1 \omega}{\eta_Q(x_c)}, \tag{6.9}$$

with $A \approx 0.5$ near T_c and $\eta_Q(x_c)$ the value of the minimum quantum viscosity calculated on the symmetry axis at T_c. It occurs that for the experimental conditions of Refs. [53, 54], $|\delta c|/c$ turns out to be 0.01 with the parameters: $N = 3\times 10^5$, $\omega_z = 2\pi \times 23.31 Hz$ and $\omega_\perp = 2\pi \times 1226 Hz$. Notice that the condition $\frac{|\delta c|}{c} \ll 1$ actually requires a less stringent condition as compared to Eq. (6.1) because of the small prefactor $A/(8\times 49\pi)$ in the right-hand side of Eq. (6.9).

It is interesting also to produce calculations in the classical regime of high temperatures. Here $\eta = \eta_{Cl}$ does not depend on density nor, consequently, on $r_\perp$. The result is given by (6.9) with η_Q replaced by $\eta_{Cl} = \frac{15}{32\sqrt{\pi}}\frac{(mk_BT)^{3/2}}{\hbar^2}$ [118] and $A = 1$. We find that also in this case $|\delta c|/c$ is small enough and that the condition for the 1D approximation is satisfied.

A condition analogous to Eq. (6.4) should be also satisfied for the thermal conductivity κ. We do not present here the corresponding calculation, because there are no reliable data on κ from experiments. It is however important to point out that the temperature fluctuations are always $r_\perp$-independent in the superfluid phase due to the conditions of mechanical equilibrium of the superfluid component in the radial direction. Furthermore, the thermal conductivity κ diverges at transition temperature [113] so that there are good reasons to believe that the corresponding corrections to the sound velocity are less important than the ones due to the shear viscosity.

Chapter 7

Conclusions and Perspectives

We have provided a systematic discussion of the two-fluid hydrodynamic behavior exhibited by the unitary Fermi gas in the presence of a highly elongated harmonic potential. The main achievements contained in the thesis are summarized below.

(i) We have presented an exhaustive discussion of the relevant 3D and 1D thermodynamic functions, like the pressure, the entropy and the specific heats at constant density and at constant pressure, whose knowledge is required in order to solve the hydrodynamic equations. The thermodynamic functions are identified using the most recent experimental data obtained at MIT [55], through the introduction of universal scaling functions which emphasize the universality of the unitary Fermi gas. The matching of the MIT data with the low temperature behavior of the 3D thermodynamic functions fixed by the thermal excitation of phonons and with the high temperature virial expansion has been explicitly discussed. Particularly interesting results concern the behavior of the 1D quantities which are calculated by radial integration of the 3D thermodynamic functions using the local density approximation. The behavior of the 1D thermodynamic functions at low temperature is not uniquely fixed by the thermal excitation of phonons as happens in uniform superfluids, but involves also the thermal regimes at higher temperature in the peripheral radial region. Their temperature dependence at low T has been explicitly calculated.

(ii) We have solved the 1D hydrodynamic equations derived in [37] using a variational formulation of the hydrodynamic equations. Explicit results are given for

both the first and second sound modes. While the first sound solutions are basically determined by the 1D adiabatic compressibility the second sound solutions are sensitive, in addition to the entropy and the specific heat, to the superfluid density of the system, a rather elusive quantity which cannot be determined by the knowledge of the equation of state of the system.

(iii) We have provided results for both 1D uniform and axially trapped configurations. In the first case the solutions of the hydrodynamic equations take the form of sound wave whose velocity has been systematically investigated for both first and second sound, employing different models for the superfluid density, and a detailed analysis of recent experimental results was presented [36]. In the presence of axial trapping the lowest excitations take the form of discretized collective oscillations whose frequencies are calculated as a function of temperature. The theoretical predictions for the first discretized sound solutions are compared with recent experiments carried out both below and above the critical temperature for superfluidity [53].

(iv) An important feature emerging from our studies is that the finite value of the thermal expansion coefficient makes the second sound mode an oscillation at constant 1D pressure, rather than at constant 1D density and an explicit formula for the resulting density fluctuations has been derived as a function of temperature. This has the important consequence that, except at very low temperature, the density fluctuations characterizing second sound are not negligible, thereby making this mode observable in experiments.

(v) The applicability of the 1D hydrodynamic approach employed in the thesis is based on the assumption that the dependence of the temperature fluctuation and of the velocity field on the radial coordinates can be safely ignored. We have discussed the validity of this assumption by properly including the effects of viscosity in the hydrodynamic equations and calculating the first corrections to the velocity of sound. Explicit estimates near the critical temperature and in the classical regime show that these corrections are small in the experimentally available trapping conditions.

(vi) A still open question concerns the theoretical calculation of the temperature dependence of the superfluid density near the superfluid transition. *Ab initio* Monte Carlo calculations could provide a quantitative estimate of the superfluid fraction in this relevant region, now accessible experimentally, where fermionic quasiparticle

excitations are expected to provide the dominant contribution, as recently discussed in [102]. We hope our work encourages more theoretical calculations in order to improve the accuracy of the theoretical predictions for superfluid density.

Another open question remains the theoretical understanding of damping phenomena characterizing the first and second sound oscillations of the strongly interacting Fermi gas.

Appendix A

1D variational formulation of the Landau two-fluid hydrodynamic equations

The continuity equation (4.4) and the equation for the entropy (4.5) can be easily recovered by taking the time derivative of the density fluctuation δn_1 and that of the entropy fluctuation $\delta s_1 = n_1^0 \delta \bar{s}_1 + \bar{s}_1^0 \delta n_1$ (in linear regime) according to their definition given in Sec. 5.3. The equation for the superfluid field (4.6) can be recovered by minimizing the frequency defined in Eq. (5.54) with respect to the superfluid displacement field u_s. Similarly, the equation for the total current (4.7) can be recovered by minimizing the frequency with respect to u_n, as shown below.

Minimizing the frequency (5.54) with respect to the superfluid displacement field, namely, $\frac{\delta\omega^2}{\delta u_s} = 0$ results in the equation below:

$$\begin{aligned} m\omega^2 n_{s1}^0 u_s &= n_{s1}^0 \frac{\partial}{\partial z}[\frac{1}{n_1^0}(\frac{\partial P}{\partial n_1})_{\bar{s}_1}\delta\rho_1] \\ &\quad + n_{s1}^0 \frac{\partial}{\partial z}[n_1^0(\frac{\partial T}{\partial n_1})_{\bar{s}_1}\delta\bar{s}_1] - n_{s1}^0 \frac{\partial}{\partial z}[\bar{s}_1(\frac{\partial T}{\partial n_1})_{\bar{s}_1}\delta n_1] \\ &\quad - n_{s1}^0 \frac{\partial}{\partial z}[\bar{s}_1^0(\frac{\partial T}{\partial \bar{s}_1})_{n_1}\delta\bar{s}_1] \\ &= n_{s1}^0 \frac{\partial}{\partial z}\delta\mu. \end{aligned} \tag{A.1}$$

The equation above is equivalent to $-m\partial_t v_s = \frac{\partial}{\partial z}(\mu + V_{ext})$ by assuming $u_s \propto e^{-i\omega t}$.

So Eq. (4.6) is proved. We mainly used the formula:

$$\int dz f(z)\nabla[\delta(z-z')g(z)] = -g(z')\nabla f(z'), \tag{A.2}$$

and the thermodynamic identity:

$$(\frac{\partial T}{\partial n_1})_{\bar{s}_1} = \frac{1}{n_1^2}(\frac{\partial P_1}{\partial \bar{s}_1})_{n_1}. \tag{A.3}$$

A simple proof is the following: we get from the Gibbs-Duhem relation $d\mu = d\frac{P_1}{n_1} + \frac{P_1}{n_1^2}dn_1 - d(T\bar{s}_1) + Td\bar{s}_1$, which gives that $d(\mu - \frac{P_1}{n_1} + T\bar{s}_1) = \frac{P_1}{n_1^2}dn_1 + Td\bar{s}_1$. Therefore, $(\frac{\partial T}{\partial n_1})_{\bar{s}_1} = \frac{1}{n_1^2}(\frac{\partial P_1}{\partial \bar{s}_1})_{n_1}$.

Similarly, taking these into account and using the expansion of δP_1 and δT in terms of n_1 and $\bar{s}_1$, we get an equation for the normal velocity field following the requirement $\frac{\delta\omega^2}{\delta u_n} = 0$:

$$m\omega^2 n_{n1}^0 u_n = \frac{\partial P_1}{\partial z} + n_1\nabla_z V_{ext} - m\omega^2 n_{s1}^0 u_s \tag{A.4}$$

Therefore, $\mathrm{m}\omega^2(n_{n1}^0 u_n + n_{s1}^0 u_s) = -m(n_{n1}^0\partial_t v_n + n_{s1}^0\partial_t v_s) = \frac{\partial P_1}{\partial z} + n_1\nabla_z V_{ext}$, Eq. (4.7) is proved.

Appendix B

Some derivation details

B.1 Derivation for the simplified first sound equation (5.61)

In this section, we show how to simplify the general equation (5.54) under the first sound ansatz ($u_s = u_n = u$). For instance, the first term can be written as:

$$\begin{aligned}\frac{1}{n_1}\left(\frac{\partial P_1}{\partial n_1}\right)_{\bar{s}_1}(\delta n_1)^2 &= n_1\left(\frac{\partial P_1}{\partial n_1}\right)_{\bar{s}_1}(\frac{\partial u}{\partial z})^2 + \frac{u^2}{n_1}\left(\frac{\partial P_1}{\partial n_1}\right)_{\bar{s}_1}(\frac{\partial n_1}{\partial z})^2 \\ &\quad +2u\left(\frac{\partial P_1}{\partial n_1}\right)_{\bar{s}_1}\frac{\partial n_1}{\partial z}\frac{\partial u}{\partial z}. \end{aligned} \tag{B.1}$$

The second cross-term between the density fluctuations and the entropy fluctuations take the form:

$$\begin{aligned}2n_1\left(\frac{\partial T}{\partial n_1}\right)_{\bar{s}_1}\delta n_1\delta\bar{s}_1 &= 2n_1u^2\left(\frac{\partial T}{\partial n_1}\right)_{\bar{s}_1}\frac{\partial n_1}{\partial z}\frac{\partial \bar{s}_1}{\partial z} + 2n_1^2u\left(\frac{\partial T}{\partial n_1}\right)_{\bar{s}_1}\frac{\partial \bar{s}_1}{\partial z}\frac{\partial u}{\partial z} \\ &= n_1u^2\left(\frac{\partial T}{\partial n_1}\right)_{\bar{s}_1}\frac{\partial n_1}{\partial z}\frac{\partial \bar{s}_1}{\partial z} + \frac{u^{^2}}{n_1}\left(\frac{\partial P_1}{\partial \bar{s}_1}\right)_{n_1}\frac{\partial \bar{s}_1}{\partial z}\frac{\partial n_1}{\partial z} \\ &\quad +2u\left(\frac{\partial P_1}{\partial \bar{s}_1}\right)_{n_1}\frac{\partial \bar{s}_1}{\partial z}\frac{\partial u}{\partial z}. \end{aligned} \tag{B.2}$$

In obtaining the second step, we have used the identity: $\left(\frac{\partial T}{\partial n_1}\right)_{\bar{s}_1} = \frac{1}{n_1^2}\left(\frac{\partial P}{\partial \bar{s}_1}\right)_{n_1}$ (see App. A). Inserting the expression for the entropy fluctuation (5.59) into the last

term in Eq. (5.54), we get

$$n_1 \left(\frac{\partial T}{\partial \bar{s}_1}\right)_{n_1} (\delta \bar{s}_1)^2 = n_1 u^2 \left(\frac{\partial T}{\partial \bar{s}_1}\right)_{n_1} \frac{\partial \bar{s}_1}{\partial z} \frac{\partial \bar{s}_1}{\partial z}. \tag{B.3}$$

Equation (B.3) actually cancels with the first term in Eq. (B.2) due to the condition $\nabla_z T = 0$ holding at equilibrium. Then by recombining the remaining terms in Eq. (B.1) and Eq. (B.2), we get the simplified integrand in the numerator: $n_1 \left(\partial P_1/\partial n_1\right)_{\bar{s}_1} (\partial_z u)^2 - \omega_z^2 z \partial_z (m n_1 u^2)$ where we have employed the thermodynamic relation $\partial_z P_1 = -n_1 \partial_z V_{ext}(z)$ holding at equilibrium (see Eq. (4.7)). Carrying out the partial integral when necessary, finally, the expression for the frequency (5.54) takes the simplified form:

$$\omega^2 = \frac{\int dz n_1 \left(\frac{\partial P_1}{\partial n_1}\right)_{\bar{s}_1} \left(\frac{\partial u}{\partial z}\right)^2}{\int dz m n_1 u^2} + \omega_z^2. \tag{B.4}$$

B.2 Derivation of the general equation (5.63)

A detailed derivation in reaching the general matrix equation (5.63) for the first sound discretized modes via variational approach is given below. Taking variation of expression (5.61) with respect to X_k, we get:

$$\frac{\delta K}{\delta X_k} = R_z^2 \sum_l X_l \int dz' R_z m n_1 z'^{k+l}, \tag{B.5}$$

where $K = \frac{1}{2} \int dz m n_1 u^2$. In order to make use of experiment data of Ref. [55], we reformulate the moment of density. By proper scaling, asymmetrical harmonic trap can be transformed to spherical form: $V_{ext} = \frac{1}{2} m(\omega_x^2 x^2 + \omega_y^2 y^2 + \omega_z^2 z^2) = \frac{1}{2} m(\tilde{x}^2 + \tilde{y}^2 + \tilde{z}^2) = \frac{1}{2} m \tilde{r}^2$, where $\tilde{j} = \omega_j j, j = x, y, z$. So the moment of 1D density

can be reformulated in terms of the 3D harmonic potentials.

$$\begin{aligned}
\tilde{M}_{k,l} &= \int dz' R_z m n_1 z'^{k+l} \\
&= \frac{2\pi R_z}{\omega_x\omega_y(\omega_z R_z)^{k+l+1}} \frac{2}{k+l+1} (\frac{2}{m})^{\frac{k+l+1}{2}} \int dV_{ext} V_{ext}^{\frac{k+l+1}{2}} n(V_{ext}) \\
&= \frac{2\pi R_z}{\omega_x\omega_y} \frac{2}{k+l+1} \frac{\beta^{-1}}{\lambda_T^3} \int_{\beta(\mu_0 - V_{ext}(R))}^{\beta\mu_0} dx (\beta\mu_0 - x)^{\frac{k+l+1}{2}} \lambda_T^3 n(x) \\
&\equiv \frac{2\pi R_z}{\omega_x\omega_y} \frac{2}{k+l+1} \frac{\beta^{-1}}{\lambda_T^3} M_{k,l}. \qquad \text{(B.6)}
\end{aligned}$$

We have also introduced the dimensionless quantity: $x = \beta(\mu_0 - V_{ext})$ where μ_0 is the chemical potential in the center of the harmonic trap. $\beta = 1/k_B T$ at finite temperature. Similarly, for the numerator $U = \frac{1}{2}\int dz \frac{7}{5} P_1 \left(\frac{\partial u}{\partial z}\right)^2 + \frac{1}{2}\omega_z^2 \int dz m n_1 u^2$ we get (we also used partial integral so part of the second part joins the first part):

$$\frac{\delta U}{\delta X_k} = \frac{7k+5}{5}\omega_z^2 R_z^2 \sum_l \tilde{M}_{k,l} X_l - \frac{7}{5}k(k-1)\omega_z^2 R_z^2 \sum_l \tilde{H}_{k,l} X_l, \qquad \text{(B.7)}$$

where,

$$\begin{aligned}
\tilde{H}_{k,l} &= \int dz' \frac{P_1}{\omega_z^2 R_z} z'^{k+l-2} \\
&= \frac{2\pi}{\omega_x\omega_y(\omega_z R_z)^{k+l}} \frac{1}{k+l-1} (\frac{2}{m})^{\frac{k+l+1}{2}} \int dV_{ext} \frac{P}{\omega_z} V_{ext}^{\frac{k+l-1}{2}} \\
&= \frac{2\pi R_z}{\omega_x\omega_y} \frac{1}{k+l-1} \frac{k_B T}{\lambda_T^3} \int_{\beta(\mu_0 - V_{ext}(R))}^{\beta\mu_0} dx \frac{P(x)\lambda_T^3}{k_B T} (\beta\mu_0 - x)^{\frac{k+l-1}{2}} \\
&\equiv \frac{2\pi R_z}{\omega_x\omega_y} \frac{1}{k+l-1} \frac{k_B T}{\lambda_T^3} H_{k,l}. \qquad \text{(B.8)}
\end{aligned}$$

Minimization of the frequency with respect to the velocity field requires that $\omega^2 \frac{\delta K}{\delta X_k} = \frac{\delta U}{\delta X_k}$. So by combining Eqs. (B.5)–(B.8), we get,

$$\sum_l [(\frac{\omega^2}{\omega_z^2} - \frac{7k+5}{5}) \frac{2}{k+l+1} M_{k,l} + \frac{7}{5}k(k-1) \frac{1}{k+l-1} H_{k,l}] X_l = 0. \qquad \text{(B.9)}$$

In the case of $T = 0$, we change the variable from x to $x' = x/(\mu_0/k_B T)$. Note that at zero temperature, the size of the cloud is determined by μ_0 according to

the Thomas Fermi approximation, so the lower bound in the integrals entering the coefficient matrix is 0, and the upper bound is 1. An extra term of the prefactor μ_0/k_BT will correspondingly be produced, but can be included into X_l, therefore doesn't affect the final form for the coefficient matrix. We use M^0_{k+l} and H^0_{k+l} for the moments to distinguish from the moments at finite temperatures.

Appendix C

Convergence revealed by the 3×3 matrix equation solution

In order to check the convergence of the frequency for the $k = 2$ and $k = 3$ modes, we solve Eq. (5.63) involving the next order terms, i.e., taking up to the third terms in the generic expression and get the 3×3 matrix of even parity below:

$$\begin{bmatrix} (\epsilon-1)M_0 & \frac{1}{3}(\epsilon-1)M_2 & \frac{1}{5}(\epsilon-1)M_4 \\ \frac{1}{3}(\epsilon-1)M_2 & \frac{1}{5}(\epsilon-\frac{43}{15})M_4 & \frac{1}{7}(\epsilon-\frac{81}{25})M_6 \\ \frac{1}{5}(\epsilon-1)M_4 & \frac{2}{7}(\epsilon-\frac{81}{25})M_6 & \frac{1}{9}(\epsilon-\frac{21}{5})M_8 \end{bmatrix} \begin{bmatrix} X_0 \\ X_2 \\ X_3 \end{bmatrix} = 0, \tag{C.1}$$

where, $\epsilon \equiv \frac{\omega^2}{\omega_z^2}$. In order to compare with 2×2 matrix, we expand the coefficient matrix in terms of the third row and get:

$$\begin{aligned} D &= 8(\epsilon-1)M_0M_4M_8[(\frac{1}{45}-\frac{d_0}{81})(\epsilon-\epsilon_0)(\epsilon-\frac{21}{5})+\frac{2d_1}{105}(\epsilon-1)(\epsilon-\frac{81}{25}) \\ &\quad -\frac{d_2}{125}(\epsilon-1)(\epsilon-\frac{43}{15})-\frac{d_3}{49}(\epsilon-\frac{81}{25})^2], \end{aligned} \tag{C.2}$$

where $d_0 = \frac{M_2^2}{M_0M_4} = 1/t_2$, $d_1 = \frac{M_2M_6}{M_0M_8}$, $d_2 = \frac{M_4^2}{M_0M_8}$, $d_3 = \frac{M_6^2}{M_4M_8}$, whose values, in the zero temperature and classical limit, can be obtained by adopting the moments of density (5.67) and (5.70) and $\epsilon_0 = \frac{129-25d_0}{45-25d_0}$ is the second frequency we obtained from the 2×2 matrix. As expected, one of the roots for the determinant to be zero is $\epsilon = 1$ because the dipole mode is the exact solution of the Landau two-fluid

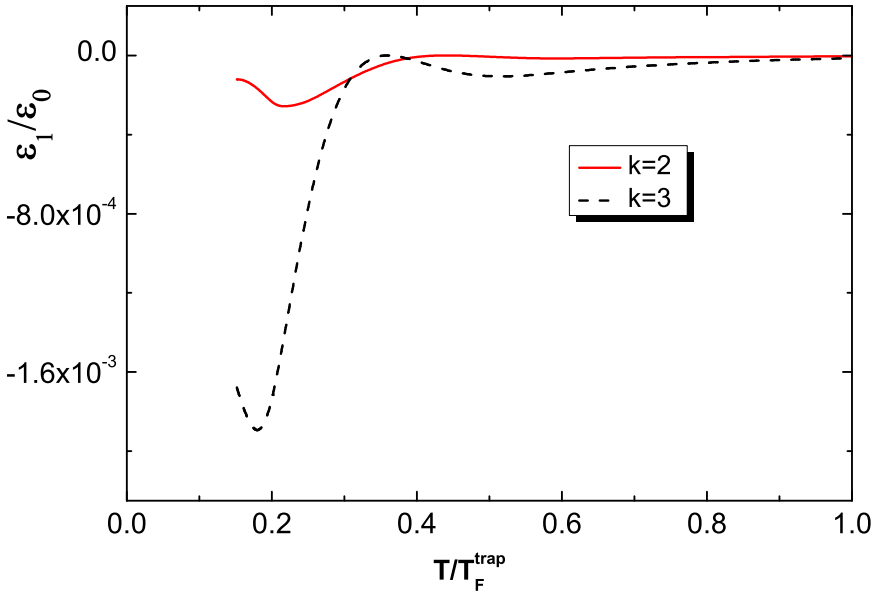

Figure C.1: First order correction to the frequency of the $k = 2$ and $k = 3$ modes by considering the 3×3 matrix.

equations. Besides, we get another two roots from the following equation:

$$\begin{aligned} I &= (\frac{1}{45} - \frac{d_0}{81})(\epsilon - \epsilon_0)(\epsilon - \frac{21}{5}) + \frac{2d_1}{105}(\epsilon - 1)(\epsilon - \frac{81}{25}) \\ &\quad - \frac{d_2}{125}(\epsilon - 1)(\epsilon - \frac{43}{15}) - \frac{d_3}{49}(\epsilon - \frac{81}{25})^2 = 0. \end{aligned} \tag{C.3}$$

Next we try to understand better Eq. (C.3) to see whether 3×3 matrix gives only a small correction to the $k = 2$ mode compared to the frequency obtained from 2×2 matrix. At $T = 0$, by substituting all the parameters into I we get $I = \frac{7}{4500}(\epsilon - \frac{21}{5})(\epsilon - 9)$, yielding the same analytic solutions as the 2×2 matrix, i.e., $\epsilon = \frac{21}{5}$ and in addition, $\epsilon = 9$ (as expected from the exact solution at zero temperature (5.7)). In the $T \gg T_c$ limit, $I = \frac{16}{4725}(\epsilon - \frac{19}{5})(\epsilon - \frac{33}{5})$, hence the roots are: $\epsilon = \frac{19}{5}$ and $\epsilon = \frac{33}{5}$, consistent with the previous exact solutions (5.51) in the high temperature limit. But in the intermediate temperature, the corrections are not straightforwardly visible. To study the correction in the intermediate temperature, we assume $\epsilon = \epsilon_0 + \epsilon_1$ and $\epsilon_1 \ll \epsilon_0$. Substituting $\epsilon = \epsilon_0 + \epsilon_1$ into I and neglecting

the terms of ϵ_1^2, we get: $I \approx [(\frac{1}{45} - \frac{d_0^e}{81})(\epsilon_0 - \frac{21}{5}) + \frac{4d_1^e}{105}(\epsilon_0 - \frac{53}{25}) - \frac{2d_2^e}{125}(\epsilon_0 - \frac{29}{15}) - \frac{2d_3^e}{49}(\epsilon_0 - \frac{81}{25})]\epsilon_1 + \frac{2d_1^e}{105}(\epsilon_0 - 1)(\epsilon_0 - \frac{81}{25}) - \frac{d_2^e}{125}(\epsilon_0 - 1)(\epsilon_0 - \frac{43}{15}) - \frac{d_3^e}{49}(\epsilon_0 - \frac{81}{25})^2 = 0$. So, the correction is given by

$$\frac{\epsilon_1}{\epsilon_0} = -\frac{\frac{2d_1^e}{105}(\epsilon_0 - 1)(\epsilon_0 - \frac{81}{25}) - \frac{d_2^e}{125}(\epsilon_0 - 1)(\epsilon_0 - \frac{43}{15}) - \frac{d_3^e}{49}(\epsilon_0 - \frac{81}{25})^2}{(\frac{1}{45} - \frac{d_0^e}{81})\epsilon_0(\epsilon_0 - \frac{21}{5}) + \frac{4d_1^e}{105}\epsilon_0(\epsilon_0 - \frac{53}{25}) - \frac{2d_2^e}{125}\epsilon_0(\epsilon_0 - \frac{29}{15}) - \frac{2d_3^e}{49}\epsilon_0(\epsilon_0 - \frac{81}{25})}. \quad \text{(C.4)}$$

One can check that in the limits $T = 0$ and $T \gg T_c$, $\epsilon_1 = 0$. We make use of the experiment data and show that $\frac{\epsilon_1}{\epsilon_0} \ll 1$ in the intermediate temperature regime as well. We have checked that the correction is small also for the $k = 3$ mode (see Fig. C.1).

Appendix D

Numerical solutions of the displacement field equation (5.89)

In the presence of the axial harmonic trapping, we verify that the variational predictions for the collective frequencies of the $k = 2$ and $k = 3$ modes are practically indistinguishable from the exact numerical solution of Eq. (5.89), governing the first sound collective modes [112]. Equation (5.89) is a second order non-linear differential equation with a single variable. It can be solved numerically in a rather straightforward way. To compute u numerically, we subdivide the z axis equally into many small elements Δz within the region of interest that typically covers a few Thomas-Fermi radii from the trap center. We then label the point at a distance $i\Delta z$ ($i \in Z$) away from the origin as point i. When Δz is sufficiently small compared to the characteristic feature scale of the displacement field u, one can represent u and its derivatives accurately using

$$u(i\Delta z) = u_i, \tag{D.1}$$

$$\partial_z u_i = \frac{u_{i+1} - u_{i-1}}{2\Delta z}, \tag{D.2}$$

$$\partial_z^2 u_i = \frac{u_{i+1} + u_{i-1} - 2u_i}{\Delta z^2}. \tag{D.3}$$

Below, we adopt the finite temperature Thomas Fermi radius $R_z = \sqrt{\frac{2k_BT}{m\omega_z^2}}$ to achieve the dimensionless expressions in order to make direct use of the universal functions

discussed in chapter 2. Using the discretized displacement field and rearranging, Eq. (5.89), we get

$$u_{i+1} = 2u_i - u_{i-1} + \frac{\frac{7}{5}iu_{i-1} + au_i - \frac{7}{5}iu_i}{\frac{7}{10}i - \frac{f_i}{\Delta\bar{z}^2}}, \tag{D.4}$$

where the quantities $a = \frac{\omega^2}{\omega_z^2} - 1$, $\Delta\bar{z} = \frac{\Delta z}{R_z}$ (in the relevant figures below, we take $\Delta\bar{z} = 0.001$), $f_i = \frac{7}{10}\frac{f_q(x_0 - i^2\Delta\bar{z}^2)}{f_p(x_0 - i^2\Delta\bar{z}^2)}$ are all dimensionless. Here, f_i can be determined from the measured EOS for any given $x_0 = \beta\mu_0$ at the trap center. For the symmetric displacement fields, one has $u_{+i} = u_{-i}$, we can set $u_0 = 1$ and obtain $u_1 = 1 - a\Delta\bar{z}^2/2f_0$ using Eq. (D.4) and the symmetry requirement. Similarly, for the anti-symmetrical displacement fields, one has $u_{+i} = -u_{-i}$, we can set $u_0 = 0$ and $u_1 = 1$. The complete displacement field can then be obtained using the recurrence relation in Eq. (D.4). The physical eigen-collective modes are obtained by keeping the divergence of u at large z as small as possible (i.e. keeping the divergence as polynomials instead of exponential). This can be achieved by varying the mode frequency through the parameter a in Eq. (D.4).

Once the displacement field is obtained, the corresponding mode profile is available by using Eq. (5.58), namely:

$$\begin{aligned} \delta n_1 &= -\frac{\partial n_1 u}{\partial z} = -\frac{n_{1,i+1}u_{i+1} - n_{1,i-1}u_{i-1}}{2\Delta z} \\ &\propto \frac{f_p(x_0 - (i+1)^2\Delta\bar{z}^2)u_{i+1} - f_p(x_0 - (i-1)^2\Delta\bar{z}^2)u_{i-1}}{2\Delta\bar{z}}. \end{aligned} \tag{D.5}$$

The results from the exact numerical calculation show that the approximate variational method gives very good prediction for the mode frequencies and mode profiles (see Figs. D.1 and D.2).

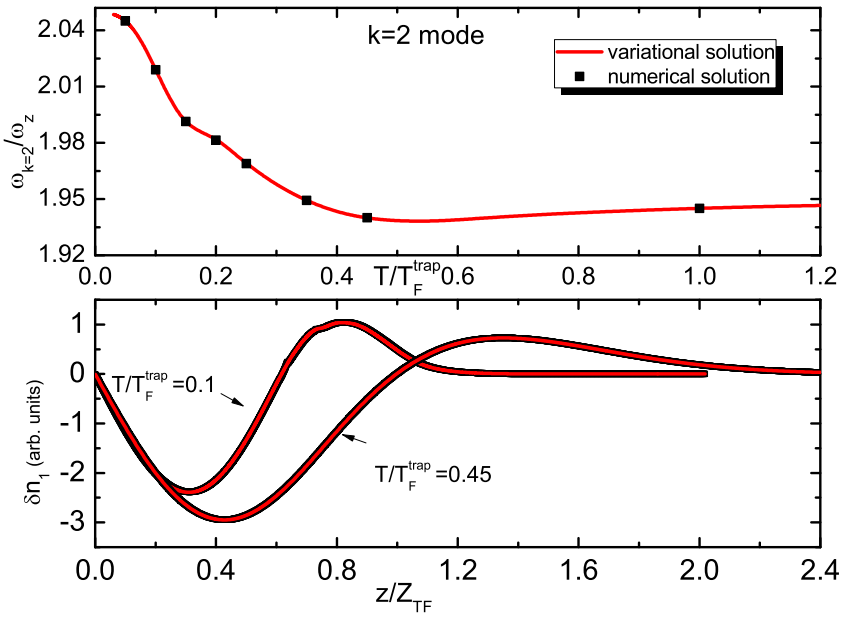

Figure D.1: Comparing the frequency and the corresponding mode profile of the $k = 2$ mode obtained from the variational method to the exact numerical solutions. In the lower panel, the density fluctuations are shown at two different temperatures, for the lowest ($T/T_F^{trap} \approx 0.1$) and for the highest temperature ($T/T_F^{trap} \approx 0.45$) explored in the experiment of Refs. [53], [54].

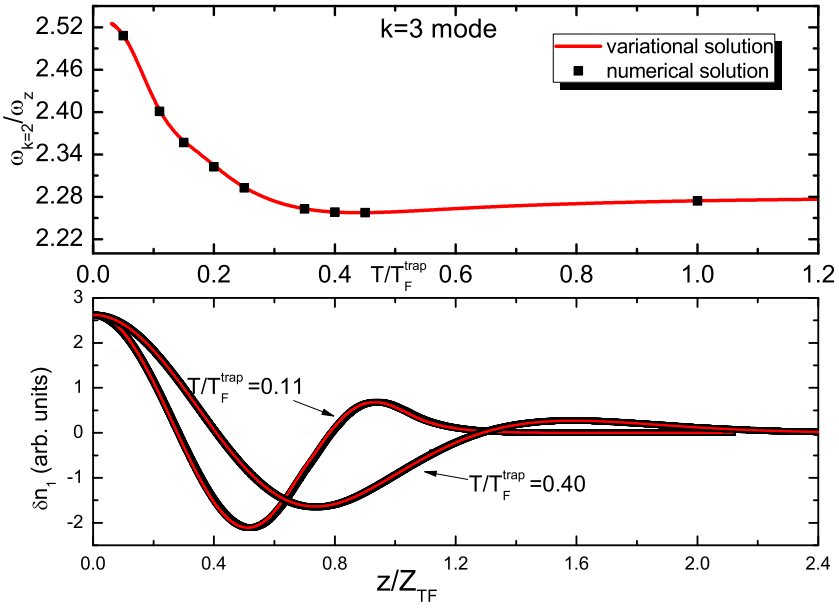

Figure D.2: Comparing the frequency and the corresponding mode profile of the $k = 3$ mode obtained from the variational method to the exact numerical solutions. In the lower panel, the density fluctuations are shown at two different temperatures.

Bibliography

[1] P. Kapitza, Viscosity of Liquid Helium below the λ-Point. Nature **141**, 74 (1938).

[2] J.F. Allen, A.D. Misener, Flow of Liquid Helium II. Nature **141**, 75 (1938).

[3] L. Tisza J. Phys. Radium **1**, 164 (1940).

[4] L. Tisza J. Phys. Radium **1**, 350 (1940).

[5] L.D. Landau, The theory of superfluidity of helium II. J. Phys. USSR **5**, 71 (1941).

[6] V. Peshkov, "Second Sound" in Helium II. J. Phys. USSR **8**, 381 (1944).

[7] V. Peshkov, Determination of the Velocity of Propagation of the Second Sound in Helium II. J. Phys. USSR **10**, 389 (1946).

[8] L.D. Landau, On the theory of superfluidity of helium II. J. Phys. USSR **11**, 91 (1947).

[9] M.H. Anderson, J.R. Ensher, M.R. Matthews, C.E. Wieman, E.A. Cornell, Observation of Bose-Einstein Condensation in a Dilute Atomic Vapor. Science **269**, 198 (1995).

[10] K.B. Davis, M.-O. Mewes, M.R. Andrews, N.J. van Druten, D.S. Durfee, D.M. Kurn, W. Ketterle, Bose-Einstein condensation in a gas of sodium atoms. Phys. Rev. Lett. **75**, 3969 (1995).

[11] C.C. Bradley, C.A. Sackett, J.J. Tollett, R.G. Hulet, Evidence of Bose-Einstein Condensation in an Atomic Gas with Attractive Interactions. Phys. Rev. Lett. **75**, 1687 (1995).

[12] B. DeMarco, D.S. Jin, Onset of Fermi Degeneracy in a Trapped Atomic Gas. Science **285**, 1703 (1999).

[13] F. Schreck, L. Khaykovich, K.L. Corwin, G. Ferrari, T. Bourdel, J. Cubizolles, C. Salomon, Quasipure Bose-Einstein Condensate Immersed in a Fermi Sea. Phys. Rev. Lett. **87**, 080403 (2001).

[14] A.G. Truscott, K.E. Strecker, W.I. McAlexander, G.B. Partridge, R.G. Hulet, Observation of Fermi Pressure in a Gas of Trapped Atoms. Science **291**, 2570 (2001).

[15] G. Roati, F. Riboli, G. Modugno, M. Inguscio, Fermi-Bose Quantum Degenerate ^{40}K-^{87}Rb Mixture with Attractive Interaction. Phys. Rev. Lett. **89**, 150403 (2002).

[16] Z. Hadzibabic, S. Gupta, C.A. Stan, C.H. Schunck, M.W. Zwierlein, K. Dieckmann, W. Ketterle, Fiftyfold Improvement in the Number of Quantum Degenerate Fermionic Atoms. Phys. Rev. Lett. **91**, 160401 (2003).

[17] K.M. O'Hara, S.L. Hemmer, M.E. Gehm, S.R. Granade, J.E. Thomas, Observation of a Strongly Interacting Degenerate Fermi Gas of Atoms. Science **298**, 2179 (2002).

[18] C. Chin, R. Grimm, P. Julienne, E. Tiesinga, Feshbach resonances in ultracold gases. Rev. Mod. Phys. **82**, 1225 (2010).

[19] T.-L. Ho, Universal Thermodynamics of Degenerate Quantum Gases in the Unitarity Limit. Phys. Rev. Lett. **92**, 090402 (2004).

[20] F. Dalfovo, S. Giorgini, L.P. Pitaevskii, S. Stringari, Theory of Bose-Einstein condensation in trapped gases. Rev. Mod. Phys. **71**, 463 (1999).

[21] L. Pitaevskii, S. Stringari, *Bose-Einstein condensation* (Oxford University Press, Oxford, 2003).

[22] C.J. Pethick, H. Smith, *Bose-Einstein Condensation in Dilute Gases* (Cambridge University Press, Cambridge, 2001).

[23] M. Inguscio, W. Ketterle, C. Salomon, *Ultracold Fermi Gases, Proceedings of the international school of physics Enrico Fermi, Course CLXIV, Varenna, June 2006* (IOS Press, Amsterdam, 2008).

[24] S. Giorgini, L.P. Pitaevskii, S. Stringari, Theory of ultracold atomic Fermi gases. Rev. Mod. Phys. **80**, 1215 (2008).

[25] I. Bloch, J. Dalibard, W. Zwerger, Many-body physics with ultracold gases. Rev. Mod. Phys. **80**, 885 (2008).

[26] M.R. Andrews, D.M. Kurn, H.-J. Miesner, D.S. Durfee, C.G. Townsend, S. Inouye, W. Ketterle, Propagation of Sound in a Bose-Einstein Condensate. Phys. Rev. Lett. **79**, 553 (1997).

[27] J. Joseph, B. Clancy, L. Luo, J. Kinast, A. Turlapov, J.E. Thomas, Measurement of Sound Velocity in a Fermi Gas near a Feshbach Resonance. Phys. Rev. Lett. **98**, 170401 (2007).

[28] M. Horikoshi, S. Nakajima, M. Ueda, T. Mukaiyama, Measurement of Universal Thermodynamic Functions for a Unitary Fermi Gas. Science **327**, 442 (2010).

[29] E. Zaremba, Sound propagation in a cylindrical Bose-condensed gas. Phys. Rev. A **57**, 518 (1998).

[30] P. Capuzzi, P. Vignolo, F. Federici, M.P. Tosi, Sound propagation in elongated superfluid fermionic clouds. Phys. Rev. A **73**, 021603 (2006).

[31] A. Griffin, T. Nikuni, E. Zaremba, *Bose-Condensed Gases at Finite Temperature* (Cambridge University Press, Cambridge, 2009).

[32] D.M. Stamper-Kurn, H.-J. Miesner, S. Inouye, M.R. Andrews, W. Ketterle, Collisionless and Hydrodynamic Excitations of a Bose-Einstein Condensate. Phys. Rev. Lett. **81**, 500 (1998).

[33] R. Meppelink, S.B. Koller, J.M. Vogels, H.T.C. Stoof, P. van der Straten, Damping of Superfluid Flow by a Thermal Cloud. Phys. Rev. Lett. **103**, 265301 (2009).

[34] R. Meppelink, S.B. Koller, P. van der Straten, Sound propagation in a Bose-Einstein condensate at finite temperatures. Phys. Rev. A **80**, 043605 (2009).

[35] E. Arahata, T. Nikuni, Dynamical Simulation of Sound Propagation in a Highly Elongated Trapped Bose Gas at Finite Temperatures. J. Low Temp. Phys. **171**, 369 (2013).

[36] L.A. Sidorenkov, M.K. Tey, R. Grimm, Y.-H. Hou, L. Pitaevskii, S. Stringari, Second sound and the superfluid fraction in a Fermi gas with resonant interactions. Nature **498**, 78 (2013).

[37] G. Bertaina, L. Pitaevskii, S. Stringari, First and Second Sound in Cylindrically Trapped Gases. Phys. Rev. Lett. **105**, 150402 (2010).

[38] D.S. Jin, J.R. Ensher, M.R. Matthews, C.E. Wieman, E.A. Cornell, Collective Excitations of a Bose-Einstein Condensate in a Dilute Gas. Phys. Rev. Lett. **77**, 420 (1996).

[39] M.-O. Mewes, M.R. Andrews, N.J. van Druten, D.M. Kurn, D.S. Durfee, C.G. Townsend, W. Ketterle, Collective Excitations of a Bose-Einstein Condensate in a Magnetic Trap. Phys. Rev. Lett. **77**, 988 (1996).

[40] S. Stringari, Collective Excitations of a Trapped Bose-Condensed Gas. Phys. Rev. Lett. **77**, 2360 (1996).

[41] S. Stringari, Collective oscillations of a trapped superfluid Fermi gas near a Feshbach resonance. Europhys. Lett. **65**, 749 (2004).

[42] J. Kinast, S. Hemmer, M. Gehm, A. Turlapov, J. Thomas, Evidence for Superfluidity in a Resonantly Interacting Fermi Gas. Phys. Rev. Lett. **92**, 150402 (2004).

[43] M. Bartenstein, A. Altmeyer, S. Riedl, S. Jochim, C. Chin, J. Denschlag, R. Grimm, Collective Excitations of a Degenerate Gas at the BEC-BCS Crossover. Phys. Rev. Lett. **92**, 203201 (2004).

[44] D.S. Jin, M.R. Matthews, J.R. Ensher, C.E. Wieman, E.A. Cornell, Temperature-Dependent Damping and Frequency Shifts in Collective Excitations of a Dilute Bose-Einstein Condensate. Phys. Rev. Lett. **78**, 764 (1997).

[45] R. Onofrio, D.S. Durfee, C. Raman, M. Köhl, C.E. Kuklewicz, W. Ketterle, Surface Excitations of a Bose-Einstein Condensate. Phys. Rev. Lett. **84**, 810 (2000).

[46] O.M. Maragò, S.A. Hopkins, J. Arlt, E. Hodby, G. Hechenblaikner, C.J. Foot, Observation of the Scissors Mode and Evidence for Superfluidity of a Trapped Bose-Einstein Condensed Gas. Phys. Rev. Lett. **84**, 2056 (2000).

[47] F. Chevy, V. Bretin, P. Rosenbusch, K.W. Madison, J. Dalibard, Transverse Breathing Mode of an Elongated Bose-Einstein Condensate. Phys. Rev. Lett. **88**, 250402 (2002).

[48] G.E. Astrakharchik, R. Combescot, X. Leyronas, S. Stringari, Equation of State and Collective Frequencies of a Trapped Fermi Gas Along the BEC-Unitarity Crossover. Phys. Rev. Lett. **95**, 030404 (2005).

[49] A. Altmeyer, S. Riedl, C. Kohstall, M.J. Wright, R. Geursen, M. Bartenstein, C. Chin, J.H. Denschlag, R. Grimm, Precision Measurements of Collective Oscillations in the BEC-BCS Crossover. Phys. Rev. Lett. **98**, 040401 (2007).

[50] J. Kinast, A. Turlapov, J.E. Thomas, Damping of a Unitary Fermi Gas. Phys. Rev. Lett. **94**, 170404 (2005).

[51] M.J. Wright, S. Riedl, A. Altmeyer, C. Kohstall, E.R.S. Guajardo, J.H. Denschlag, R. Grimm, Finite-Temperature Collective Dynamics of a Fermi Gas in the BEC-BCS Crossover. Phys. Rev. Lett. **99**, 150403 (2007).

[52] S. Riedl, E.R. Sánchez Guajardo, C. Kohstall, A. Altmeyer, M.J. Wright, J.H. Denschlag, R. Grimm, G.M. Bruun, H. Smith, Collective oscillations of a Fermi gas in the unitarity limit: Temperature effects and the role of pair correlations. Phys. Rev. A **78**, 053609 (2008).

[53] M.K. Tey, L.A. Sidorenkov, E.R.S. Guajardo, R. Grimm, M.J.H. Ku, M.W. Zwierlein, Y.-H. Hou, L. Pitaevskii, S. Stringari, Collective Modes in a Unitary Fermi Gas across the Superfluid Phase Transition. Phys. Rev. Lett. **110**, 055303 (2013).

[54] E.R.S. Guajardo, M.K. Tey, L.A. Sidorenkov, R. Grimm, Higher-nodal collective modes in a resonantly interacting Fermi gas. Phys. Rev. A **87**, 063601 (2013).

[55] M.J.H. Ku, A.T. Sommer, L.W. Cheuk, M.W. Zwierlein, Revealing the Superfluid Lambda Transition in the Universal Thermodynamics of a Unitary Fermi Gas. Science **335**, 563 (2012).

[56] T.-L. Ho, E.J. Mueller, High Temperature Expansion Applied to Fermions near Feshbach Resonance. Phys. Rev. Lett. **92**, 160404 (2004).

[57] X.-J. Liu, Virial expansion for a strongly correlated Fermi system and its application to ultracold atomic Fermi gases. Phys. Rep. **524**, 37 (2013).

[58] E. Taylor, A. Griffin, Two-fluid hydrodynamic modes in a trapped superfluid gas. Phys. Rev. A **72**, 053630 (2005).

[59] E. Taylor, H. Hu, X.-J. Liu, A. Griffin, Variational theory of two-fluid hydrodynamic modes at unitarity. Phys. Rev. A **77**, 033608 (2008).

[60] E. Taylor, H. Hu, X.-J. Liu, L.P. Pitaevskii, A. Griffin, S. Stringari, First and second sound in a strongly interacting Fermi gas. Phys. Rev. A **80**, 053601 (2009).

[61] E. Burovski, N. Prokof'ev, B. Svistunov, M. Troyer, Critical Temperature and Thermodynamics of Attractive Fermions at Unitarity. Phys. Rev. Lett. **96**, 160402 (2006).

[62] R. Haussmann, W. Rantner, S. Cerrito, W. Zwerger, Thermodynamics of the BCS-BEC crossover. Phys. Rev. A **75**, 023610 (2007).

[63] A. Bulgac, J.E. Drut, P. Magierski, Quantum Monte Carlo simulations of the BCS-BEC crossover at finite temperature. Phys. Rev. A **78**, 023625 (2008).

[64] M.M. Forbes, S. Gandolfi, A. Gezerlis, Resonantly Interacting Fermions in a Box. Phys. Rev. Lett. **106**, 235303 (2011).

[65] J. Carlson, S. Gandolfi, K.E. Schmidt, S. Zhang, Auxiliary-field quantum Monte Carlo method for strongly paired fermions. Phys. Rev. A **84**, 061602 (2011).

[66] K. van Houcke, F. Werner, E. Kozik, N. Prokof'ev, B. Svistunov, M.J.H. Ku, A.T. Sommer, L.W. Cheuk, A. Schirotzek, M.W. Zwierlein, Feynman diagrams versus Fermi-gas Feynman emulator. Nat. Phys. **8**, 366 (2012).

[67] J.E. Drut, T.A. Lähde, G. Wlazłowski, P. Magierski, Equation of state of the unitary Fermi gas: An update on lattice calculations. Phys. Rev. A **85**, 051601 (2012).

[68] O. Goulko, M. Wingate, Thermodynamics of balanced and slightly spin-imbalanced Fermi gases at unitarity. Phys. Rev. A **82**, 053621 (2010).

[69] H. Hu, X.-J. Liu, P.D. Drummond, Universal thermodynamics of a strongly interacting Fermi gas: theory versus experiment. New J. Phys. **12**, 063038 (2010).

[70] H. Hu, X.-J. Liu, P.D. Drummond, Comparative study of strong-coupling theories of a trapped Fermi gas at unitarity. Phys. Rev. A **77**, 061605 (2008).

[71] P. Nozires, S. Schmitt-Rink, Bose Condensation in an Attractive Fermion Gas: From Weak to Strong Coupling Superconductivity. J. Low Temp. Phys. **59**, 195 (1985).

[72] V.K. Akkineni, D.M. Ceperley, N. Trivedi, Pairing and superfluid properties of dilute fermion gases at unitarity. Phys. Rev. B **76**, 165116 (2007).

[73] A. Bulgac, J.E. Drut, P. Magierski, Spin 1/2 Fermions in the Unitary Regime: A Superfluid of a New Type. Phys. Rev. Lett. **96**, 090404 (2006).

[74] N. Prokof'Ev, B. Svistunov, Bold Diagrammatic MonteCarlo Technique: When the Sign Problem Is Welcome. Phys. Rev. Lett. **99**, 250201 (2007).

[75] L. Luo, J.E. Thomas, Thermodynamic Measurements in a Strongly Interacting Fermi Gas. J. Low Temp. Phys. **154**, 1 (2009).

[76] S. Nascimbène, N. Navon, K.J. Jiang, F. Chevy, C. Salomon, Exploring the thermodynamics of a universal Fermi gas. Nature **463**, 1057 (2010).

[77] In a recent paper [100] the temperature dependence of the superfluid density was calculated beyond the phonon regime applying Landau's equation for n_n in a BEC-BCS famework to account for the effects of the single-particle excitations.

[78] B.D. Josephson, Relation between the superfluid density and order parameter for superfluid He near Tc. Phys. Lett. **21**, 608 (1966).

[79] G. F. Bertsch, 1999, in the announcement of the Tenth International Conference on Recent Progress in Many-Body Theories (unpublished).

[80] E. Beth, G.E. Uhlenbeck, The quantum theory of the non-ideal gas. II. Behaviour at low temperatures. Physica **4**, 915 (1937).

[81] X.-J. Liu, H. Hu, P.D. Drummond, Virial Expansion for a Strongly Correlated Fermi Gas. Phys. Rev. Lett. **102**, 160401 (2009).

[82] L.D. Landau, E.M. Lifshitz, *Course of Theoretical Physics, vol.5 -Statistical Physics, Part 1* (Pergamon Press, 1980).

[83] T.-L. Ho, Q. Zhou, Obtaining the phase diagram and thermodynamic quantities of bulk systems from the densities of trapped gases. Nat. Phys. **6**, 131 (2010).

[84] Using the values of f_p and f_n, determined according to the procedure discussed in chapter 2, we find the value $\gamma = 63.2$.

[85] D.J. Papoular, G. Ferrari, L.P. Pitaevskii, S. Stringari, Increasing Quantum Degeneracy by Heating a Superfluid. Phys. Rev. Lett. **109**, 084501 (2012).

[86] I.M. Khalatnikov, *An Introduction to the Theory of Superfluidity* (Benjamin, 1965).

[87] L.D. Landau, E.M. Lifshitz., *Course of Theoretical Physics, vol.6 - Fluid Mechanics, 2nd edition* (Pergamon Press, 1987).

[88] T.D. Lee, C.N. Yang, Low-Temperature Behavior of a Dilute Bose System of Hard Spheres. II. Nonequilibrium Properties. Phys. Rev. **113**, 1406 (1959).

[89] A. Griffin, E. Zaremba, First and second sound in a uniform Bose gas. Phys. Rev. A **56**, 4839 (1997).

[90] Y. He, Q. Chen, C.-C. Chien, K. Levin, First- and second-sound-like modes at finite temperature in trapped Fermi gases from BCS to BEC. Phys. Rev. A **76**, 051602 (2007).

[91] E. Arahata, T. Nikuni, Propagation of second sound in a superfluid Fermi gas in the unitary limit. Phys. Rev. A **80**, 043613 (2009).

[92] H. Hu, E. Taylor, X.-J. Liu, S. Stringari, A. Griffin., Second sound and the density response function in uniform superfluid atomic gases. New J. Phys. **12**, 043040 (2010).

[93] Y.-H. Hou, L.P. Pitaevskii, S. Stringari, First and second sound in a highly elongated Fermi gas at unitarity. Phys. Rev. A **88**, 043630 (2013).

[94] The regime we consider here should not be confused with the strict 1D regime where all the particles occupy the lowest single particle state of the radial harmonic potential.

[95] G. Bertaina, Study of Ultracold Fermi Gases in the BCS-BEC Crossover: Quantum Monte Carlo Methods, Hydrodynamics and Local Density Approximation., PhD thesis, Universita degli Studi di Trento, 2010.

[96] K.R. Atkins, Third and Fourth Sound in Liquid Helium II. Phys. Rev. **113**, 962 (1959).

[97] The quantitative differences exhibited by Fig. 4.6 with respect to Fig. 2 of [37] are due to the more accurate thermodynamic ingredients used in the present calculation.

[98] S. Jochim, M. Bartenstein, A. Altmeyer, G. Hendl, S. Riedl, C. Chin, J. Hecker Denschlag, R. Grimm, Bose-Einstein Condensation of Molecules. Science **302**, 2101 (2003).

[99] N. Andrenacci, P. Pieri, G.C. Strinati, Evolution from BCS superconductivity to Bose-Einstein condensation: Current correlation function in the broken-symmetry phase. Phys. Rev. B **68**, 144507 (2003).

[100] L. Salasnich, Low-temperature thermodynamics of the unitary Fermi gas: Superfluid fraction, first sound, and second sound. Phys. Rev. A **82**, 063619 (2010).

[101] J.G. Dash, R.D. Taylor, Hydrodynamics of Oscillating Disks in Viscous Fluids: Density and Viscosity of Normal Fluid in Pure ^{4}He from 1.2K to the Lambda Point. Phys. Rev. **105**, 7 (1957).

[102] G. Baym, C.J. Pethick, Normal mass density of a superfluid Fermi gas at unitarity. Phys. Rev. A **88**, 043631 (2013).

[103] H. Hu, X.-J. Liu, Probing the critical exponent of superfluid fraction in a strongly interacting Fermi gas. arXiv:1310.3559 (2013).

[104] L. Pitaevskii, S. Stringari, Elementary Excitations in Trapped Bose-Einstein Condensed Gases Beyond the Mean-Field Approximation. Phys. Rev. Lett. **81**, 4541 (1998).

[105] H. Heiselberg, Collective Modes of Trapped Gases at the BEC-BCS Crossover. Phys. Rev. Lett. **93**, 040402 (2004).

[106] M. Amoruso, I. Meccoli, A. Minguzzi, M.P. Tosi, Collective excitations of a degenerate Fermi vapour in a magnetic trap. Eur. Phys. J. D **7**, 441 (1999).

[107] Y. Castin, Exact scaling transform for a unitary quantum gas in a time dependent harmonic potential. C. R. Physique **5**, 407 (2004).

[108] C. Cercignani, *The Boltzmann equation and its applications* (Springer Verlag, 1988).

[109] D.T. Son, Vanishing Bulk Viscosities and Conformal Invariance of the Unitary Fermi Gas. Phys. Rev. Lett. **98**, 020604 (2007).

[110] V.B. Shenoy, T.-L. Ho, First and Second Sound Modes of a Bose-Einstein Condensate in a Harmonic Trap. Phys. Rev. Lett. **80**, 3895 (1998).

[111] E. Taylor, Variational Theory for Two-Fluid Modes In Trapped Fermi Gases, PhD thesis, University of Toronto, 2008.

[112] The calculation was first provided by M. K. Tey.

[113] P.C. Hohenberg, B.I. Halperin, Theory of dynamic critical phenomena. Rev. Mod. Phys. **49**, 435 (1977).

[114] G. Wlazłowski, P. Magierski, J.E. Drut, Shear Viscosity of a Unitary Fermi Gas. Phys. Rev. Lett. **109**, 020406 (2012).

[115] A. LeClair, On the viscosity-to-entropy density ratio for unitary Bose and Fermi gases. New J. Phys. **13**, 055015 (2011).

[116] C. Cao, E. Elliott, J. Joseph, H. Wu, J. Petricka, T. Schäfer, J.E. Thomas, Universal Quantum Viscosity in a Unitary Fermi Gas. Science **331**, 58 (2011).

[117] C. Cao, E. Elliott, H. Wu, J.E. Thomas, Searching for perfect fluids: quantum viscosity in a universal Fermi gas. New J. Phys. **13**, 075007 (2011).

[118] G.M. Brunn, H. Smith, Shear viscosity and damping for a Fermi gas in the unitary limit. Phys. Rev. A **75**, 043612 (2007).

List of Publications

The major contents of this thesis have already appeared in some of the following papers:

- **Yan-Hua Hou**, Lev P. Pitaevskii and Sandro Stringari,
  First and second sound in a highly elongated Fermi gas at unitarity,
  Phys. Rev. A **88**, 043630 (2013).

- **Yan-Hua Hou**, Lev P. Pitaevskii and Sandro Stringari,
  Scaling solutions of the two fluid hydrodynamic equations in a harmonically trapped gas at unitarity,
  Phys. Rev. A **87**, 033620 (2013).

- Leonid A. Sidorenkov, Meng Khoon Tey, Rudolf Grimm, **Yan-Hua Hou**, Lev Pitaevskii, Sandro Stringari,
  Second sound and the superfluid fraction in a Fermi gas with resonant interactions,
  Nature **498**, 78 (2013).

- Meng Khoon Tey, Leonid A. Sidorenkov, Edmundo R. Snchez Guajardo, Rudolf Grimm, Mark J. H. Ku, Martin W. Zwierlein, **Yan-Hua Hou**, Lev Pitaevskii, Sandro Stringari,
  Collective Modes in a Unitary Fermi Gas across the Superfluid Phase Transition,
  Phys. Rev. Lett. **110**, 055303 (2013).